

Mechanisms of communication from mitochondria to lysosomes

Dissertation

For the award of the degree

“Doctor of Philosophy” (Ph.D.)

in the Molecular Medicine Study Program

at the Georg-August University Göttingen

submitted by

Lorena Fernández Mosquera

born in Vigo, Spain

Göttingen, 2016

Thesis Committee

Dr. Nuno Raimundo (Supervisor and first referee)

Institute of Cellular Biochemistry

Georg-August University Göttingen, Germany

Prof. Dr. Silvio O. Rizzoli (Second referee)

Department of Neuro- and Sensory Physiology

University Medical Center Göttingen, Germany

Prof. Dr. Stephan E. Lehnart

Heart Center - Translational cardiology

University Medical Center Göttingen, Germany

Extended Thesis Committee

Dr. Ruth Geiss-Friedlander

Department of Molecular Biology

Georg-August University Göttingen, Germany

Dr. Ira Milosevic

European Neuroscience Institute Göttingen

Georg-August University Göttingen, Germany

Prof. Matthias Dobbstein

Department of Molecular Oncology

Georg-August University Göttingen, Germany

Affidavit

I hereby declare that my dissertation, entitled 'Mechanisms of communication from mitochondria to lysosomes', has been written independently and with no other aids or sources than quoted.

Lorena Fernández Mosquera

Göttingen, December 2016

**Science knows no country, because knowledge belongs to humanity,
and is the torch which illuminates the world.**

Louis Pasteur

To Antonio and Antonia

Acknowledgements

First of all I would like to thank Dr. Nuno Raimundo, who gave me this great opportunity. I thank him for the challenges that this project brought and which showed me that it is necessary to always look for the correct path. I am also grateful for always having the opportunity to discuss with him any results or idea. And overall I thank him for the encouragement and motivation that he provides. Thanks for being a great mentor.

I further thank the rest of members of my thesis committee Prof. Silvio O. Rizzoli and Prof. Stephan Lehnart for their ideas, suggestions and advices which I took in consideration during my thesis. Also, I thank Dr. Ruth Geiss-Friedlander, Dr. Ira Milosevic and Prof. Matthias Dobbelstein for joining my extended thesis committee.

I would like also to acknowledge Dr. Massimiliano Stagi for his help with Matlab analysis and his great advices about pH and Ca^{2+} determinations.

Many thanks to Dr. Milosevic group for the help with microscopy, in special Sindhu Gowrisankaran for helping me and for the nice advice.

Also thanks to the members of my lab for all the help and support, in science and in my life abroad. Thank you for creating an environment that is scientifically stimulating and fun at the same time.

I also would like to acknowledge Divya Bala for the for language proofreading. Also thanks to King Faisal, Dr. Anita Krisko and Catia Diogo for their advice and support during the writing of this thesis.

Thanks also to the former members of the lab in special to Daniela Gerke for her technical support and Dr. John Murdoch for his suggestions.

As not everything can be about work, I would like to thank again my lab for the nice moments together. To Leonardo, King and Anita for the sushi, beers and conversations about science and life.

To my Spanish 'family' in Germany Maria, Antonio, Barbara, Kinga, David y Julius. Thanks for the support!

To my friends that supported me from a distance: Hari, Manu, Heidy, Rober, Belen, Ruben, Yoli, Zule, Feli, Alba, Victor, Aida, Pei, Tiger, Merce... Muchas gracias bastardos!

Y sobre todo gracias a mi familia, que siempre me ha apoyado en este loco plan de llegar a ser Dr. Especialmente gracias a mis padres que me han enseñado a luchar y sobreponerme a todo. Gracias por sacrificarlo todo por mi, para que llegara a ser lo que quisiera. Gracias por animarme cuando sentía que no podía seguir y sobre todo gracias por quererme tal y como soy.

Y por último, aunque no por ello menos importante, gracias a Víctor. La persona que ha apoyado todas mis decisiones, que me ha dado fuerzas en momentos de debilidad y que ha hecho reír cuando me sentía triste. Gracias por estar siempre a mi lado.

List of abbreviations

Acetyl-CoA - Acetyl coenzyme A

ADP - Adenosine diphosphate

AIF - Apoptosis inducing factor

AMP - Adenosine monophosphate

AMPK - AMP-activated protein kinase

Ar18 - Arf-like GTPase

ATP - Adenosine triphosphate

ATP6V0A1 - vATPase Subunit A1

ATP6V1A - vATPase Subunit V1 Subunit A

BNIP3 - BCL2-interacting protein 3

BORC - BLOC-one-related complex

BSA - Bovine serum albumin

CCCP - Carbonyl cyanide-m-chlorophenyl hydrazine

CnA - Dominant negative calcineurin

CTSD - Cathepsin D

CTSF - Cathepsin F

CO₂ - Carbon dioxide

DMEM - Dulbecco's modified eagle's medium

DMSO – Dimethyl sulfoxide

Drp1 - Dynamin-related protein 1

EBSS - Earl's balanced salt solution

ER - Endoplasmic reticulum

ERMES - Endoplasmic reticulum-mitochondria encounter structure

ETC - Electron transport chain

FACS - Fluorescence-activated cell sorting

FBS - Fetal bovine serum

FIS1 - Fission 1 protein

FAD - Flavin adenine dinucleotide

FADH₂ - Flavin adenine dinucleotide, reduced form

FCCP - Carbonyl cyanide-p-trifluoromethoxyphenol hydrazone

FK506 - Tracolimus

FUNDC1 - Fun14 Domain containing 1

GAA - Acid alpha glucosidase

GFP - Green fluorescent protein

H₂O – Water

H₂O₂ - Hydrogen peroxide

IMS - Intermembrane space

IMM - Inner mitochondrial membrane

LAMP1 - Lysosomal associated membrane protein 1

LAMP2 - Lysosomal associated membrane protein 2

LC3B - Microtubule-associated protein 1 light chain-3B

LIMP2 - Lysosomal integral membrane protein 2

LSDs - Lysosomal storage disorders

MCOLN1 - Muco lipin 1

MFF - Mitochondrial fission factor

MiD49 - Mitochondrial dynamics protein of 49kDa

MiD51 - Mitochondrial dynamics protein of 51kDa

MITF - Microphthalmia-associated transcription factor

mtDNA - Mitochondrial DNA

Mtf1 - Mitofusin 1

Mtf2 - Mitofusin 2

mTORC1 - Mammalian target of rapamycin complex 1

NAD⁺ - Nicotinamide adenine dinucleotide

NADH - Nicotinamide adenine dinucleotide, reduced form

NaN₃ - Sodium azide

OCR - Oxygen consumption rate

OMM - Outer mitochondrial membrane

OPA1 - Optic atrophic 1

Oxa1 - Mitochondrial membrane oxidase assembly protein1

OXPHOS - Oxidative phosphorylation

O₂ - Oxygen

PAM - Presequence-associated motor complex

PBS - Phosphate-buffered saline

pcDNA - Plasmid cytomegalovirus promoter DNA

PCR - Polymerase chain reaction

PGC1- α - Peroxisome proliferator-activated receptor gamma coactivator alfa

PINK1 - PTEN-induced putative kinase 1

Pi - Orthophosphate

PI3P - Phosphatidylinositol 3-phosphate

PI(3, 5) P2 - Phosphatidylinositol 3,5-bisphosphate

PIKFYVE - FYVE finger-containing phosphoinositide kinase

P/S - Penicillin/Streptomycin

PVDF - Polyvinylidene fluoride membrane

QH2 - Ubiquinol

qPCR - Quantitative real time polymerase chain reaction

Rab7 - Ras related protein 7

RFP - Red fluorescent protein

RHEB - Ras homolog enriched in brain

RILP - Rab-interacting lysosomal protein

ROS - Reactive oxygen species

RNA - Ribonucleic acid

rRNAs - Ribosomal RNAs

SAM - Sorting and assembly machinery

SDH - Succinate dehydrogenase

SDS-PAGE - Sodium dodecyl sulfate polyacrylamide gel electrophoresis

shRNA - Short hairpin RNA

siRNA - Small interfering RNA

SOD - Superoxide dismutase

TCA - Tricarboxylic acid

TFAM - Mitochondrial transcription factor A

TFEB - Transcription factor EB

TFE3 - Transcription factor E3

TFEC - Transcription factor EC

TGN - Trans-Golgi network

TIM23 - Translocase of the inner mitochondria membrane 23

TIM22 - Translocase of the inner mitochondria membrane 22

TPC2 - Two-pore channel 2

tRNAs - transfer RNAs

TRPML1 - Mucolipin TRP channel 1

ULK1 - unc-51 like autophagy activating kinase 1

ULK2 - unc-51 like autophagy activating kinase 2

UQCRC1 - Ubiquinol-cytochrome-c reductase complex core protein 1

V-ATPase - V-type-H⁺-ATPase

vCLAMP - Vacuole and mitochondria patch

VDAC - Voltage-dependent anion-selective channel

$\Delta\Psi$ – Mitochondrial transmembrane potential

List of figures

Figure 1. Mitochondrial network

Figure 2. Mitochondrial structure

Figure 3. Mitochondrial dynamic balance

Figure 4. Mitochondrial respiratory chain and oxidative phosphorylation

Figure 5. Cytochrome reductase deficiency in humans

Figure 6. Patients with mutations that affect cytochrome oxidase

Figure 8. Roles of the lysosome in cellular processes

Figure 9. Schematic view of a lysosome

Figure 10. Assembly of V-ATPase in mammalian cells

Figure 11. mTORC1-lysosome amino acid sensing pathway

Figure 12. List of some autophagy related genes in yeast and their mammalian homologs

Figure 13. Scheme of types of autophagy in mammalian cells

Figure 14. Scheme of ubiquitin-dependent and ubiquitin-independent autophagy in selective macroautophagy

Figure 15. Scheme of Parkin-dependent mitophagy

Figure 16. Scheme of Parkin-independent mitophagy

Figure 17. Scheme of autophagy

Figure 18. Membrane sources for phagophores

Figure 19. Model of the Atg12–Atg5–Atg16 complex autophagosome formation

Figure 20. Scheme of mitochondrial signals

Figure 21. Mitochondrial respiratory chain and ROS

Figure 22. mTORC1 amino acid regulation

Figure 23. Response of lysosomal genes to TFEB

Figure 24. TFEB regulation by mTORC

Figure 25. TFEB and MITF regulation by mTORC1

Figure 26. Regulation of TFEB and MITF by calcineurin

Figure 28. Mitochondrial malfunction affects lysosomes

Figure 27. Mitochondria-vacuole contact sites

Figure 29. Lysosomal malfunction affects mitochondria

Figure 30. Induction of acute mitochondrial malfunction by chemicals

Figure 31. Representative images of mitochondria and lysosomes under acute mitochondrial malfunction triggered by chemicals

Figure 32. Representative images of mitochondria and lysosomes under acute mitochondrial malfunction triggered by chemicals, in cells with LAMP1-GFP

Figure 33. Autophagy under acute mitochondrial malfunction

Figure 34. Induction of acute mitochondrial malfunction by transient knock--down

Figure 35. Representative images of mitochondria and lysosomes in cells under acute mitochondrial malfunction triggered by transient UQCRC1kd

Figure 36. Representative image of lysosomes and autophagosomes in cells under acute mitochondrial malfunction triggered by transient UQCRC1kd

Figure 37. Effects on transcript levels of lysosomal-related genes caused by acute mitochondrial malfunction

Figure 38. Effects on TFEB protein amount caused by acute mitochondrial malfunction

Figure 39. Effects TFEB and MITF transcript levels caused by acute mitochondrial malfunction

Figure 40. Effects of TFEB knock-down on MITF and of MITF knock-down on TFEB

Figure 41. Effects on transcript levels of lysosomal-related genes caused by acute mitochondrial malfunction on TFEB and MITF knock-downs

Figure 42. Pathway that connects acute mitochondrial malfunction with lysosomal biogenesis

Figure 43. Effects on transcript levels of lysosomal-related genes and MITF family caused by acute mitochondrial malfunction in presence of an AMPK inhibitor

Figure 44. Effects on transcript levels of lysosomal-related genes by an AMPK

Figure 45. Acute mitochondrial malfunction and calcineurin

Figure 46. Western blot of stable UQCRC1 knock-down

Figure 47. Representative images of cells with and without chronic mitochondrial malfunction

Figure 48. Effects on mitochondria caused by chronic mitochondrial malfunction

Figure 49. Effects on lysosomes caused by chronic mitochondrial malfunction

Figure 50. Effects on lysosomal mass caused by chronic mitochondrial malfunction

Figure 51. Effects on lysosomal proteolytic capacity caused by chronic mitochondrial malfunction

–

Figure 52. Effects of chronic mitochondrial malfunction on autophagy

Figure 53. Effects of chronic mitochondrial malfunction on autophagosomes

Figure 54. Representative image of autophagolysosomes in cells under chronic mitochondrial malfunction

Figure 55. Effect of chronic mitochondrial malfunction on lysosomal biogenesis

Figure 56. Effects of chronic mitochondrial malfunction on TFEB

Figure 57. Effects of chronic mitochondrial malfunction on TFEB localization

Figure 58. Effects of chronic mitochondrial malfunction on TFEB regulation

Figure 59. Effects of chronic mitochondrial malfunction on lysosomal Ca²⁺ homeostasis

Figure 60. Representative images showing the effects of MCOLN1 manipulation on lysosomal size in chronic mitochondrial malfunction

Figure 61. Effects of chronic mitochondrial malfunction on AMPK

Figure 63. Effects of AMPK activation chronic on lysosomal biogenesis under mitochondrial malfunction

Figure 64. Effects of chronic mitochondrial malfunction on lysosomal pH

Figure 65. Lysosomal biogenesis pathway in acute mitochondrial malfunction

Figure 66. Lysosomal biogenesis pathway in chronic mitochondrial malfunction

List of tables

Table 1. Companies and institutions that have provided the materials and instruments

Table 2. List of reagents

Table 3. Kits and disposals

Table 4. Buffers and solutions

Table 5. List of primers

Table 6. Cell culture media

Table 7. Cell culture compounds

Table 8. Cell culture devices

Table 9. Plasmids and siRNAs

Table 10. Primary antibodies for western blot and immunocytochemistry

Table 11. Secondary antibodies for western blot and immunocytochemistry

Table 12. Equipment

Table 13. Software

Content

Abbreviations	viii
List of figures	xiii
List of tables	xvi
Abstract	1
1. Introduction	3
1.1 Mitochondrion.....	3
1.1.1 Origin of the mitochondrion.....	3
1.1.2 Mitochondrial structure and morphology.....	4
1.1.3 Mitochondrial dynamics.....	6
1.1.4 Mitochondrial metabolism.....	7
1.1.4.1 Citrate cycle.....	7
1.1.4.2 Respiratory chain and oxidative phosphorylation	8
1.1.5 Uncoupler of respiratory chain.....	9
1.1.6 Cytochrome c reductase or bc ₁ complex	10
1.1.7 Cytochrome c oxidase.....	11
1.2 Lysosomes.....	14
1.2.1 Endolysosomal pathway and lysosomal formation.....	14
1.2.2 Lysosomal structure.....	16
1.2.3 Lysosomal pH.....	17
1.2.4 Lysosomal Ca ²⁺	18
1.2.5 Lysosomal amino acid sensing.....	19
1.3 Autophagy.....	21
1.3.1 Types of autophagy.....	22

1.3.2 Mitophagy.....	24
1.3.3 Autophagosome.....	26
1.4 Signaling pathways.....	29
1.4.1 Stress signaling and mitochondria.....	29
1.4.2 Mitochondria and ROS.....	30
1.4.3 Lysosomes and signaling.....	31
1.4.4 TFEB.....	32
1.4.5 AMPK.....	36
1.5 Interactions between mitochondria and lysosomes.....	37
1.5.1 Contact sites between mitochondria and lysosomes.....	37
1.5.2 Signaling pathways between mitochondria and lysosomes.....	38
1.4.3 Lysosomes and signaling.....	31
1.4.4 TFEB.....	32
1.4.5 AMPK.....	36
Aims.....	41
2. Materials and methods.....	42
2.1 Materials.....	42
2.1.1 Suppliers.....	42
2.1.2 Reagents.....	44
2.1.3 Kits and disposals.....	46
2.1.4 Buffers and solutions.....	48
2.1.5 Primers.....	50
2.1.6 Cell culture media and compounds.....	51
2.1.7 Cell culture devices.....	52

2.1.8 Plasmids and siRNA.....	53
2.1.9 Antibodies.....	54
2.1.10 Cell lines.....	55
2.1.11 Instruments.....	55
2.1.12 Software.....	57
2.2 Methods.....	58
2.2.1 Cell work.....	58
2.2.1.1 Growth conditions.....	58
2.2.1.2 Starvation treatment.....	58
2.2.1.3 Chemical treatments.....	58
2.2.1.4 Transient knock-downs.....	59
2.2.1.5 Selection of stable knock-downs.....	59
2.2.2 Molecular biology.....	60
2.2.2.1 RNA isolation from cells.....	60
2.2.2.2 cDNA synthesis.....	60
2.2.2.3 qPCR.....	62
2.2.2.4 DQ-BSA.....	63
2.2.2.5 Lysosomal quantification plate reader.....	63
2.2.2.6 Protein concentration determination using Pierce BCA assay.....	63
2.2.2.7 FACS determinations.....	64
2.2.2.8 Mitochondrial oxygen consumption determination.....	64
2.2.2.9 Nuclear isolation.....	65
2.2.3 Protein biochemistry.....	66
2.2.3.1 Sample preparation.....	66

2.2.3.2 Protein concentration determination using Bradford assay.....	66
2.2.3.3 SDS-PAGE.....	66
2.2.3.4 Western blotting.....	67
2.2.3.5 Immunostaining.....	67
2.2.4 Microscopy.....	67
2.2.4.1 Mitochondria/Lysosomes microscopy.....	67
2.2.4.2 Immunostaining in stable UQCRC1kd.....	68
2.2.4.3 Lysosomal pH determination with acridine orange.....	68
2.2.5 Statistical analysis.....	69
3. Results.....	70
3.1 Acute mitochondrial malfunction.....	71
3.1.1 Effect of acute mitochondrial malfunction caused by chemicals on lysosomes and autophagy	71
3.1.2 Effect of acute mitochondrial malfunction caused by transient UQCRC1 knock-down on lysosomes and autophagy	74
3.1.3 Effect of acute mitochondrial malfunction on lysosomal biogenesis.....	76
3.1.3 Effect of acute mitochondrial malfunction on TFEB/MITF levels.....	77
3.1.4 Acute mitochondrial malfunction and AMPK.....	81
3.1.5 Acute mitochondrial malfunction and calcineurin.....	84
3.2 Chronic mitochondrial malfunction.....	86
3.2.1 Chronic mitochondrial malfunction model.....	86
3.2.2 Effects of stable UQCRC1 knock-down on mitochondria.....	87
3.2.3 Effects of chronic mitochondrial malfunction on lysosomal morphology and function.....	88
3.2.4 Effects of chronic mitochondrial malfunction on autophagy.....	92

3.2.5 Effect of chronic mitochondrial malfunction on lysosomal biogenesis.....	94
3.2.6 Effect of chronic mitochondrial malfunction on TFEB localization.....	96
3.2.7 Effect of chronic mitochondrial malfunction on TFEB regulation.....	98
3.2.8 Effects of chronic mitochondrial malfunction on lysosomal Ca ²⁺ homeostasis.....	99
3.2.9 Effects of chronic mitochondrial malfunction on AMPK signaling.....	102
3.2.10 Effects of chronic mitochondrial malfunction on lysosomal pH.....	105
4. Discussion.....	107
4.1 Acute mitochondrial malfunction triggers lysosomal biogenesis and autophagy.....	107
4.2 Acute mitochondrial malfunction triggers TFEB/MITF-dependent lysosomal biogenesis.....	108
4.3 TFEB/MITF-dependent lysosomal biogenesis is AMPK-dependent.....	108
4.4 TFEB/MITF-dependent lysosomal biogenesis is calcineurin-independent.....	109
4.5 Chronic mitochondrial malfunction triggers uncoordinated lysosomal biogenesis and dysfunctional lysosomes.....	111
4.6 Chronic mitochondrial malfunction triggers a non-canonical TFEB pathway.....	112
4.7 Chronic mitochondrial malfunction caused dysfunctional calcium lysosomal homeostasis AMPK-dependent.....	112
4.8 Chronic mitochondrial malfunction increases lysosomal pH misregulating lysosomal calcium homeostasis.....	113
Summary and conclusions.....	116
References.....	117
Curriculum vitae.....	134

Abstract

The importance of mitochondria for cellular respiration, ATP synthesis and involvement in cell signaling pathways impacting cell proliferation, differentiation or death is now recognized. Due to the broad roles of mitochondria in cellular function, it is not surprising that mitochondrial malfunction has been shown to be a crucial factor in several diseases, including metabolic and neuromuscular diseases and also pathophysiological processes such as aging. However, it remains unclear how mitochondria interact with other organelles. While it is known that mitochondria have physical contact sites with other organelles, the communication via signaling pathways remains unclear. This thesis focuses on the mechanisms by which acute and chronic mitochondrial stresses impact lysosomal biogenesis and function.

In order to approach our goals, cellular models of acute and chronic mitochondrial malfunction were generated using chemical inhibitors of mitochondrial function or silencing the expression of a key mitochondrial respiratory chain subunit. This thesis shows that mitochondrial malfunction regulates lysosomal biogenesis via microphthalmia transcription factor family. Furthermore, we found that this increase in lysosomal biogenesis correlates with an increase in autophagic flux.

Interestingly, we found that the effect of mitochondrial malfunction over lysosomal biogenesis acts in different manners depending on the persistence of the mitochondrial defect. Acute mitochondrial malfunction triggers lysosomal biogenesis which is AMPK-dependent. However, chronic mitochondrial malfunction results in AMPK repression, in an uncoordinated transcriptional program lysosomal biogenesis and in dysfunctional swollen lysosomes, with the consequent accumulation of autophagolysosomes. This thesis also shows that cells with chronic mitochondrial malfunction are not able to trigger the canonical TFEB pathway.

Furthermore, we found that those dysfunctional lysosomes that have a pH less acidic than the control cells could be the cause of the decreased lysosomal performance since the optimal pH for lysosomal enzymes is acidic (4.5-5). We also found that pharmacologic activation of a lysosomal calcium channel, MCOLN1, is able to rescue the aberrant morphology of the swollen lysosomes present in chronic mitochondrial malfunction and most interestingly, also rescues the pH in those lysosomes taking it back to the range observed in control cells.

This work contributes to the knowledge of mitochondrial-lysosomal interactions, revealing an integrated perspective which shows differences between acute and chronic mitochondrial malfunction and the diversity of their effects on lysosomal homeostasis. Moreover, the discovery

of the pivotal role played by the MCOLN1 channel, in lysosomal impairment caused by chronic mitochondrial malfunction, provides a target of interest for mitochondrial diseases.

1. Introduction

1.1 Mitochondrion

The word mitochondrion arises from the Greek words mitos (thread) and khondros (granule). The first references to mitochondria are from the mid-1800s when Albert von Kölliker described the presence of “granules” in the cells of striated muscles. These “granules” were named mitochondria only in 1898 by Carl Benda. In the beginning of the 20th century, mitochondria were described as the “power house” of the cell by Albert Claude. However, nowadays it is known that the role of mitochondria in the cell has evolved to include many other functions as well (Raimundo 2014). Mitochondria are involved in amino acid, sugar and fatty acid catabolism, calcium homeostasis, synthesis of heme, Fe-S clusters and steroids. Also, mitochondria are instrumental in many pathways related to cell signaling like cell proliferation and differentiation as well as in autophagy (Nunnari & Suomalainen 2012; Pernas & Scorrano 2015; Raimundo 2014) .

In view of the fact that mitochondria are involved in such extensive variety of processes, it is not surprising that mitochondrial malfunction is implicated in several diseases, particularly neuromuscular diseases and metabolic disorders as well as pathophysiological processes such as aging or even cancer (Nunnari & Suomalainen 2012; Bratic & Larsson 2013; Tsai et al. 2009).

1.1.1 Origin of the mitochondrion

Since mitochondria were discovered, several theories about their origin have been proposed. The currently accepted theory is the Endosymbiotic Theory. This theory, proposed by Francis Taylor in 1974, was specially supported by Lynn Margulis and has been widely supported by genetic data (Scheffler 2008). According to the Endosymbiotic Theory, mitochondria resulted from an alpha-proteobacterium engulfed by a eukaryotic progenitor over two billion years ago (Scheffler 2008; Dolezal et al. 2006), resulting in the formation of mitochondrial double membrane and in the presence of a second genome in the cell, the mitochondrial DNA (mtDNA).

It is commonly accepted today that mitochondria have a monophyletic origin wherein a singular event in evolution originated this organelle. However, there is still a surprising difference among organisms with respect to the number and function of mitochondrial genes encoded by the mtDNA. For example, in mammals, 13 polypeptides of mitochondrial respiratory chain are encoded by mtDNA, whereas in freshwater protozoon *Reclinomonas Americana*, 23 polypeptides of mitochondrial respiratory chain are encoded by mtDNA (Lang et al. 1997). As part of evolution,

several genes were transferred from the mitochondrial to the nuclear genome. The following sections of this thesis will focus on mammalian mitochondria.

1.1.2 Mitochondrial structure and morphology

At structural level, mitochondria are described as very dynamic double-membrane-bound organelles, with a huge diversity in their morphology (Youle et al. 2012). Mitochondria look similar to small bacteria, usually with a spaghetti-like shape, of no fixed length and about 1 μm in diameter (Fig. 1) (Palade, 1953; Sjostrand, 1953).

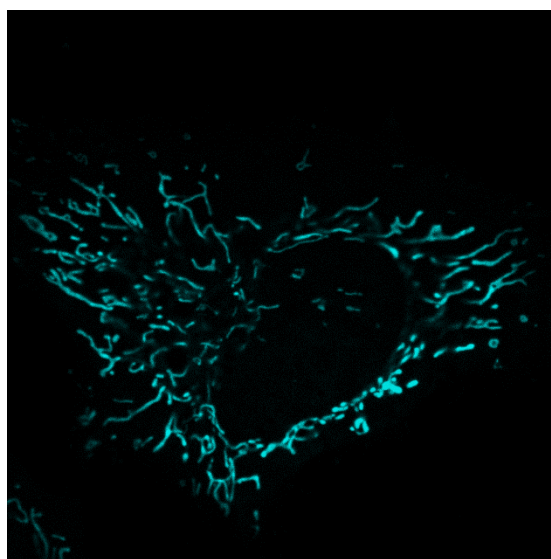


Figure 1. Mitochondrial network – Mitochondrial network in HeLa cell (100X). The cells were transfected with cyan fluorescent protein targeted to mitochondria (mito-CFP).

The mitochondrion is an organelle present in Eukaryotic cells delimited by two membranes. The outer mitochondrial membrane (OMM), separates the cytoplasm from the intermembrane space (IMS). The inner mitochondrial membrane (IMM) separates the mitochondrial matrix from the IMS.

The OMM is permeable to molecules up to 8 kDa due to the presence of a β -barrel protein called porin, also known as voltage-dependent anion-selective channel (VDAC), that has a diameter of 2 to 3 nanometers (Zalman et al. 1980; Benz 1994). On the other hand IMM has a protein:lipid ratio higher than usual and its permeability is tightly controlled in order to maintain the proton gradient generated by the mitochondrial respiratory chain and used by the ATP synthase. Furthermore, another difference between the IMM and the OMM is the presence of invaginations

called cristae in the IMM. The mitochondrial respiratory chain and the oxidative phosphorylation complexes reside in the areas of the IMM that form these cristae (Bernardi & Azzone 1981; Ishihara et al. 2006; Pernas & Scorrano 2015). Recently, it has been identified that the intra-cristae space is another mitochondrial compartment (Raimundo et al. 2016; Pernas & Scorrano 2016). The number of cristae in the mitochondrion seems to correlate with the energy demands of the cell (Rossignol et al. 2004) (Fig. 2).

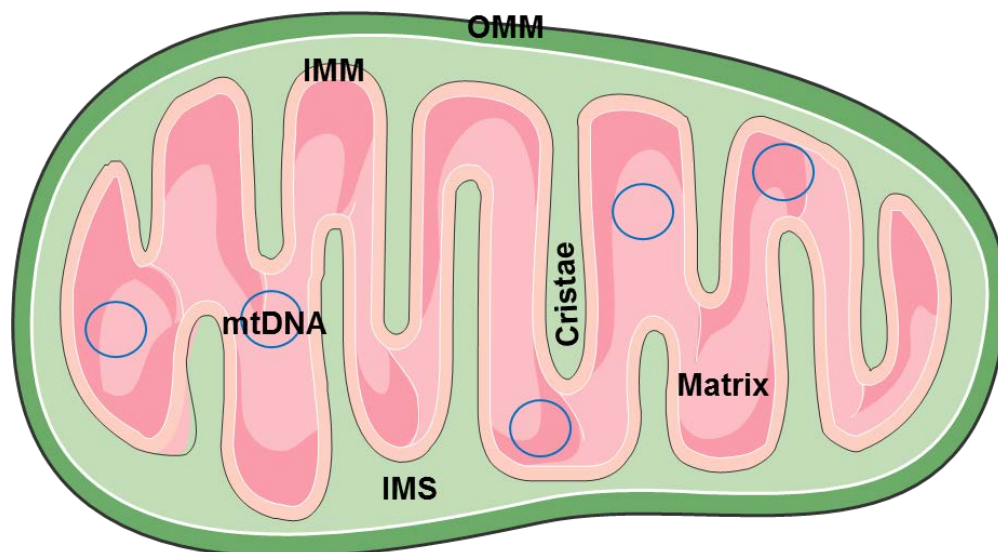


Figure 2. Mitochondrial structure – Scheme of a mitochondrion with the outer mitochondrial membrane (OMM), the inner mitochondrial membrane (IMM) and between them is the inter membrane space (IMS). The IMM is folded, thus generating the cristae (where the respiratory chain complexes are located) and encloses the mitochondrial matrix. In the mitochondrial matrix resides the mitochondrial DNA (mtDNA).

Inside the IMM is the mitochondrial matrix, where the processes involved in mitochondrial metabolism as well as the maintenance, replication, transcription and translation of mtDNA take place (Scalettar et al. 1991). One of the principal characteristics of the mitochondrion is that it has its own genetic material, the mitochondrial DNA. In mammals this mtDNA, which has 16569 base pairs, encodes 2 ribosomal RNAs (rRNAs), 13 polypeptides of mitochondrial respiratory chain and 22 transfer RNAs (tRNAs). The rest of the proteins present in the mitochondrion, around 1500, are nuclear-encoded, translated by ribosomes in the cytoplasm and translocated into the mitochondria through dedicated protein import complexes. These include, for example, the translocase of the outer mitochondria membrane (TOM) complex, placed in the OMM (Chacinska et al. 2009; Lightowlers et al. 2015; Chacinska et al. 2010) and the translocase of the inner

mitochondria membrane 23 (TIM23) complex. TOM and TIM, in cooperation with the presequence-associated motor (PAM) complex, catalyze the translocation of the nuclear encoded protein precursors to the matrix. The TIM23 complex also mediates the sorting of precursor proteins with a 'stop' signal into IMM (Chacinska et al. 2009). There is also the translocase of the inner mitochondria 22 (TIM22) complex that assembles carrier proteins into the inner membrane, as well as the membrane mitochondrial oxidase assembly protein1 (Oxa1) that also mediates protein insertion from the matrix into the inner membrane (Neupert & Herrmann 2007; Chacinska et al. 2009). Furthermore, the tiny Tim proteins guide β -barrel precursor proteins, imported by TOM complex, across the IMS to the sorting and assembly machinery (SAM) that drives their integration in the OMM (Koehler 2000; Schleiff & Becker 2011).

1.1.3 Mitochondrial dynamics

Data obtained through in vivo microscopy show that mitochondria are dynamic organelles since they can move along their axis at a speed of 2 to 30 $\mu\text{m}/\text{min}$. This displacement correlates with changes in the mitochondrial shape, thinning and thickening of mitochondrion and rearrangement of cristae (Scheffler 2008). However there are other ways in which mitochondria change their shape, like fission and fusion. The rates of mitochondrial fission/fusion are usually equilibrated, however they can favor one of the directions of this equilibrium in order to adapt to different stress conditions (Youle et al. 2012; Wai & Langer 2016) (Fig. 3). Several proteins are involved in mitochondrial fission and fusion. In mammals, the core proteins involved in fission are dynamin-related protein 1 (Drp1) which cycles on and off to the mitochondria from the cytoplasm and the mitochondrial proteins placed in OMM that recruit Drp1, such as fission 1 protein (FIS1), mitochondrial fission factor (MFF) and mitochondrial dynamics proteins of 49 and 51 kDa (MiD49 and MiD51) (Smirnova et al. 1998; Gandre-Babbe & Bliiek 2008; Yoon et al. 2003; James et al. 2003; Losón et al. 2012). For example, when the cell is growing and dividing, under conditions of impaired oxidative phosphorylation (OXPHOS) or loss of mitochondrial membrane potential, Drp1 translocates to the OMM where it oligomerizes, forming spirals that constrict OMM and IMM until the fragmentation of the mitochondrion. On the other hand, when there is an increase in mtDNA, such as in cells with mitochondrial Transcription Factor 1 (TFAM) depletion, mitochondria fuse becoming hyperfused. The proteins involved in the mitochondrial fusion are the mammalian orthologues mitofusin 1 (Mtf1) and mitofusin 2 (Mtf2) (Santel & Fuller 2001; Ishihara et al. 2004; West et al. 2015), which are anchored in the OMM and are required to fuse the OMM while the

fusion of IMM needs optic atrophic 1 (OPA1), which is in the membrane of the mitochondrial cristae facing the IMM (Olichon et al. 2003; Frezza et al. 2006; Wai & Langer 2016).

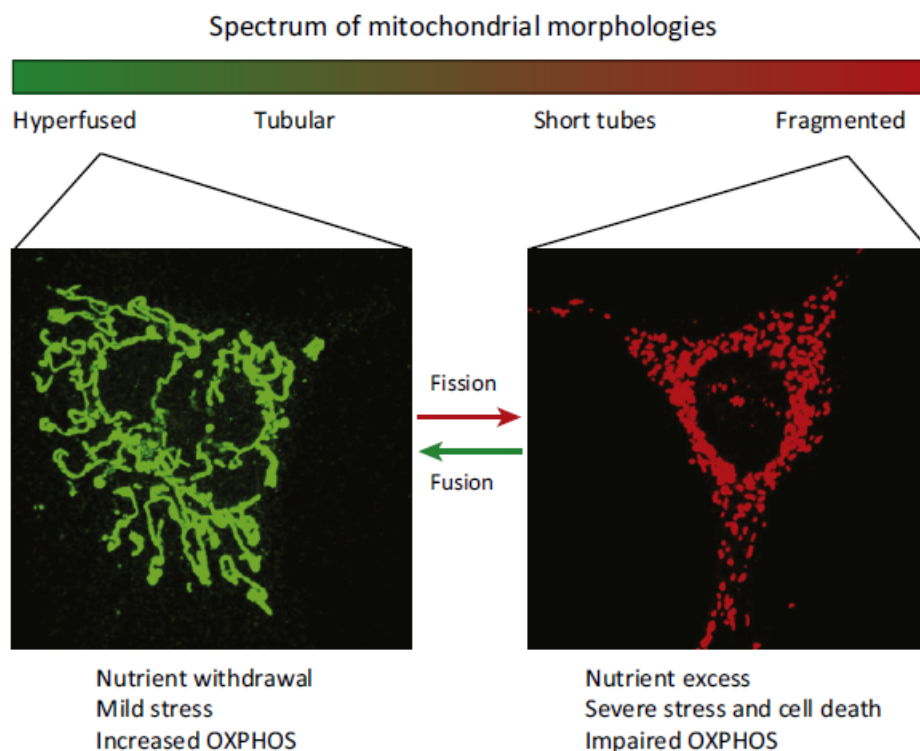


Figure 3. Mitochondrial dynamic balance – Mitochondria in mouse embryonic fibroblast under different metabolic stimuli. Under nutrient withdrawal, mild stress and increase of OXPHOS, there is an increase in mitochondrial fission (green), while under nutrient excess, severe stress and decreased of OXPHOS, there is an increase in mitochondrial fusion (red). Figure from Wai & Langer 2016.

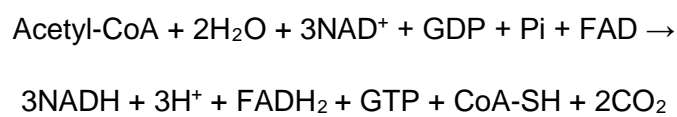
1.1.4 Mitochondrial metabolism

1.1.4.1 Citrate cycle

The citrate cycle and OXPHOS are two essential sets of reactions in order to satisfy the energy demands in eukaryotic cells. These two processes are connected by the generation of NADH and FADH₂ in the citrate cycle, which then transfer electrons to molecular oxygen, reducing it to water in the mitochondrial respiratory chain. The transfer of electrons is coupled with the transfer of protons from the matrix to the IMS generating an electrochemical gradient that is used to generate energy and store it in form of ATP (Korla & Mitra 2013).

The citrate cycle, also known as tricarboxylic acid (TCA) cycle or Krebs cycle, was proposed by Krebs and Johnson in 1937 (Krebs & Johnson 1937). The enzymes that catalyze the reactions of the citrate cycle are in the mitochondrial matrix, except succinate dehydrogenase (SDH) which is associated with the matrix side of the inner membrane and is a part of both the citrate cycle and the respiratory chain (complex II) (Addink et al. 1972).

Acetyl-CoA is the initial substrate of citrate cycle, it is mainly generated by oxidation of pyruvate but also from fatty acid and amino acid metabolism. Once that acetyl-CoA enters the citrate cycle, a series of chemical reactions start. The overall reaction of the citrate cycle is represented by the equation:



The citrate cycle and the mitochondrial respiratory chain have several “contact” points, such as complex II which catalyzes the oxidation of succinate to fumarate with the associated reduction of FAD to FADH₂. Furthermore, the reduction of NAD⁺ to NADH is also accomplished in the citrate cycle and NADH is used to feed complex I of the mitochondrial respiratory chain (Scheffler 2008; Korla & Mitra 2013).

1.1.4.2 Respiratory chain and oxidative phosphorylation

Mitochondrial respiratory chain or electron transport chain (ETC) defines a group of protein complexes placed in the IMM, where it operates as the site of OXPHOS through the use of ATP synthase. The respiratory chain is involved in the transfer of electrons from electron donors to electron acceptors via redox reactions. This transfer of electrons is coupled with the pumping of H⁺ across the membrane and the generation of an electrochemical gradient, composed by pH gradient and membrane potential ($\Delta\psi$) across the inner membrane. This electrochemical gradient is used by the mitochondrial ATP synthase, also referred to as Complex V, to transform adenosine diphosphate (ADP) in adenosine triphosphate (ATP) (Mitchell & Moyle 1969; Scheffler 2008).

The operation of the respiratory chain is well characterized. NADH and FADH₂ are oxidized to NAD⁺ and FAD in the complex I and complex II respectively. Ubiquinol carries electrons from both complexes to the complex III which in turn, through the ubiquinone cycle, transfers the electrons to cytochrome c. This protein will then pass the electrons to complex IV (cytochrome c oxidase). In complex IV, the electrons are passed to their terminal acceptor O₂ thus forming H₂O. During

this process, protons are pumped from the mitochondrial matrix into IMS in complex I, III, and IV, thereby generating the electrochemical gradient that is used by ATP synthase to generate ATP - the energy “currency” of the cell (Andreyev et al. 2005) (Fig. 4).

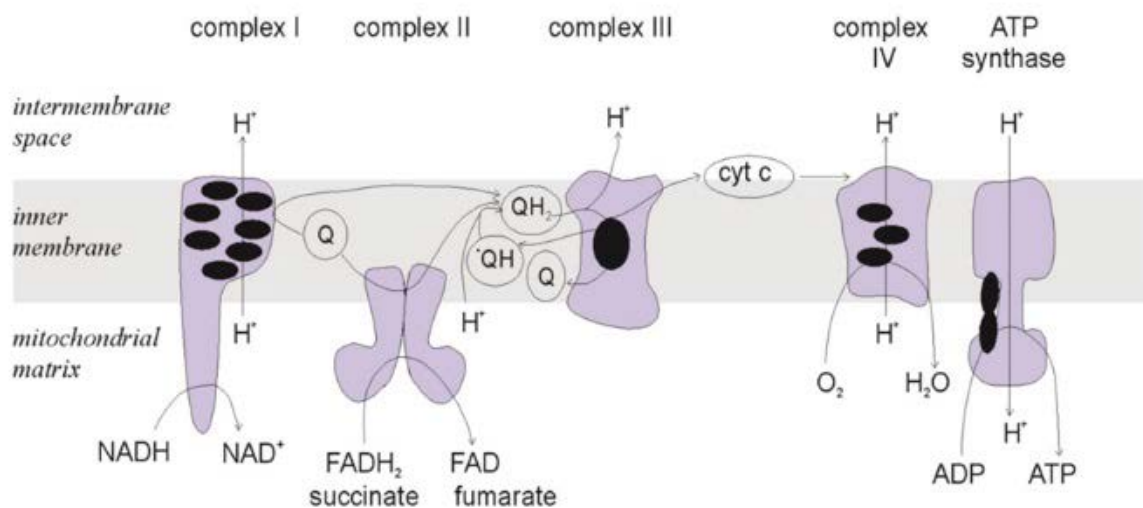


Figure 4. Mitochondrial respiratory chain and oxidative phosphorylation – The respiratory chain complexes (I-IV), ubiquinone and cytochrome c (cyt c) and ATP synthase are displayed. The black dots in the complexes represent the subunits encoded by mtDNA. Figure adapted from DiMauro and Schon, 2008.

Currently it is known that the respiratory chain complexes form multimeric structures called respirasomes or supercomplexes (Schägger & Pfeiffer 2000). For example, in mammals almost all of complex I is associated to dimers of complex III (III_2); there are supercomplexes formed by complex $I_1-III_2-IV_n$ (Schägger & Pfeiffer 2000); ATP synthase can form dimers (Schäfer et al. 2006; Wittig et al. 2006). It has been shown that the deficiencies in complex III or IV affect complex I (Enríquez 2016). Furthermore supercomplexes are also related to the increase in the efficiency of electron transfer and a consequent decrease in the production of reactive oxygen species (Maranzana et al. 2013; Enríquez 2016).

1.1.5 Uncoupler of respiratory chain

The generation of the ATP by ATP synthase requires orthophosphate (Pi), ADP and energy. The energy is provided by the electrochemical gradient across the inner membrane, generated by the

respiratory chain. One of the methods employed in this thesis to induce mitochondrial malfunction includes using uncouplers which are protonophores that move protons through IMM due to their ability to diffuse through the membrane. The uncouplers decrease the membrane potential uncoupling the proton gradient and reducing the ability of ATP synthase to function optimally. Some commonly used uncouplers are carbonyl cyanide m-chlorophenyl hydrazone (CCCP), carbonyl cyanide-p-trifluoromethoxyphenol hydrozone (FCCP), 2,4-dinitrophenol or dicumarol (Kessler et al. 1976; Lim et al. 2001; Lou et al. 2007). The uncoupling of mitochondrial respiratory chain allows the return of protons from the IMS into the mitochondrial matrix without ATP production. In this system, proton leakage causes a decrease in the membrane potential across the inner membrane and an increase in the mitochondrial respiration rate. This means that in the presence of an uncoupler, for example CCCP, the complexes I-IV of respiratory chain function normally but the synthesis of ATP cannot occur although ATP synthase is not inhibited (Terada 1990; Miles 2003; Lou et al. 2007).

1.1.6 Cytochrome c reductase or bc₁ complex

Cytochrome c reductase, bc₁ complex or complex III is a transmembrane protein complex that is the third complex of ETC. This complex receives electrons from complex I and II, through ubiquinol, and transfers these electrons to cytochrome c, through the Q-cycle or ubiquinone cycle.

In mammals, complex III is formed by 11 subunits with a molecular weight of 240 kb. Only one complex III subunit is encoded by mtDNA, namely cytochrome b. All other complex III subunits are nuclear encoded. This complex has three redox components: cytochrome b with two hemes, FeS protein with a Rieske [Fe-S] center and cytochrome c₁ (Iwata et al. 1998; Fry & Green 1978; Rieske 1976; Xia et al. 1997).

The cytochrome bc₁ has two active sites. Ubiquinol is oxidized at site Q₀ and releases protons to the IMS and ubiquinone is reduced in Q₁ and uptakes protons from the matrix. The existence of these two sites is essential for the Q-cycle. The Q-cycle takes advantage of the lipid-solubility of ubiquinone and ubiquinol, which allows them to diffuse in the membrane (Saraste 1999). A key point in the Q cycle is the separation of the electron paths of the two electrons received from ubiquinol at Q₀. The first electron goes to the Rieske Fe-S which shuttles it to the cytochrome c₁ while the second electron from ubiquinol goes to cytochrome b. The bifurcation of this pathway couples the transfer of electrons to cytochrome c with the pumping of protons to the IMS (Iwata et al. 1998; Xia et al. 1997; Saraste 1999).

It has been shown that defects in bc_1 complex lead to several mitochondrial disorders like mitochondrial myopathy, encephalomyopathy, or cardiomyopathy (Fig. 5) (Hoffman et al. 1993; Kennaway 1988) .

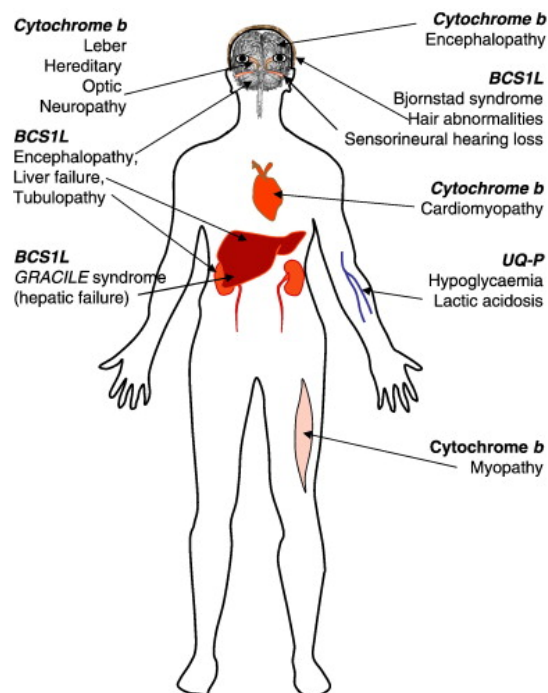


Figure 5. Cytochrome reductase deficiency in humans – Examples of organ/system involvement in patients with mutations in mitochondrial and nuclear genes affecting complex III of mitochondrial respiratory chain, Figure from Bénit et al. 2009.

In order to generate a model of mitochondrial malfunction in this thesis, knock-downs of ubiquinol-cytochrome-c reductase complex core protein 1 (UQCRC1), which is the largest nuclear encoded subunit of the complex (Hoffman et al. 1993), were generated. UQCRC1 is a core subunit of the cytochrome-c reductase and is involved in the mitochondrial electrochemical gradient (Hoffman et al. 1993).

1.1.7 Cytochrome c oxidase

Cytochrome c oxidase or complex IV is a large transmembrane protein complex that is the last complex of the ETC. Its function is to accept electrons that cytochrome c carries from complex III and reduce O_2 into water while simultaneously pumping protons into the IMS to maintain the electrochemical gradient. In mammals, complex IV is formed by 13 different subunits and has a

molecular weight of 204 kDa. Ten of these subunits are nuclear encoded, but the three biggest (COX I, II and III) are encoded by mtDNA and are essential for the function of the complex. Cytochrome c oxidase is a metalloprotein containing two heme iron and two copper as well as zinc and magnesium (Tsukihara et al. 1996; Kadenbach et al. 2000; Li et al. 2006; Brunori et al. 1987). The transfer of electrons from cytochrome c to complex IV is mediated by four metal centers. The electrons are delivered to the CuA of COX II, then transferred to the heme center of COX I before reducing the oxygen that binds the heme a_3 -CuB. The electron transport through the metal centers is coupled with proton pumping to IMS (Vygodina et al. 2013; Shoubridge 2001; Scheffler 2008).

Patients with mutations in genes (nuclear or mitochondrial) related with the cytochrome c oxidase show a heterogeneous range of phenotypes. Cytochrome c oxidase deficiencies are mainly autosomal recessive disorders. Mutations in the mtDNA affecting this complex are rare (Shoubridge 2001). There are several phenotypes linked to cytochrome c oxidase deficiency including cardioencephalomyopathy, hepatic fail, stroke and Leigh syndrome (Fig. 6) (Shoubridge 2001; Barrientos et al. 2002)

Gene	Clinical features
Mitochondrial encoded COX subunits	
COXI	Sideroplastic anemia Motor neuro-like degeneration Multisystemic disorder Myoglobinuria
COXII	Encephalomyopathy Myopathy
COXIII	MELAS Myoglobinuria Encephalomyopathy Leigh-like syndrome
Heme A biosynthesis	
COX10	Ataxia, tubulopathy
Copper metabolism and insertion	
SCO1 SCO2	Hepatic failure, encephalopathy Cardioencephalomyopathy
COX assembly	
SURF1	Leigh's syndrome

Figure 6. Patients with mutations that affect cytochrome oxidase – Genetic and clinical heterogeneity of patients with COX deficiencies. Figure adapted from Barrientos et al. 2002.

In this thesis, sodium azide was used to inhibit cytochrome c oxidase (complex IV) by binding the oxygen reduction site in COX I (heme a_3 -CuB), without affecting the activities of complexes I and III in a significant way (Bennett et al. 2002; Ishii et al. 2014).

1.2 Lysosomes

Lysosomes were first described in 1955 when Christian de Duve identified a new organelle that formed a pool of soluble hydrolases capable of degrading proteins, carbohydrates, lipids or nuclear acids (de Duve 2005; Ballabio 2016; Lim & Zoncu 2016). For a long time, lysosomes were considered to be the “trash can” or “suicide bag” of the cells; the place where all materials that were not useful anymore were degraded. There are several routes to deliver materials to the lysosomes; the extracellular material is delivered through endocytosis or phagocytosis, while the intracellular material is delivered through autophagy (Lim & Zoncu 2016; Ballabio 2016). Lysosomes are no longer seen as just ‘trash cans’ of the cell. Currently it is known that the activity of lysosomes go beyond cellular clearance; lysosomes are involved in other processes like exocytosis, plasma membrane repair, transcriptional regulation and a reservoir of amino acids, metabolites and ions (Fig. 7) (Perera & Zoncu 2016; Lim & Zoncu 2016; Ballabio 2016).

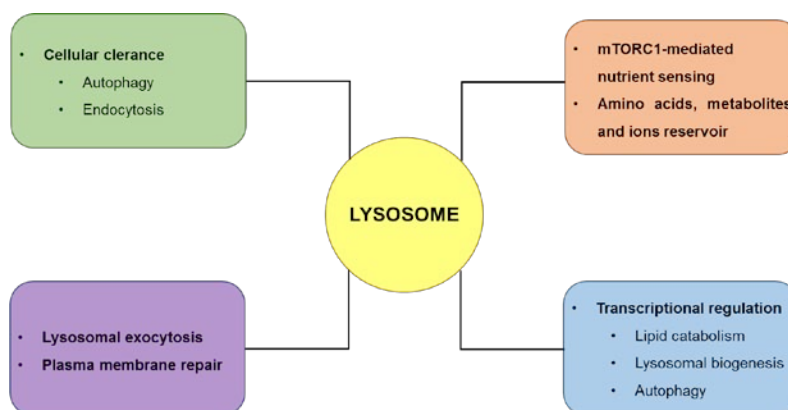


Figure 7. Roles of the lysosome in cellular processes. Figure adapted from Lim & Zoncu 2016.

Since lysosomes are involved in a broad range of processes, it is not surprising that lysosomal malfunction is implicated in several diseases like lysosomal storage disorders (LSDs), neurodegeneration, as well as pathophysiological process such as aging or cancer (Platt et al. 2012; Cuervo 2008; Perera & Zoncu 2016).

1.2.1 Endolysosomal pathway and lysosomal formation

The biogenesis of lysosomes requires a continuous replenishment of newly synthesized components. Both the soluble hydrolases and lysosomal membrane proteins have to be

transported along the biosynthetic pathway that comprises the endoplasmic reticulum (ER), the Golgi apparatus and the trans-Golgi network (TGN).

The lysosomes result from a combined pool of vesicles that are derived from TGN and early endosomes budding from the plasma membrane. Due to this complexity there are several theories to explain the endosome-lysosome relationship (Luzio et al. 2000; Perera & Zoncu 2016; Luzio et al. 2007). The most accepted theory explains that, in general, early endosomes are formed in the peripheral cytoplasm budding from the plasma membrane. These organelles have a slightly acidic intraluminal pH of approximately 6.0. The early endosomes can fuse again with the plasma membrane or go through a gradual maturation process (Perera & Zoncu 2016; Appelqvist et al. 2013; Hu et al. 2015; Luzio et al. 2003). The maturation is accompanied by intravacuolar acidification, and the reception of hydrolases and lysosomal membrane proteins from the TGN. The correct targeting of lysosomal proteins from the TGN to the endo-lysosomal system is an essential process in lysosomal biogenesis and maintenance. The process can be direct, from the TGN to the endosomal system, or indirect involving transport to the plasma membrane and endocytosis (Fig. 8) (Appelqvist et al. 2013; Braulke & Bonifacino 2009; Van Meel & Klumperman 2008).

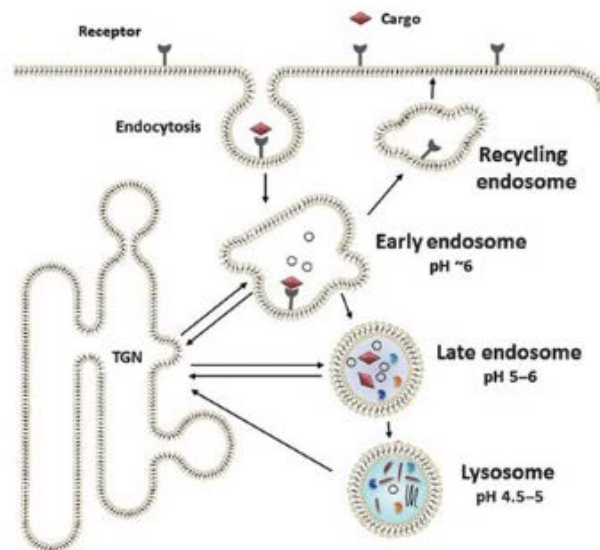


Figure 8. Endolysosomal pathway - The pathway starts with budding from the plasma membrane of the early endosomes that can mature gradually and become late endosomes or fuse back with the plasma membrane. From the trans-Golgi network (TGN) begins the budding of vesicles with lysosomal proteins cargo that fuse with endosomes and lysosomes. Figure adapted from Appelqvist et al. 2013

1.2.2 Lysosomal structure

Lysosomes are membrane bound organelles present in Eukaryotic cells and are found in different shapes, sizes and numbers varying among species. In high eukaryotes, lysosomes are spherical organelles, with a typical size between 0.5-1 μ m, that contain about 60 different acid hydrolases at an acidic pH of 4.5-5 (Mindell 2012; Zhou et al. 2013).

These organelles are limited by a phospholipid bilayer membrane of 7-10 nm. This membrane contains lysosomal membrane proteins like lysosomal integral membrane protein 2 (LIMP2) or the most abundant lysosomal transmembrane proteins like lysosomal associated membrane protein 1 or 2 (LAMP1 and LAMP2). These proteins are usually highly glycosylated, probably forming a continuous glycoprotein layer at the luminal side called glycocalix. This glycocalix acts as a barrier that protects the lysosomes against self-digestion (Perera & Zoncu 2016; Schwake et al. 2013; Settembre et al. 2013) (Fig. 9).

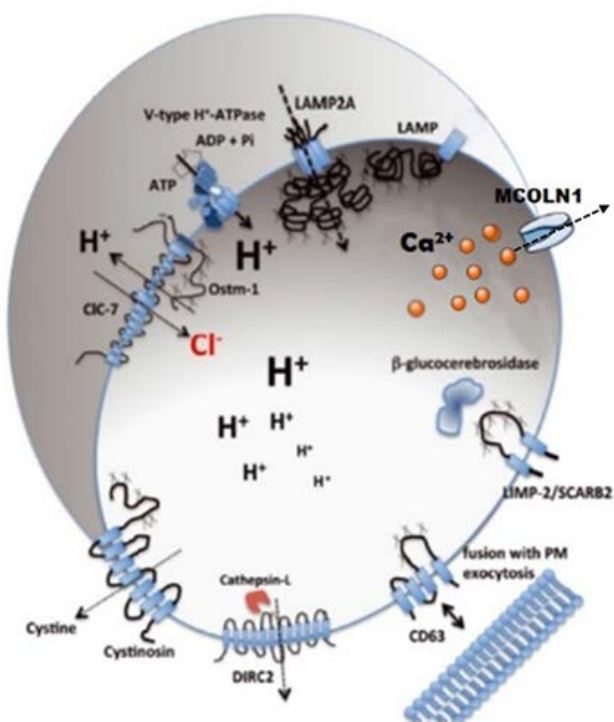


Figure 9. Schematic view of a lysosome - The schematic above illustrates the most relevant lysosomal proteins namely lysosomal associated membrane protein 1 or 2 (LAMP1 and LAMP2), lysosomal integral membrane protein 2 (LIMP2) and lysosomal associated membrane protein 3 (CD63), as well as the proton pump V-type-H⁺-ATPase (V-ATPase), the MCOLN1 channel and the BORC complex. Figure adapted from Schwake et al. 2013

Lysosomes contain approximately 60 different acid hydrolases which can digest a huge variety of molecules like proteins, lipids, carbohydrates and nucleic acids. These acid hydrolases are active at optimal pH of 4.5-5 (Ballabio 2016; Perera & Zoncu 2016). In order to get a lumen with the optimal acidic pH, the lysosomes have a proton pump, the V-type-H⁺-ATPase (V-ATPase), which is involved in acidification of endocytic vacuoles like lysosomes (Merkulova et al. 2015; Cotter et al. 2015).

Lysosomes are dynamic organelles that move in the cytoplasm influenced by the processes they are involved in, for example, it has been shown that lysosomal position regulates mammalian target of rapamycin complex 1 (mTORC1) signaling. When lysosomes are peripheral, mTORC1 is activated by nutrients (Korolchuk et al. 2011). The lysosomal positioning is regulated by the BLOC-one-related complex (BORC) which is a multi-subunit complex formed by eight subunits (Pu et al. 2015). This complex associates to the lysosome, recruiting the Arf-like GTPase (Arl8) and starting a chain of reactions that ends with the translocation of the lysosomes to the peripheral cytoplasm (Pu et al. 2015). However BORC is not the only entity involved in lysosomal positioning. The small GTPase Rab7, which recruits Rab-interacting lysosomal protein (RILP), has also been shown to be involved in lysosomal centripetal movement (Pu et al. 2015; Cantalupo et al. 2001). In addition, recently the mucolipin 1 (MCOLN1 or TRPML1), most relevant for its role as the principal Ca²⁺ channel in the lysosomes, has been reported as a mediator of lysosomal movement (Li et al. 2016). It is thus evident that motility of lysosomes is a complex process with several regulators.

1.2.3 Lysosomal pH

As previously stated, it is fundamental for the optimal functioning of the lysosomal acid hydrolases, that the lysosomal pH is maintained at 4.5-5. In order to acidify the lysosomal lumen, there is a proton gradient from the cytoplasm to the lumen of the lysosomes which is due to the activity of the V-ATPase, a transmembrane protein that uses ATP energy to pump the protons into the lysosome. The V-ATPases are formed by 14 subunits divided into cytosolic V₁ domains and integral V₀ domains. These domains can dissociate in a reversible manner, in order to regulate the activity of the pump (Fig. 10) (Merkulova et al. 2015; de Duve 2005; Cotter et al. 2015).

The proton gradient generated by the ATPase also generates a difference in the voltage in the lysosomal membrane. To dissipate the transmembrane voltage generated by the ATPase, which can inhibit the proton pumping, proton movement is accompanied by the movement of a

counterion. This counterion could be a cation release to the cytoplasm or an anion transport into the lysosomal lumen (Mindell 2012; DiCiccio & Steinberg 2011).

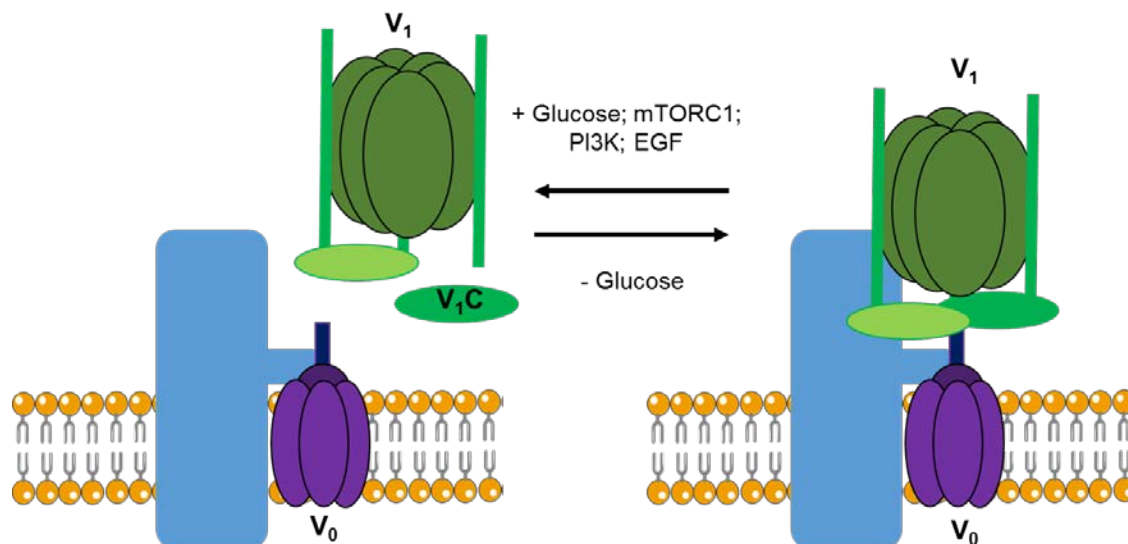


Figure 10. Assembly of V-ATPase in mammalian cells – The assembly of the V-ATPase is related to its activity. The assembly of the V_1 and V_0 domains occurs in response to increase of glucose and in response to epidermal growth factor (EGF), phosphoinositide 3 kinase (PI3K) and mechanistic target of rapamycin complex 1 (mTORC1). Figure adapted from Cotter et al. 2015.

1.2.4 Lysosomal Ca^{2+}

Lysosomes have been reported as organelles that store calcium. The concentration of Ca^{2+} in lysosomes is 400 to 600 μM while in the cytosol it is about 100nM (Christensen et al. 2002). However, while the hydrolytic function of the lysosomes is well known, the Ca^{2+} related functions are not completely elucidated. With its elevated lysosomal concentration, it is reasonable to assume that the calcium levels are tightly regulated by channels (Raffaello et al. 2016). There are several channels involved in Ca^{2+} homeostasis in lysosomes like MCOLN1, H^+/Ca^{2+} exchanger or the two-pore channel 2 (TPC2) (Raffaello et al. 2016; Galione 2011). However, the MCOLN1 cation-permeable channel, also called TRPML1, has been reported as the principal Ca^{2+} channel in the lysosomes. Human mutations in MCOLN1 result in mucopolipidosis type IV (ML-IV), a neurodegenerative LSD that exhibits membrane trafficking defects. It has been reported that reactivation of MCOLN1 channel in FIG4 cells, a mutation that leads to LSD with accumulation of

Ca^{2+} in the lysosomes, induces a release of lysosomal Ca^{2+} and an improvement in the phenotype of the disease, showing the relevance of Ca^{2+} homeostasis in lysosomes (Li et al. 2016).

1.2.5 Lysosomal amino acid sensing

Lysosomes are the center of nutrient sensing and metabolic regulation thanks to the physical and functional relation existing between lysosomes and mammalian target of rapamycin complex 1 (mTORC1), which is a highly conserved regulator of cell growth (Laplante & Sabatini 2009; Bar-Peled & Sabatini 2014). V-ATPases, placed in the lysosomal membrane, are essential for the amino acid activation of mTORC1 that control cell proliferation and growth according to nutrient availability.

The V-ATPase responds with conformational changes to the amino acid concentration in the lysosomes. Besides, V-ATPase interacts directly with the Ragulator complex on the lysosomal surface, and Ragulator, a trimeric complex that interacts with Rag GTPases when the concentration of amino acids in the lysosomes is high, recruits mTORC1 to the lysosomal surface where it is activated by Ras homolog enriched in brain (RHEB) (Fig. 11). The response of mTORC1 to amino acids depends on the interaction of Ragulator with the V-ATPase domains.

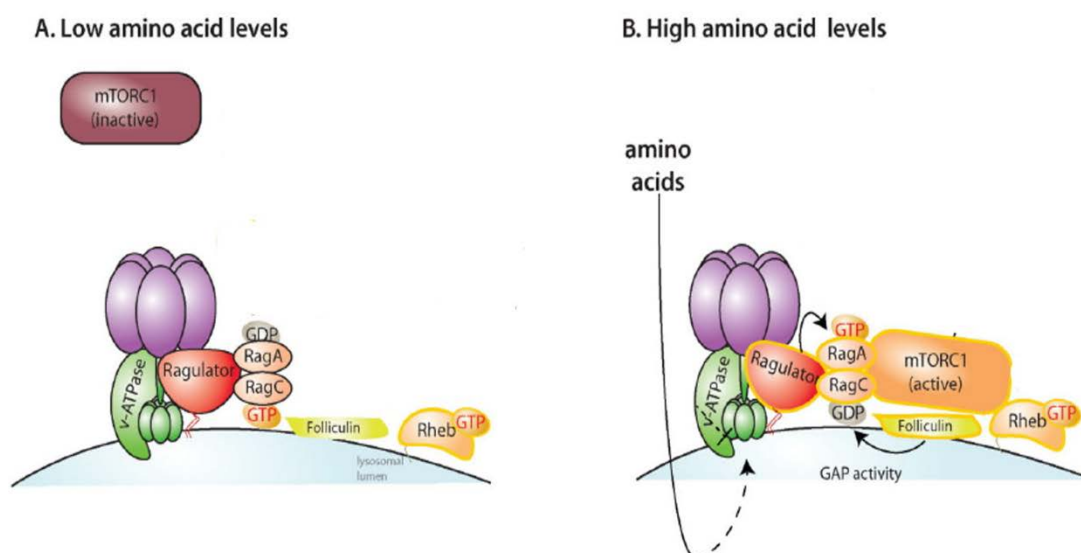


Figure 11. mTORC1-lysosome amino acid sensing pathway – A) Under low amino acid levels Ragulator binds to V-ATPase in the inactive conformation. B) Under high amino acid levels Ragulator and V-ATPase change their conformations to an active state thereby changing the conformation of Rags that recruit mTORC1 to the lysosomal surface where it is activated by Rheb. Figure adapted from Bar-Peled & Sabatini 2012.

The interaction between the membrane domain V_0 and Ragulator is independent of amino acid levels but the interaction of Ragulator with the cytosolic domain V_1 becomes weak with increasing amino acid levels (Peña-Llopis et al. 2011; Stransky & Forgac 2015; Bar-Peled, Schweitzer & Zoncu 2013; Bar-Peled & Sabatini 2012).

It is necessary to mention that mTORC1 also regulates the transcription factor EB (TFEB), reported as the master regulator of lysosomal biogenesis, which will be discussed in the following chapter (Settembre et al. 2012).

In conclusion, the relation between V-ATPase assembly and mTORC1 activation is a method to control cell growth that would take place in presence of enough nutrients to sustain it.

1.3 Autophagy

The concept of autophagy emerged during the 1960s, from Christian de Duve, a term that denotes “self-eating”. A few years after de Duve discovered the lysosomes, he observed that the cell was able to degrade intracellular components by enclosing them into membranes and delivering them to the lysosomes. Unfortunately, the advances in this field were limited. Only in the early 1990s, Yoshinori Ohsumi was able to identify essential genes for autophagy called autophagy related genes (Atg) in the yeast *Saccharomyces cerevisiae* through the use of a genetic approach (Shen & Mizushima 2014; Ohsumi 2014; Tsuboi & Ohsumi 1992; Tsukada 1993). These genes were used to elucidate the mechanisms involved in autophagy and to demonstrate that it is a highly conserved process among eukaryotes (Fig. 12).

Yeast	Mammals	Function
Atg1	ULK1, 2	Kinase
Atg2	Atg2A, B	Atg9/Atg2-Atg18 complex
Atg3	Atg3	E2-like enzyme
Atg4	Atg4A, B, C, D	Hydrolases
Atg5	Atg5	E3-like enzyme
Atg6	Beclin-1	Regulator
Atg7	Atg7	E1-like enzyme
Atg8	LC3A, B, C GABARAP, L1, L2	Ubiquitin-like modifiers and regulators
Atg9	Atg9A, B	Atg9/Atg2-Atg18 complex
Atg10	Atg10	E2-like enzyme
Atg12	Atg12	Modifier
Atg13	Atg13	Regulator
Atg14	Atg14	Regulator
Atg16	Atg16L1, 2	Regulator
Atg17	RB1CC1	E3-like enzyme
Atg18	WIPI-1	Atg9/Atg2-Atg18 complex

Figure 12. List of some autophagy related genes in yeast and their mammalian homologs - Adapted from Kesidou et al. 2013.

1.3.1 Types of autophagy

Autophagy is a highly conserved pathway that recycles cellular components in order to keep cellular homeostasis, becoming an essential quality control mechanism in cells. Autophagy is divided in three different principal types: macroautophagy, chaperone-mediated autophagy (CMA) and microautophagy (Fig. 13) (Cuervo 2008; Zaffagnini & Martens 2016).

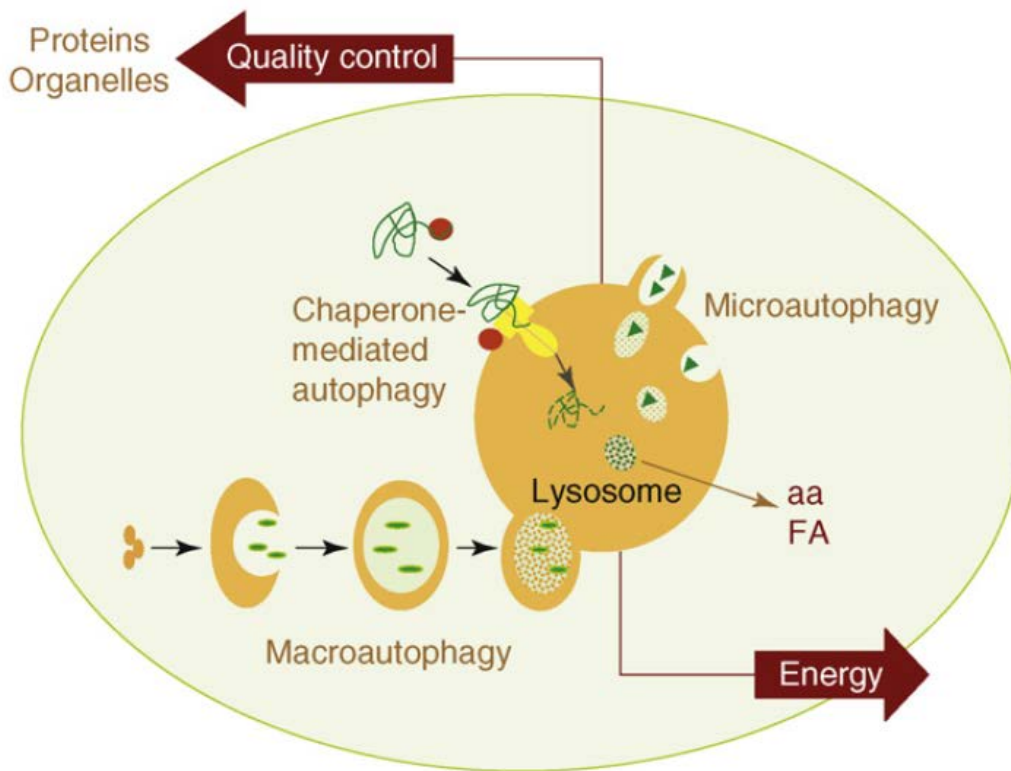


Figure 13. Scheme of types of autophagy in mammalian cells – In microautophagy, complete regions of cytosol are sequestered by lysosomal projections or invaginations. In chaperone-mediated autophagy, cytosolic proteins are targeted with chaperones recognized by the lysosomal protein LAMP2. In macroautophagy, regions of the cytosol are sequestered by newly formed double membrane organelles and delivered to the lysosomes. Figure from Cuervo 2008.

Microautophagy: This type of autophagy is not well characterized in mammalian cells. It is a process in which the lysosomal membrane is invaginated or projected in order to sequester cytosolic components into intralysosomal vesicles. Microautophagy is mainly characterized like a non-selective type of autophagy even though there are pieces of evidence that show that

peroxisomes can be selectively degraded through this way in yeast (Sakai et al. 1998). The main roles of microautophagy are membrane homeostasis, cell survival under nitrogen restriction and maintenance of size of organelles (Cuervo 2008; Li et al. 2012).

Chaperone-mediated autophagy: CMA is a type of selective autophagy for soluble cytosolic proteins that require unfolding of the protein before being delivered to the lysosomes. The selectivity comes through the recognition of the KFERQ motif, by a cytosolic chaperone, in the protein that is targeted for degradation and it is then delivered to the surface of the lysosome. In order to arrive to the lysosomal lumen, the protein interacts with the lysosome-associated protein type 2A (LAMP-2A) and a complex of lysosomal chaperones. Chaperone-mediated autophagy reaches its maximum activity under oxidative stress (Kaushik et al. 2006; Cuervo 2008; Kiffin et al. 2005).

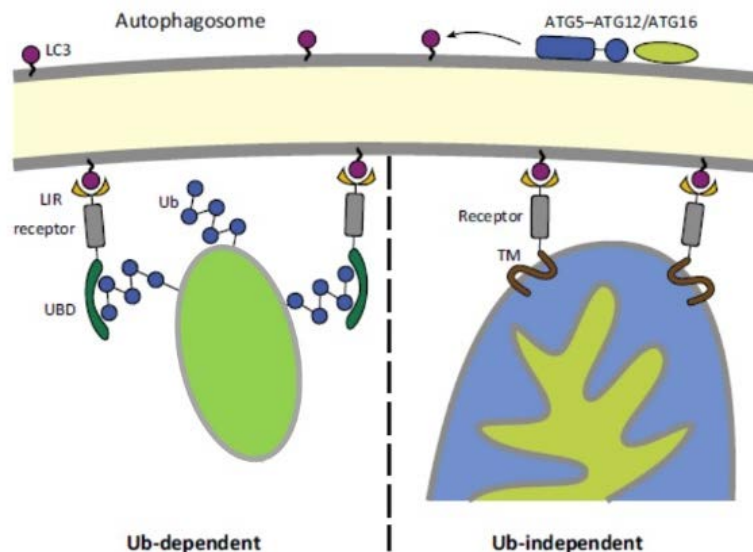


Figure 14. Scheme of ubiquitin-dependent and ubiquitin-independent autophagy in selective macroautophagy - LC3 proteins can recognize LIR motif (yellow) of organelles marked for selective autophagy. The left side represents the ubiquitin-dependent autophagy where the organelle was marked with ubiquitin chains that recruit autophagy receptor, which have LIR motif, that are recognized by LC3. On the right is the ubiquitin-independent autophagy in which LC3 interacts with the LIR motif present in the autophagy receptors that are in the organelle membrane. Figure adapted from Khaminets 2016.

Macroautophagy: Macroautophagy (hereafter autophagy) is the most extensively studied and quantitatively more important type of autophagy. This type of autophagy is a highly dynamic process in which complete regions of the cytosol, with all their contents, are sequestered by an

autophagosome. This type of non-selective autophagy is fundamental in the cell maintenance. However this process can also be highly selective, targeting specific protein aggregates or organelles, like mitochondria, ribosomes or endoplasmic reticulum, acting like an internal cell quality control mechanism. Selective autophagy is controlled by autophagy receptors that link organelles or protein aggregates with the autophagosome through their interaction with LC3II. Those autophagy receptors can be ubiquitin (Ub) chains or other autophagy receptors like sequestosome-1 (p62/ SQSTM1), which bind LC3II through a short LC3-interacting region (LIR) motif (Fig. 14) (Cuervo 2008; Khaminets 2016).

1.3.2 Mitophagy

For a long time autophagy was thought to be only a non-selective process fundamental for the maintenance of the cell. However, this simplistic view of autophagy has evolved and currently it is known that autophagy can be a highly selective process, essential for cell quality control, in which specific organelles or protein aggregates are targets. For the purpose of this study, we focus on mitophagy, the specific autophagic degradation of mitochondria. Mitophagy was observed by Christian de Duve in 1966, in mammalian cells, using electron microscopy (De Duve, Christian and Wattiaux 1966). However, the way in which the mitochondria were sequestered by the autophagosomes was unclear for a long time. Currently, there are two different main models that attempt to describe the mechanism of mitophagy.

Parkin-dependent mitophagy: This is the most studied mechanism of autophagy in mammals by which damaged mitochondria are degraded by mitophagy after the activation of PTEN induced putative kinase 1 (PINK1) and Parkin RBR E3 ubiquitin protein ligase (Parkin). When mitochondria are damaged, showing a decrease of mitochondrial potential or an increased amount of misfolded proteins, PINK1 is stabilized on the OMM and recruits Parkin which in turn ubiquitinates several proteins localized in the OMM like mitochondrial fusion proteins 1 and 2 (Mfn1 and Mfn2), translocase of outer mitochondrial membrane 20 (TOMM20), and voltage dependent anion channel (VDAC), in order to initiate mitophagy (Jin & Youle 2012; Lazarou et al. 2015; Ni et al. 2015; Ding & Yin 2012). On the other hand, PINK1/Parkin activation recruits other autophagy receptors like sequestosome-1 (p62/ SQSTM1) and optineurin to the mitochondria. These receptors interact with LC3II in order make selective autophagy possible (Fig. 15) (Geisler et al. 2010; Ni et al. 2015; Lazarou et al. 2015).

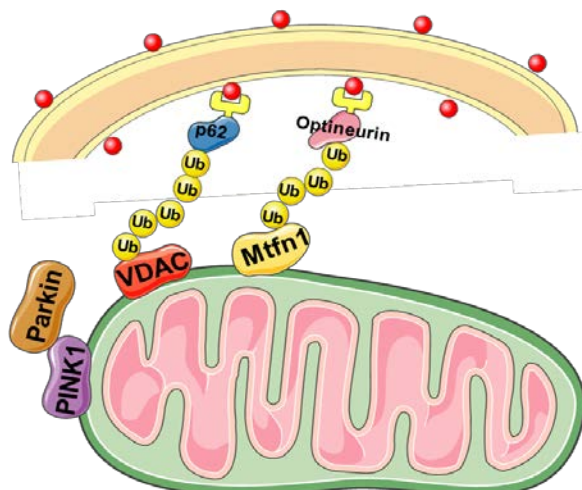


Figure 16. Scheme of Parkin-dependent mitophagy - Depolarized mitochondria stabilize PINK1 which recruits Parkin. Parkin ubiquitinates proteins of OMM and recruits autophagy receptors like p62/ SQSTM1 and optineurin that have a LIR motif that interacts with LC3II starting mitophagy.

Parkin-independent mitophagy: Even though the most accepted mitophagy mechanisms are mediated by PINK1/Parkin mediation, there are increasing studies that support the existence of mitophagy induced in a Parkin independent way. Autophagy receptors have been found in OMM and under mitochondrial damage, these receptors target mitochondria for selective autophagy.

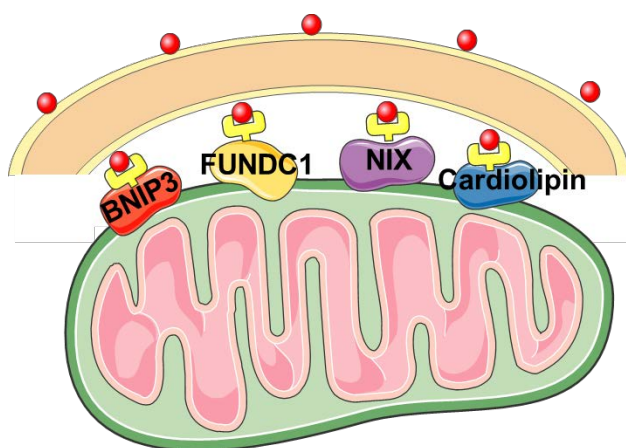


Figure 16. Scheme of Parkin-independent mitophagy - In the absence of Parkin autophagy receptors like NIX, BNIP3, FUNDC1 or cardiolipin, the cell can mediate mitophagy through the interaction of their LIR motif with LC3.

For example, Fun14 Domain containing 1 (FUNDC1), BCL2-interacting protein 3 (BNIP3) and NIX or cardiolipin under mitochondrial stress conditions presents their LIR motif targeting the damaged mitochondria for degradation (Fig. 16) (Liu et al. 2012; Novak et al. 2010; Chu et al. 2014; Ding1 & Yin 2012; Ni et al. 2015).

1.3.3 Autophagosome

Autophagosomes are double-membrane-bound organelles, unlike vesicles, involved in other pathways like microautophagy (Cuervo 2008). In mammals, these organelles have a diameter 0.5-1.5 μM and their formation occurs between 5 and 10 minutes after autophagy induction (Mizushima et al. 2002; Shibutani & Yoshimori 2014).

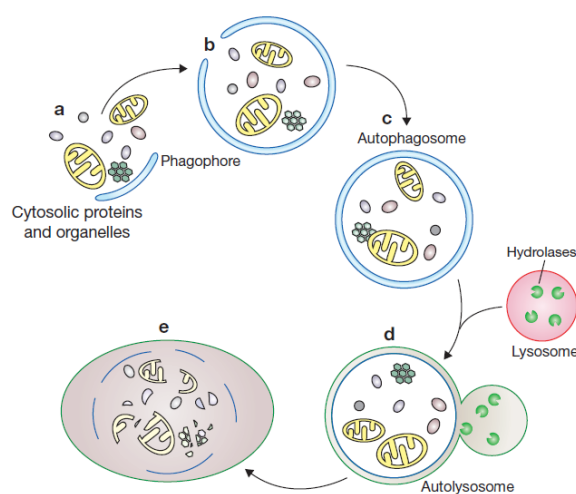


Figure 17. Scheme of autophagy - A) Formation of the phagophore. B) Cytosolic material is sequestered by an expanding membrane sac. C) The double-membrane is completely closed forming an autophagosome. D) The outer membrane of the autophagosome fuses with a lysosome to form an autophagolysosome. E) The inner membrane and the cargo is degraded in the autophagolysosomes. Figure from Zhiping Xie and Daniel J. Klionsky

Autophagosomes are formed from an expanding membrane sac or phagophore, which is a flat membrane, in the cytoplasm. This initial phagophore is an isolated membrane that expands its size engulfing portions of the cytoplasm, proteins and organelles. The phagophore formation starts in the phagophore assemble site (PAS), one in yeast and multiple in mammals. The formation process needs phosphoinositide 3-kinase (PI3K), which is largely formed by different Atg proteins (Fig. 17) (Shibutani & Yoshimori 2014; Mizushima et al. 2002).

However, this is only the classical view of the autophagosomal membrane origin. Currently new hypotheses are appearing in the field.

The relation between phagophore formation and other membranes like the plasma membrane (Ravikumar et al. 2011), the membrane of endoplasmic reticulum (Axe et al. 2008), mitochondrial membrane or even the contact sites between mitochondria and ER (Hailey et al. 2011; Hamasaki et al. 2013), open new insights into ways in which autophagosomes can be generated (Fig. 18) (Rubinsztein et al. 2012) .

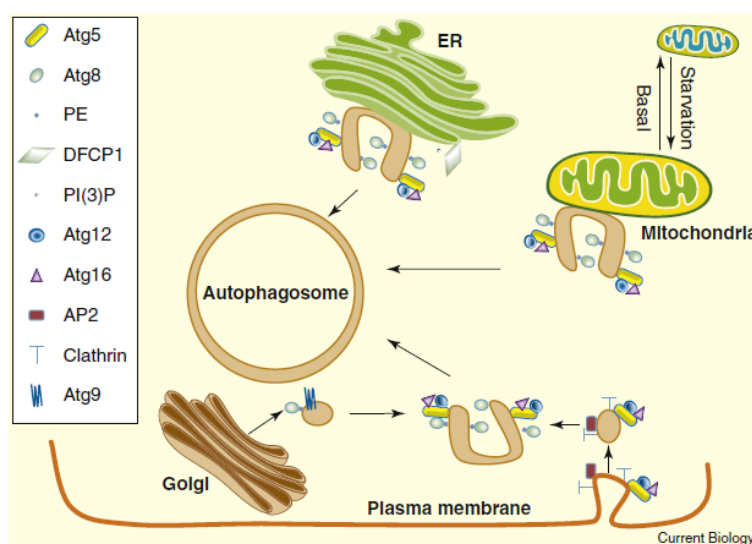


Figure 18. Membrane sources for phagophores – The proposed source of lipids and proteins for the phagophore formation are the endoplasmic reticulum, mitochondria and plasma membrane. Figure from Rubinsztein et al. 2012.

When the initial formation of the phagophore is done, the membrane continues to elongate through a complex sequence of processes in which several Atg proteins are involved. The membrane elongation starts with the recruitment of Atg12–Atg5–Atg16 complex to the membrane which in turn promotes the lipidation of microtubule-associated protein 1A/1B-light chain 3 (LC3) and its insertion into the phagophore membrane as LC3-II. The Atg12–Atg5–Atg16 complex is then detached from the membrane, to be recycled before it fuses to become an autophagosome. LC3II present in the outer membrane is delipidated, removed and recycled, but the inner membrane conserves the attached LC3II (Fig. 19) (Abada & Elazar 2014; Mizushima et al. 2002; Shibutani & Yoshimori 2014). This conversion makes LC3II a good marker for autophagosomes.

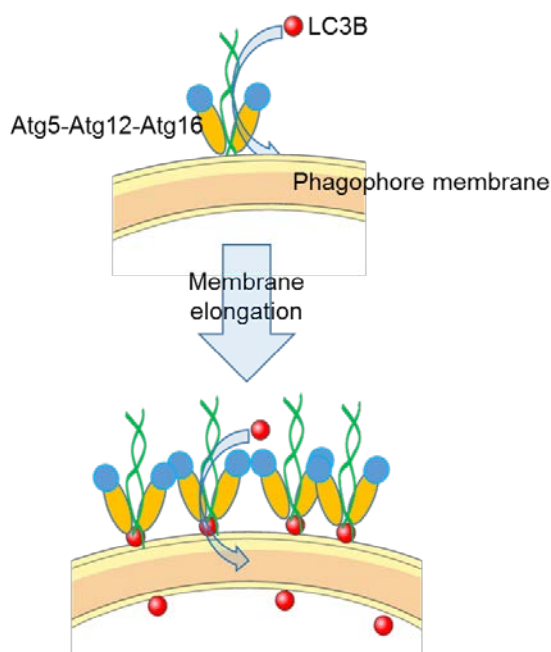


Figure 19. Model of the Atg12-Atg5-Atg16 complex autophagosome formation - The Atg12-Atg5-Atg16 complex is recruited to the initial phagophore and mediates LC3 lipidation. After the membrane starts elongating, the complex remains associated with the membrane through LC3. Atg12-Atg5-Atg16 complex with the lipidated LC3 forms a coat-like structure that stabilizes the structure of the phagophore during the elongation. Figure adapted from Abada & Elazar 2014.

Finally, the mature autophagosomes fuse with the lysosomes to become autolysosomes or autophagolysosomes. It must be stated, however, that the autophagosomes, as dynamic structures, can fuse with early and late endosomes (Mizushima et al. 2002), showing that endosomes, lysosomes and autophagosomes form a very dynamic pathway with different branches. Different groups of proteins are involved in the complicated fusion process. In higher Eukaryotes, lysosomal membrane proteins (LAMP1, V-ATPase), cytoskeleton proteins or Soluble N-ethylmaleimide sensitive fusion Attachment Protein REceptor (SNARE), like syntaxin 17 (Stx 17) or vesicle-associated membrane protein 8 (VAMP8) among others are required (Shen & Mizushima 2014). Under autophagy induction, Stx17 is recruited to the autophagosomal membrane. In the mature autophagosome, Stx17 recruits synaptosomal-associated protein 29 (SNAP-29) which interacts with VAMP8, located in the lysosomal membrane, forming a SNARE complex. The formation of this complex drives the fusion of autophagosomal and lysosomal membranes (Itakura et al. 2012). When fusion takes place, the inner membrane of the autophagosome and its cargo are quickly degraded by lysosomal enzymes thereby finishing the recycling process.

1.4 Signaling pathways

Since this thesis is focused on the pathways that mediate communication between mitochondria and lysosomes, it is important to dedicate a part of this introduction to these organelles and the signals related to them.

1.4.1 Stress signaling and mitochondria

Defects of mitochondrial metabolism are the cause for a wide range of diseases. For a long time, the general understanding was that the cause of mitochondrial diseases was the impaired capacity of the damaged mitochondria to generate energy, i.e. to synthesize ATP. This decrease in ATP synthesis implies that the cells with higher energetic needs, like neurons or cardiomyocytes, would be affected in mitochondrial disorders. However, it is currently accepted that mitochondrial signaling and mitochondria-related pathologies are connected. Numerous studies support such views, some of them for example showing that mitochondria can release cytochrome c (cyt c) to initiate apoptosis or reactive oxygen species (ROS) to activate hypoxic gene expression (HIF) (Liu et al. 1996; Chandel et al. 2000; Raimundo 2014). Moreover, it is known that there are signaling pathways connecting mitochondria, nucleus and cytoplasm like AMPK signaling, mitochondrial unfolded protein response (mito^{UPR}) or Ca²⁺ release (Rizzuto et al. 2012; Cereghetti et al. 2008; Raimundo 2014; Pellegrino et al. 2012). There are several mitochondrial signals, like citrate, which through regulation of acetyl-coenzyme A (acetyl-CoA) levels affect the acetylation of numerous proteins which in turn affect the activity of several signaling pathways (Kaelin Jr. W.G. & McKnight 2013). Also, nitric oxide (NO) which is a reactive nitrogen species (RNS) that regulates mitochondrial structure, biogenesis and the activity of proteins involved in signaling pathways like c-Jun N-terminal kinase (JNK), which is involved in autophagy, or S-Nitrosylation peptides that can trigger mito^{UPR} (Nisoli 2003; Nakamura et al. 2013). Other mitochondrial signaling pathways are regulated by metabolites like succinate and fumarate which can easily cross the OMM due to their small size and can cross IMM using carriers or transporters. Fumarate and succinate can regulate HIF pathway, while fumarate accumulation upregulates heme pathway (Fig 20) (Kaelin Jr. W.G. & McKnight 2013; Raimundo 2014; Laukka et al. 2016; Isaacs et al. 2005). There are several more mitochondria-related pathways; however, due to its relevance to this project, we will focus more on the reactive oxygen species (ROS) signaling (Fig. 20).

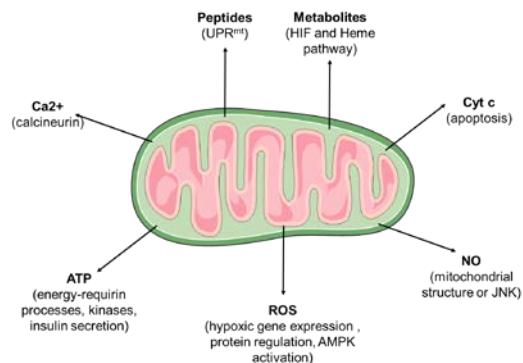


Figure 20. Scheme of mitochondrial signals – The scheme shows some of the signals that are released from the mitochondrion and their functions.

1.4.2 Mitochondria and ROS

The reactive oxygen species or ROS include all chemical species with an unpaired electron in an oxygen atom such as superoxide anion radical $O_2^{\cdot-}$, hydroxyl ($\cdot OH$) and singlet oxygen. The half-life of $O_2^{\cdot-}$ is very short and it is rapidly converted in hydrogen hydroperoxide (H_2O_2) by the superoxide dismutases (SOD) (Zorov et al. 2014; Murphy 2009). There are several sources of ROS in the cells like peroxisomes (Sandalió et al. 2013), endoplasmic reticulum (Cao & Kaufman 2014) and mitochondria (Murphy 2009). In mitochondria ROS is generated by the respiratory chain, where $O_2^{\cdot-}$ is produced in the complexes I and III (Fig. 21). Most of the $O_2^{\cdot-}$ is released to the mitochondrial matrix and converted into H_2O_2 by SOD2, while the $O_2^{\cdot-}$ released to the IMS is converted into H_2O_2 by SOD1 (Murphy 2009; Reczek & Chandel 2015).

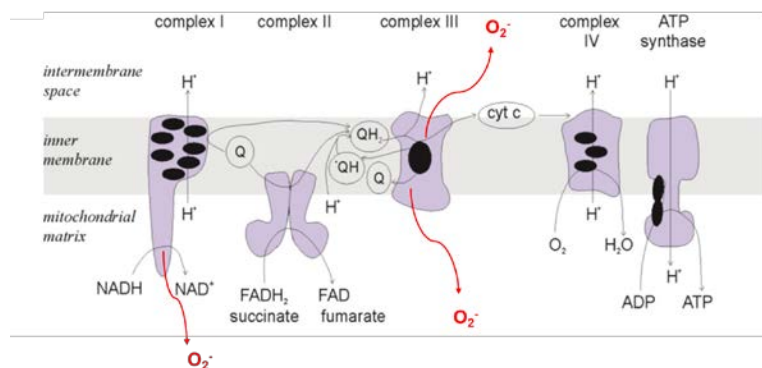


Figure 21. Mitochondrial respiratory chain and ROS – The majority of mitochondrial ROS is produced in complex I and III of the respiratory chain. While complex I releases ROS into the mitochondrial matrix, complex III releases ROS to both the matrix and the IMS.

For a long time, ROS were considered only as toxic products that caused oxidative damage in the cell, but currently it is known that ROS are also involved in signaling from mitochondria to nucleus and cytosol (Murphy 2009). The signaling activity of ROS raises the question of how ROS cross the mitochondrial membrane. There are several hypotheses, albeit controversial, which try to clarify that question. In isolated mitochondria of rat heart, it has been shown that superoxide can cross through voltage dependent anion channel (VDAC) (Han et al. 2003). Furthermore, superoxide can be transformed into H_2O_2 that can then cross membranes, supporting H_2O_2 as a good mitochondrial signal (Han et al. 2003). Another way in which ROS trigger signaling is through the citrate release, since superoxide can damage the enzyme citrate aconitase (Kaelin Jr. W.G. & McKnight 2013). Currently, it is also known that ROS are involved in cellular response to hypoxia (Chandel et al. 1998), trigger AMPK activation and E2F1-dependent apoptosis (Raimundo et al. 2012).

1.4.3 Lysosomes and signaling

Given that lysosomes are the end point of multiple processes, they have emerged as a key factor in the maintenance of the metabolic homeostasis. As it was mentioned before in this thesis, lysosomes are involved in crucial cellular processes like cell and tissue remodeling, elimination of damaged cellular components or nutrient regulation during starvation (Lim & Zoncu 2016). One of the principal functions of the lysosome is related to its close physical and regulatory connection with mTORC1, as mentioned earlier. The connection between lysosomes and mTORC1 is based on the sensing of nutrients by mTORC1 and its response triggering pathways that lead to cell growth and proliferation as well as to the repression of lysosomal biogenesis (Bar-Peled & Sabatini 2014; Martina & Puertollano 2013b). Since we already described how lysosomes recruit and activate mTORC1 and the recruitment of mTORC1 to the lysosomal surface is only possible in presence of amino acids (Sancak et al. 2010), we are going to focus on the response of mTORC1 to amino acid starvation.

During amino acid starvation, mTORC1 is cytoplasmic and inactive but in the presence of amino acids the Rag GTPases, which are tethered to the lysosomal surface by the Ragulator, recruit mTORC1 to the lysosomal membrane allowing its activation by Rheb (Fig. 22) (Lim & Zoncu 2016). When mTORC1 is active, it can regulate several biological processes like, for example, protein synthesis, through allowing the eukaryotic translation initiation factor 4E (EIF4E) to promote cap-

dependent translation and the stimulation of ribosomal protein S6 kinase beta-1 (S6K1) activity. It also promotes synthesis of lipids through the positive regulation of sterol regulatory element-binding transcription factor 1 (SREBF1) and of peroxisome proliferator-activated receptor-gamma (PPAR γ) (Porstmann et al. 2008; Laplante & Sabatini 2009). Other metabolic processes that are

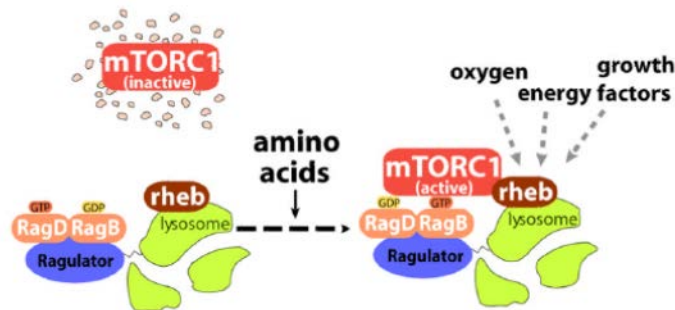


Figure 22. mTORC1 amino acid regulation – The scheme shows in the left side how under amino acid starvation mTORC1 is inactive but when there is amino acid availability, shown on the right, Rag GTPases recruit mTORC1 to the lysosomal surface where it is activated by Rheb. Figure from Sancak et al. 2010.

regulated by mTORC1 are the mitochondrial metabolism, regulating oxygen consumption, ATP and mitochondrial membrane potential (Schieke et al. 2006; Laplante & Sabatini 2009). The most relevant regulatory pathway for us is the involvement of mTORC1 in the regulation of lysosomal biogenesis by transcription factor EB (TFEB).

1.4.4 TFEB

The transcription factor EB is a basic helix–loop–helix (bHLH) leucine zipper transcription factor that belongs to a family of transcription factors called microphthalmia family. This family has four members which are microphthalmia-associated transcription factor (MITF), transcription factor EB (TFEB), transcription factor E3 (TFE3) and transcription factor EC (TFEC). The importance of this transcription factor family for this project originates from the fact that in 2009 it was shown that genes encoding for lysosomal proteins have a palindromic motif of 10 base pairs (bp), GTCACGTGAC, called Coordinated Lysosomal Expression and Regulation (CLEAR) element. The CLEAR element is located within 200 bp from the transcription start site and that mediates the start of the transcription of these lysosomal genes. In addition, overlaps were found between the CLEAR element and the E-box that is a known target site for MITF family members. With these

data the four members of the family were tested and it was reported that TFEB is the master regulator of lysosomal biogenesis and its overexpression increases the expression of lysosome-related genes like LAMP1, hexosaminidase subunit alpha (HEXA) or Cathepsin D (Fig. 23) (Sardiello & Ballabio 2009; Settembre et al. 2011).

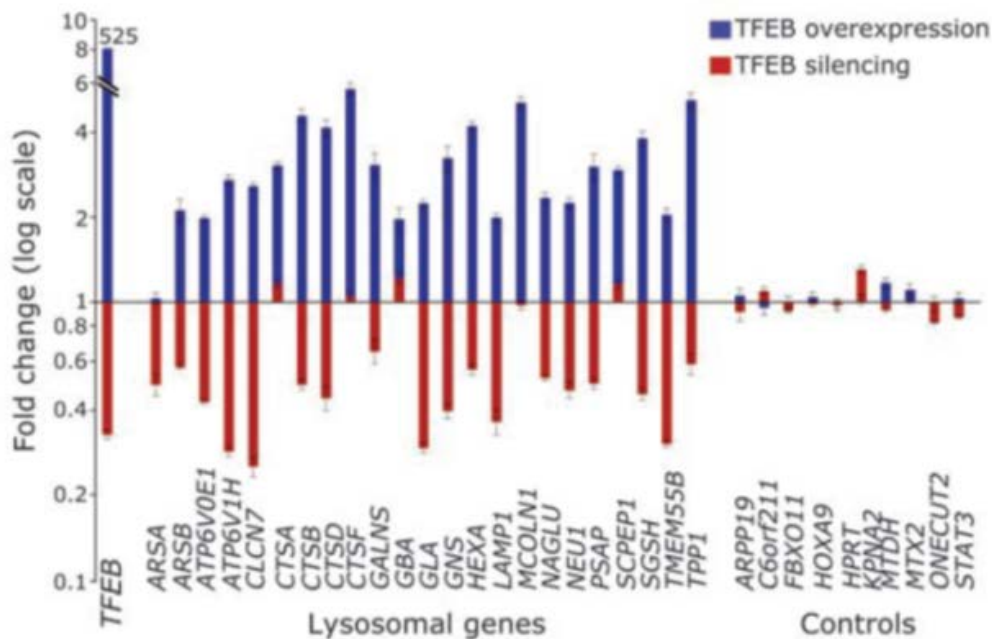


Figure 23. Response of lysosomal genes to TFEB – Fold changes of lysosomal related genes under TFEB overexpression (blue) or TFEB silencing (red). Figure from Sardiello & Ballabio 2009

In addition to TFEB regulation being connected to the lysosomes through mTORC1 (Settembre et al. 2012; Martina et al. 2012), it has been shown that under amino acid starvation TFEB is translocated to the nucleus where it is active and this translocation is regulated by mTORC1 (Sardiello & Ballabio 2009; Settembre et al. 2011). Under conditions of amino acid abundance, mTORC1 is at the lysosomal surface where it can be activated by Rheb, as described above. The activation of mTORC1 allows the phosphorylation of TFEB at S142 and S211, which keep TFEB in the cytoplasm. However, under amino acid deprivation, the conformation of Rag GTPases changes thus abolishing the presence of mTORC1 at the lysosomal surface. mTORC1 becomes cytoplasmic and inactive and also prevents phosphorylation of TFEB, enabling its translocation to the nucleus, where it can bind the CLEAR region and initiate the transcription of lysosome related-genes (Fig. 24) (Settembre et al. 2012; Martina et al. 2012; Roczniak-Ferguson et al. 2012).

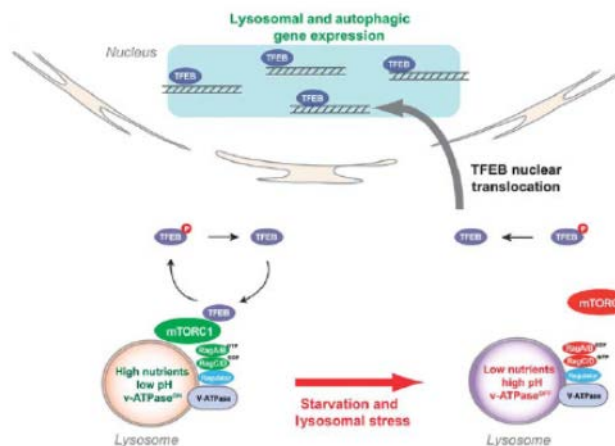


Figure 24. TFEB regulation by mTORC – Active mTORC1 phosphorylates TFEB keeping TFEB in the cytoplasm (left). Under amino acid starvation mTORC1 is cytoplasmic and inactive, TFEB is not phosphorylated and is translocated into the nucleus where it binds the CLEAR region thus regulating transcription of lysosome related-genes (right). Figure from Settembre et al. 2012

However, it has recently been shown that mTORC1-dependent activation was not the only interaction between mTORC1 and one MITF family member. Currently, it is known that mTORC1 phosphorylates TFEB and MITF allowing its binding to 14-3-3 proteins, keeping them in the cytoplasm. Also, under amino acid starvation, mTORC1 cannot phosphorylate TFEB and MITF and they are translocated into the nucleus where both can bind to the CLEAR element (Fig. 25) (Martina & Puertollano 2013). In addition, TFE3 has been reported to be retained in the cytoplasm

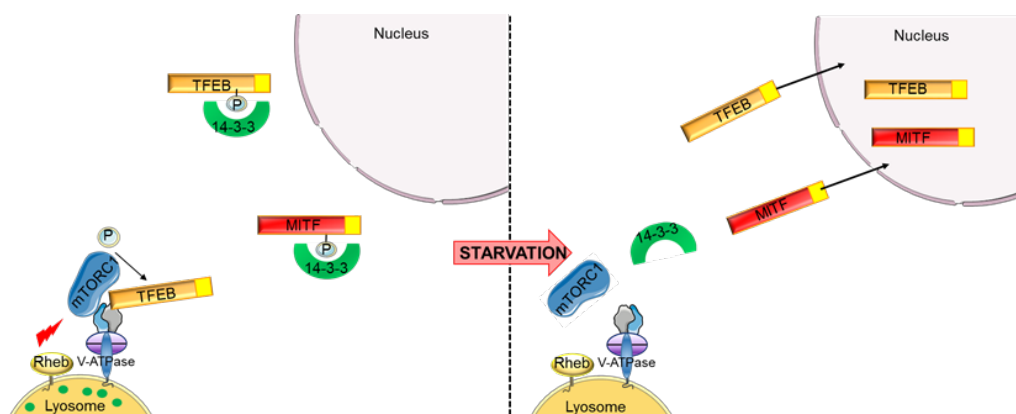


Figure 25. TFEB and MITF regulation by mTORC1 – The left side shows how active mTORC1 phosphorylates TFEB and MITF allowing that it's binding to 14-3-3 proteins keeping them in the cytoplasm. In the right, inactive mTORC1 does not phosphorylate TFEB and MITF, thus they cannot bind 14-3-3 proteins and are translocated to the nucleus. Figure adapted from Martina & Puertollano 2013

by 14-3-3 proteins due to the phosphorylation induced by mTORC1, acting in similar way as TFEB and MITF (Fig. 25) (Martina et al. 2014). Furthermore, since TFEB and MITF are bHLH leucine zipper transcription factors, it is necessary that they form a dimer to work correctly, meaning that the MITF family members can form homodimers or heterodimers making the regulation more complicated (Steingrimsson et al. 2002).

On the other hand, recent studies have shown that mTORC1 activity is not the only way to regulate TFEB. Calcineurin can dephosphorylate TFEB and allow its translocation to the nucleus due to the lysosomal Ca^{2+} signaling. The Ca^{2+} release through the MCOLN1 channel activates calcineurin which dephosphorylates TFEB, at S211, rendering it unable to bind 14-3-3 proteins. This promotes TFEB translocation to the nucleus where it binds to the CLEAR region (Fig.26) (Medina et al. 2015).

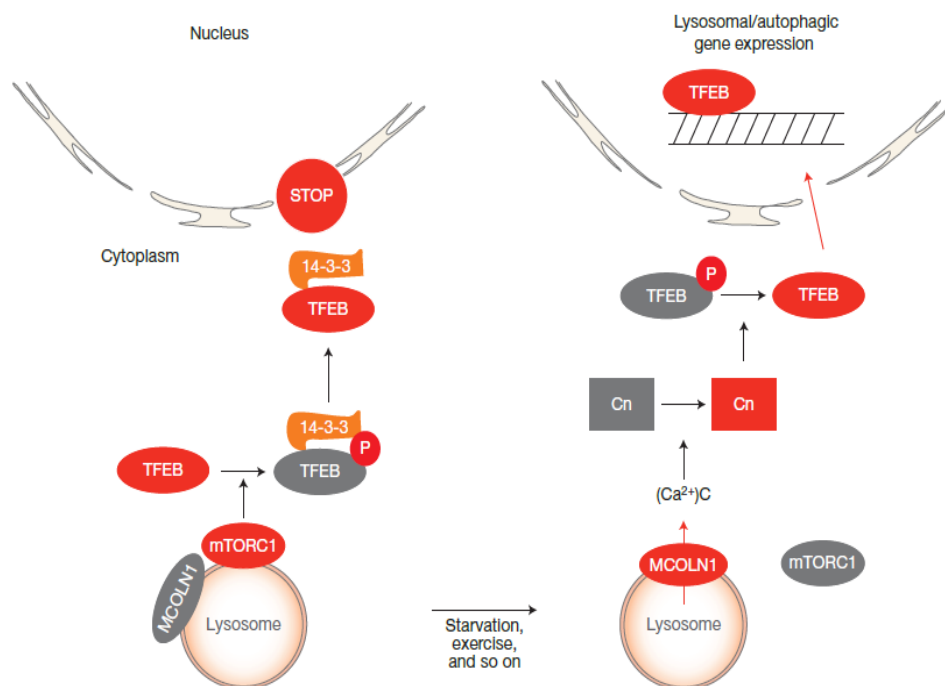


Figure 26. Regulation of TFEB and MITF by calcineurin – This scheme shows how Ca^{2+} released from lysosomes, through MCOLN1 channel, activates calcineurin that dephosphorylates TFEB. Figure from Medina et al. 2015.

However, amino acid starvation is not the only stimulus that induces MITF family members' activation. For example, nuclear translocation of TFEB, MITF and TFE3 has been reported under mitochondrial stress. But, recent studies show that deletion of different members of MITF family is compensated by the others (Nezich et al. 2015).

1.4.5 AMPK

In the context of signaling related to mitochondria and lysosomes, it is necessary to mention AMP-activated protein kinase (AMPK) due to its connection to these organelles via signaling pathways.

AMPK is a highly conserved serine/threonine kinase that is closely connected to the maintenance of cellular energy homeostasis by its ability to switch off ATP-consuming processes and switch on catabolic pathways (Hardie 2015; Jeon 2016). In order to produce more energy, AMPK activates glucose, glycolysis, acid uptake, fatty acid oxidation. AMPK also promotes mitochondrial biogenesis and mitophagy (Cantó et al. 2010; Zong et al. 2002; Hardie & Ashford 2014; Egan et al. 2011).

AMPK can be activated by AMP, also can be activated by a major increase at 100 fold of upstream kinases that phosphorylate Thr172 placed in the 'activation loop' of AMPK kinase domain. AMPK can also be activated by the v-ATPase-Ragulator complex and the Ca²⁺/calmodulin-activated protein kinase (CaMKKb) (Hurley et al. 2005; Vingtdoux et al. 2010; Zhang et al. 2014; Hardie 2015). It has been shown that mitochondria can regulate AMPK activation through ROS signaling (Emerlinga et al. 2009; Raimundo et al. 2012). Furthermore, recent studies report that mitochondrial ROS signaling can induce the release of Ca²⁺ to the cytoplasm and that Ca²⁺ translocation activates CaMKKb which in turn activates AMPK (Sinha et al. 2015; Mungai et al. 2011; Zhang et al. 2016).

In the context of the connection between AMPK and lysosomes, recent studies suggest that activation of AMPK by liver kinase B1 (LKB1) can occur at the lysosomal surface. Under the conditions of nutrient deprivation, LKB1 and AMPK are recruited to Ragulator complex, which is involved in mTORC1 activation (Zhang et al. 2014). These results suggest that nutrient availability is involved in regulation of mTORC1 and AMPK through their recruitment to the surface of lysosomes in a Ragulator-dependent manner (Bar-Peled & Sabatini 2014).

In summary, when these different pathways are considered as an elaborate network, the interactions between mitochondria and lysosomes become an interesting group of signaling alternatives that require further elucidation.

1.5 Interactions between mitochondria and lysosomes

For a long time, the organelles were studied like a group of independent islands. However, currently the interactions among organelles are receiving far more attention and are considered in two contexts: as contact sites and as signaling pathways.

1.5.1 Contact sites between mitochondria and lysosomes

Recently, a body of evidence emerged suggesting that contact sites between organelles are key points in the coordination of cellular physiology. In prior years, an increasing number of contact sites have been identified, like endoplasmic reticulum with plasma membrane, Golgi, endosomes and mitochondria (Hönscher et al. 2014), as well as between mitochondria and endosomes (Charman et al. 2010). However, while contact sites have been identified between mitochondria and vacuoles in yeast, the identification of their homologues in mammals, responsible for the contact between mitochondria and lysosomes, is not clear yet (Hönscher et al. 2014; Elbaz-Alon et al. 2015).

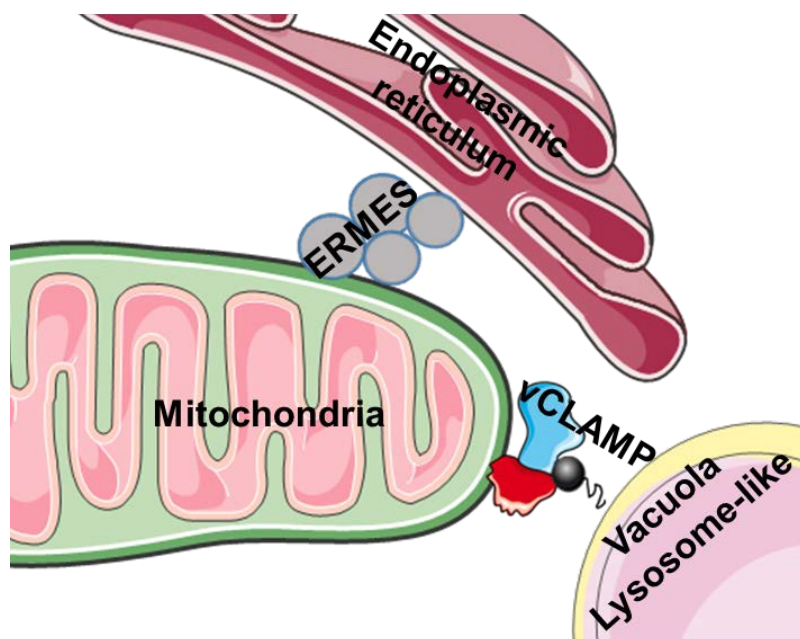


Figure 27. Mitochondria-vacuole contact sites – Representative figure of mitochondrial contact sites with lysosome-like vacuole (vCLAMP) and with endoplasmic reticulum (ERMES). Figure adapted from Hönscher et al. 2014.

Lately, the existence of a contact site named vacuole and mitochondria patch (vCLAMP) has been reported, that serves as a contact site between mitochondria and lysosome-like vacuole in yeast (Hönscher et al. 2014). vCLAMP is located close to the endoplasmic reticulum-mitochondria encounter structure (ERMES), which is a known contact site between endoplasmic reticulum and mitochondria in yeast (Fig 27) (Elbaz-Alon et al. 2014; Hönscher et al. 2014).

It has been reported that ERMES and vCLAMP have a close relation: upon diminution of one of the components there is an increase in the other, while depletion of both vCLAMP and ERMES results in cell death (Elbaz-Alon et al. 2014).

1.5.2 Signaling pathways between mitochondria and lysosomes

In prior years, several studies and reviews were focused on the cross-talk between mitochondria and lysosomes (Raimundo et al. 2016) and in the context of this project, we focus on the signaling pathways that connect these two organelles.

It is already known that damaged mitochondria trigger signaling, for example, ROS increase occurs as a consequence of mitochondrial damage in neurodegenerative diseases such as Parkinson, Alzheimer or amyotrophic lateral sclerosis (ALS) (Patten et al. 2010). In the familiar form of ALS the SOD1 is dysfunctional, leading to the increase in ROS level (Rosen et al. 1993). Interestingly, a recent study reported that mitochondrial ROS activates MCOLN1 channels triggering Ca^{2+} release from the lysosomes (Zhang et al. 2016), which in turn activates TFEB by calcineurin-dependent dephosphorylation (Medina et al. 2015; Zhang et al. 2016). However, another study shows that mitochondrial malfunction can induce lysosomal biogenesis in a TFEB-dependent manner while also triggering mitochondrial biogenesis (Ivankovic et al. 2016). Also, there are reports of TFEB nuclear translocation in a PINK1-Parkin-dependent manner in Parkin-expressing HeLa cells under chemically induced mitochondrial malfunction (Nezich et al. 2015). It is important to note that there are other studies reporting that mitochondrial malfunction leads to impaired lysosomal capacity, in mitochondrial transcription factor A (TFAM) knock-out T-lymphocytes (Baixauli et al. 2015) and in mouse fibroblast with apoptosis inducing factor (AIF), optic atrophy 1 (OPA1) or PINK1 deletion (Fig. 28) (Demers-Lamarche et al. 2016).

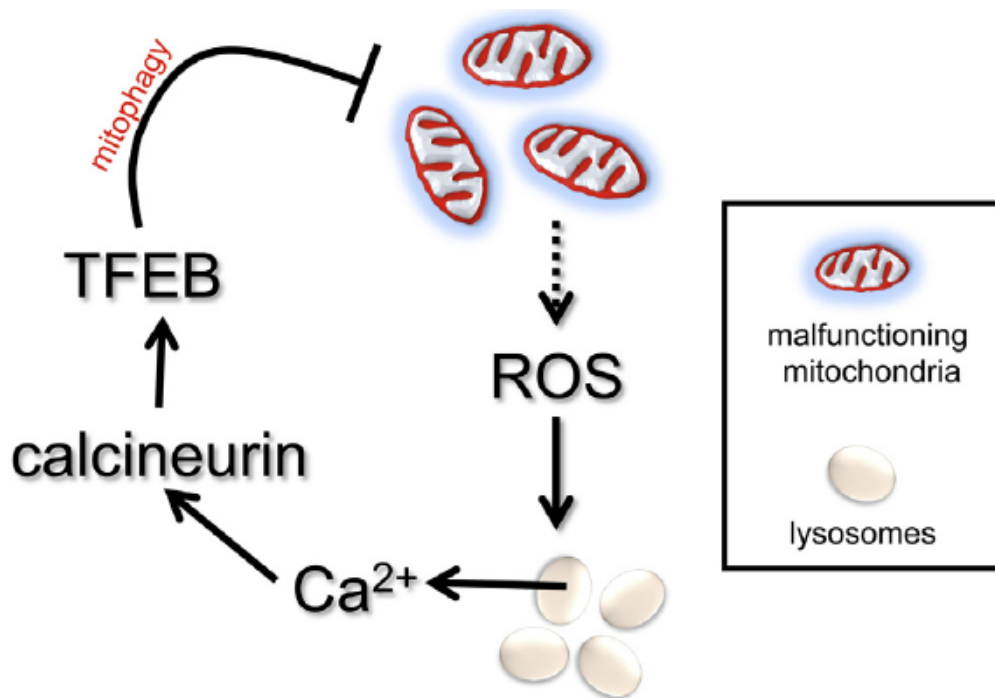


Figure 28. Mitochondrial malfunction affects lysosomes – Scheme that represents how mitochondrial malfunction affects lysosomes, triggering Ca^{2+} homeostasis dysregulation and TFEB-associated lysosomal biogenesis. The lysosomal biogenesis can be a mechanism to compensate the lysosomal impairment caused by mitochondrial malfunction as well as an attempt to remove damaged mitochondria. Figure from Raimundo et al. 2016.

On the other hand, in the context of how lysosomal malfunction affects mitochondrial function, it is important to mention lysosomal storage diseases (LSDs) in which mutations that affect lysosomal proteins induce an impaired lysosomal function (Raimundo et al. 2016). In patients affected by Pompe's disease, due to LSD caused by mutations that induce deficiency of lysosomal alpha-D-glucosidase (GAA), a decrease in the activity of complexes I, II and III of the mitochondrial respiratory chain has been reported (Selak et al. 2000). Moreover, in GAA knock-out mice, several mitochondrial defects have been reported like dysregulation in Ca^{2+} homeostasis, increase in ROS, decrease in mitochondrial membrane potential and oxygen consumption, as well as alterations in mitochondrial morphology (Lim et al. 2015). Also, mitochondrial perturbation have been reported in other LSDs like Gaucher's disease, wherein accumulation of fragmented mitochondria and diminution in the activity of complexes I, II and III of the mitochondrial respiratory chain was found (Osellame et al. 2013). Although the mechanisms that regulate how dysfunctional lysosomes affect mitochondria are not clear, recent evidence suggests the involvement of Ca^{2+} . Specifically, Ca^{2+} homeostasis experiences dysregulation (Lim et al. 2015) and cytoplasmic Ca^{2+}

displays an increase leading to the translocation of DRP1 into mitochondria, where it triggers mitochondrial fragmentation (Fig. 29) (Cereghetti et al. 2008).

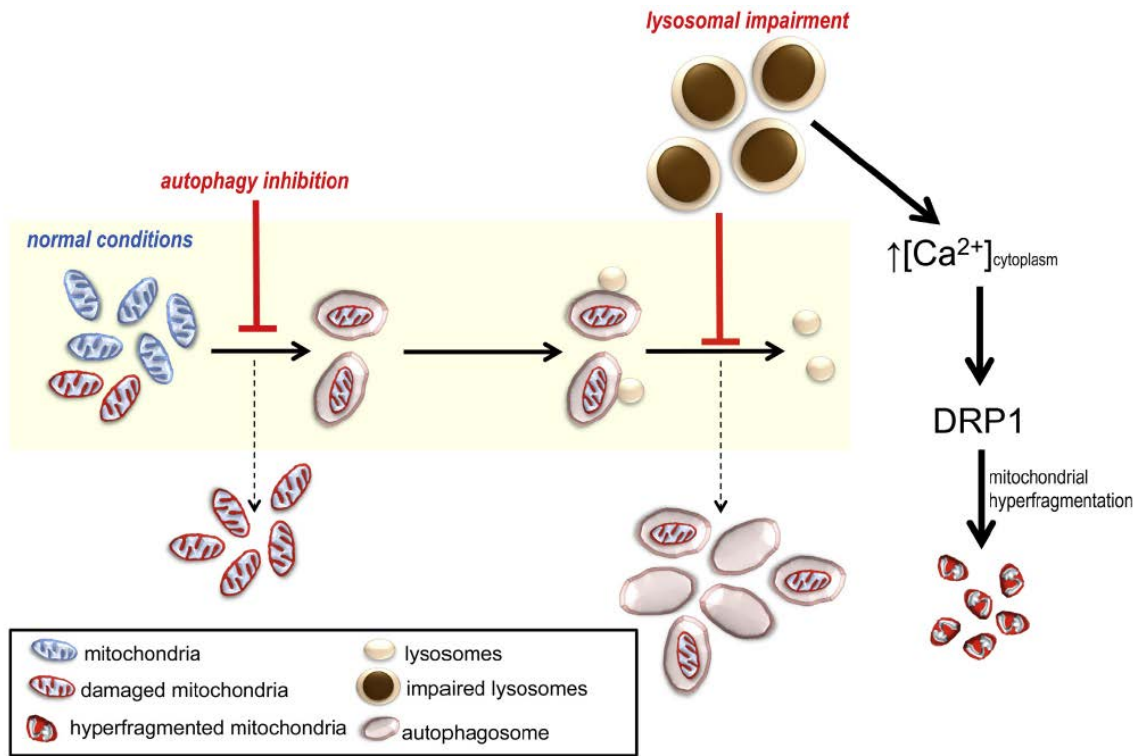


Figure 29. Lysosomal malfunction affects mitochondria - Scheme that represents how mitochondrial malfunction affects lysosomes through a decrease in lysosomal capacity which in turn leads to an accumulation of autophagosomes and lysosomes with undigested cargo. Other effects of lysosomal malfunction include the accumulation of damaged mitochondria and the dysregulation of Ca^{2+} stores with increase in cytoplasmic Ca^{2+} and translocation of DRP1 to mitochondria, resulting in mitochondrial fragmentation. Figure from Raimundo et al. 2016.

The study of organelle interactions has recently emerged as a novel field to which our results on the mechanisms of communication between mitochondria and lysosomes will contribute.

Aims

Currently, it is recognized that mitochondria function as signaling platforms and that dysfunctional mitochondria can perturb the signaling of the cells affecting decisions such as proliferation, differentiation, autophagy and death. However, little is known about the mechanisms used by mitochondria to communicate with the rest of the cell organelles and specifically with lysosomes. The main goal of this project is to explore how mitochondrial malfunction affects lysosomes and the lysosomal-related pathway of autophagy. The work described in this text aims to:

- Generate cellular models of acute and chronic mitochondrial malfunction.
- Describe how acute and chronic mitochondrial malfunction affect lysosomes and macroautophagy.
- Determine the relevance of the microphthalmia transcription factor family in lysosomal biogenesis triggered by mitochondrial malfunction.
- Identify the signaling pathways that connect acute and chronic mitochondrial malfunction with lysosomes.
- Monitor lysosomal function in chronic mitochondrial malfunction, which we hypothesize is impaired, and in the case of lysosomal dysfunction to identify the cause of the dysfunction and design a rescue strategy.

2. Materials and methods

2.1 Materials

2.1.1 Suppliers

All the reagents and the laboratory equipment used for the experiments described in this thesis were purchased from the companies listed below (Table1).

Table 1. Companies and institutions that have provided the materials and instruments

Company	City/State	Country
Abcam	Cambridge	UK
Addgene	Cambridge, MA	USA
Alfa Aesar	Haverhill, MA	USA
AMRESCO	Solon, OH	USA
AppliChem GmbH	Darmstadt	Germany
ATCC (LGC Standards GmbH)	Wesel	Germany
BD Bioscience	Heidelberg	Germany
Beckman Coulter GmbH	Krefeld	Germany
Becton, Dickinson and Company	Franklin Lakes, NJ	USA
Biometra	Göttingen	Germany
Bio-Rad	Hercules, Ca	USA
BioTek	Winooski, VE	USA
BioVision	Milpitas, CA	USA
Carl Roth, GmbH + CoKG	Karlsruhe	Germany
Carl Zeiss	Oberkochen	Germany
CAWO	Düsseldorf	Germany
Cell Signaling	Beverly, MA	USA
Corning GmbH HQ	Wiesbaden	Germany
CytoOne - USA Scientific, Inc.	Orlando FL	USA
DSHB	Iowa City, IA	USA

Dianova	Hamburg	Germany
Eppendorf	Hamburg	Germany
Epson	Suwa	Japan
Fisher Scientific	Schwerte	Germany
Fluka - Sigma-Aldrich	Schnelldorf	Germany
Foma	Bohemia	Czech Republic
GE Healthcare	Little Chalfont	UK
GE Dharmacon	Lafayette, CO	USA
Gibco	Paisley	UK
Integrated DNA Technologies	Coralville, IA	USA
InvivoGen	San Diego, CA	USA
Invitrogen	Carlsbad, CA	USA
Labnet International Inc.	Edison, NJ	USA
Life Technologies	Carlsbad, CA	USA
Millipore	Darmstadt	Germany
New England Biolabs GmbH	Frankfurt am Main	Germany
Novus	Cambridge	UK
Paul Marienfeld GmbH & Co. KG	Lauda-Königshofen	Germany
PEQLAB Biotechnologie GMBH	Erlangen	Germany
Phoenix Instrument GmbH	Garbsen	Germany
Promega	Madison, WI	USA
Sigma Aldrich	Saint Louis, MO	Germany
Sigma-Aldrich Chemie GmbH	Schnelldorf	Germany
Synaptic Systems GmbH	Göttingen	Germany
StartLab GmbH	Hamburg	Germany
Thermo Fisher Scientific	Waltham, MA	USA
TH-Geyer	Renningen	Germany
Volu-Sol	Salt Lake City, UT	USA

VWR-International	Hannover	Germany
-------------------	----------	---------

2.1.2 Reagents

The chemicals used for the experiments described in this thesis, with their correspondent suppliers and codes, can be found in the list below (Table 2).

Table 2. List of reagents

Product	Supplier	Code
A769662	InvivoGen	inh-a769
Acridine orange	Sigma Aldrich	A6014
Acrylamide solution 40%	AppliChem	A0385
Ammonium Persulfate (APS)	AMRESCO	0486
BSA	Sigma Aldrich	A7906
Bromophenol blue	Carl Roth	T116.1
CaCl ₂	Alfa Aesar	L13191
CCCP	Fluka	857815
Cold fish gelatin	Sigma	G7765
DAPI	Carl Roth	C6335.1
D(+)-Glucose	Carl Roth	275227941
DMSO	Sigma Aldrich	D8418
Dorsomorphin (compound C)	Sigma	P5499
DTT	AppliChem	A2948
Ethanol Absolut	BD Bioscience	354052
Ethanol 70%	VWR	84858.440
FCCP	Sigma Aldrich	C2920
FK506	InvivoGen	tlrl-fk5
Glycerol	Carl Roth	7530.1
Glycine	VWR	0167
Goat Serum	Life Technologies	10000C

Halt™ Protease & Phosphatase single use Inhibitor Cocktail	Thermo Scientific	78442
HEPES	Carl Roth	HN77.2
HCl	Sigma Aldrich	H1758
H ₂ O Nuclease-free	VWR	E476
KCl	Volu-Sol	83608.26
Methanol	VWR	20903.368
2-Mercapthoethanol	Carl Roth	4227.3
MgCl ₂	VWR	8.14733.0100
MgSO ₄ – 7H ₂ O	Sigma Aldrich	63138
ML-SA1	Sigma Aldrich	SML0627
Mowiol 4-88	AppliChem	A9011
NaCl	AppliChem	A1430,0010
NaHCO ₃	Carl Roth	P029.3
NaH ₂ PO ₄ – H ₂ O	Carl Roth	K300.1
NaN ₃	Sigma Aldrich	52002-1006
N-dodecylmaltoside	Carl Roth	CN26.2
Nonidet®P-40 Substitute	AMRESCO	E109-50ML
Paraformaldehyde (PFA)	AppliChem	A3813
Puromycin 100mg	Fisher Scientific	BP2956-100
SDS	Sigma Aldrich	L4509-500G
Skim Milk Powder	Fluka	70166
TEMED	Sigma Aldrich	T7024
Torin1	BioVision	2273
Tris	AMRESCO	0497
Tris Base	Sigma Aldrich	T1503
Tris-HCl	Carl Roth	9090.2
Triton X-100	AMRESCO	0694

Tween 20	AMRESCO	0777-1L
Uridine	Sigma Aldrich	U3003
YM201636	InvivoGen	inh-ym20

2.1.3 Kits and disposals

The kits and disposals used throughout this project, with their correspondent suppliers and codes, can be found in the table below (Table 3)

Table 3. Kits and disposals

Product	Supplier	Code
Amersham Hybond PO45 PVDF	GE Healthcare	10600023
Centrifuge tubes 15 mL Corning CentriStar	Corning	430791
Centrifuge tubes 50 mL Corning CentriStar	Corning	430829
CRYSTAL RNA Mini Kit	New England Biolabs	31-010-404
Cuvettes PMMA	VWR-International	634-0678
DQ-BSA Green	Life Technologies	D12050
FACS Tubes Polystyrene Round-Bottom 5 mL	Corning	352052
Fugene R 6 Transfection Reagent	Promega	E2691
High Performance chemiluminiscence film	GE Healthcare	28906837
iScrip cDNA Synthesis Kit	Bio-Rad	170-8891
iTaq™ Universal SYBR Green Supermix	Bio-Rad	172-5124
Lipofectamin 2000 Reagent	Invitrogen	11668-019
Luminata™ Classico Western HRP Substrate	Millipore	WBLUC0500
Luminata™ Crescendo Western HRP Substrate	Millipore	WBLUC0500
Lysotracker Green DND-26	Life Technologies	L7526

Lysotracker Red DND-99	Life Technologies	L7528
Medical X-Ray Film	Foma	-----
Microscope slides	Carl Roth	2111
Microseal B seal	Bio-Rad	MSB1001
MitoSOX™ Red	Life Technologies	M36008
Mitotracker Green FM	Life Technologies	M7514
Mitotracker Deep Red FM	Life Technologies	M22426
PageRuler Plus Prestained Protein Ladder	Thermo Scientific	26619
PCR plate 384-well skirted ABI-Type (Universal)	StartLab	E1042-3840
Pierce BCA Protein Assay Kit	Thermo Scientific	23225i
Protein Assay Dye Reagent Concentrate	Bio-Rad	500-0006
Serological Pipette 5 mL	StartLab	E4860-0511
Serological Pipette 10 mL	StartLab	E4860-1011
Serological Pipette 25 mL	StartLab	E4860-2511
Test Tube Soda Glass	VWR-International	212-003
Tips 10 µL TipOne	StartLab	S111-3210
Tips 20 µL TipOne	StartLab	S120-1810
Tips 200 µL TipOne	StartLab	S1120-8800
Tips 1000 µL TipOne	StartLab	S1111-6001
Tubes 8 Twin Strip Start PCR	StartLab	11402-3700
Tubes 0.5 mL molecular probes	Life Technologies	Q33856
Tubes 1.5 mL	StartLab	E1415-1500
Tubes 2 mL	StartLab	S1620-2700
XF [®] 96 extracellular flux assay kit Seahorse	BD Bioscience	102416-100
Western Blot Paper	TH-Geyer	4-01-60-0041

2.1.4 Buffers and solutions

The list of buffers and solutions used for experiments described in this thesis and their composition can be found in the table below (Table 4).

Table 4. Buffers and solutions

Buffer/solution	Composition	
BSA 5%	BSA	5 gr
	TBST	100 mL
Blocking buffer 5 % milk	Skim milk	40 gr
	TBST	800 mL
Blocking solution immunocytochemistry	PBS	5 mL
	Cold fish gelatin 10%	50 μ L
	Triton X-100 0.1%	5 μ L
	BSA	0.15 g
	Goat serum	50 μ L
EBSS medium	CaCl ₂	200 mg
	MgSO ₄ – 7H ₂ O	200 mg
	KCl	400 mg
	NaHCO ₃	2.2 gr
	NaCl	6.8 gr
	NaH ₂ PO ₄ – H ₂ O	140 mg
	D-Glucose	1 gr
	ddH ₂ O	Bring up 1 L
Freezing medium	DMEM high glucose	35 mL
	FBS	10 mL
	DMSO	5 mL
Hypertonic buffer	Tris	2.42 gr
	KCl	31.08 gr
	MgCl ₂	0.15 gr
	Glycerol	200 mL
	ddH ₂ O	Bring up 1 L
Hypotonic buffer	Tris	1.21 gr
	KCl	0.74 gr
	MgCl ₂	0.15 gr

	ddH ₂ O	Bring up 1 L
Imaging buffer	NaCl	0.75 gr
	KCl	18.64 mg
	CaCl ₂	22.19 mg
	MgCl ₂	9.52 mg
	HEPES	0.24 g
	ddH ₂ O	Bring up 100 mL
Mowiol	Mowiol 4-88	2.4 gr
	Glycerol	6 gr
	Tris 0.2 M pH 8.5	12 mL
	ddH ₂ O	12 mL
NaN ₃ 10 %	NaN ₃	1 gr
	ddH ₂ O	10 mL
N-dodecylmaltoside 1.5%	N-dodecylmaltoside	0.15 gr
	PBS	10 mL
	Protease/phosphatase	100 µL
Resolving gel 12% (4 gels)	Tris-HCl 1.5 M pH 8.8	5 mL
	10% SDS	200 µL
	40% Acrylamide	6 mL
	10% APS	100 µL
	TEMED	20 µL
	ddH ₂ O	8.7 mL
Running buffer 5X	Tris Base	15 gr
	Glycine	72 gr
	SDS	3 gr
	ddH ₂ O	Bring up 1 L
Running buffer 1X	Running buffer 5X	1 L
	ddH ₂ O	4 L
SDS loading buffer	Tris/HCl 0.5 M pH 6.8	12 mL
	Glycerol	47 mL
	SDS	12 gr
	Bromophenol blue	60 mg
	ddH ₂ O	Bring up 95 mL
	2-Mercaptoethanol	Add fresh 5 µL each 95 µL buffer

Stacking gel 4% (4 gels)	Tris-HCl 0.5 M pH 6.8	2.5 mL
	10% SDS	100 μ L
	40% Acrylamide	1 mL
	10% APS	50 μ L
	TEMED	10 μ L
	ddH ₂ O	6.43 mL
TBST 10X	Tris Base	24.2 gr
	NaCl	80 gr
	Tween 20	10 mL
	ddH ₂ O	Bring up 1 L
TBST 1X	TBST 10X	1 L
	ddH ₂ O	9 L
Transfer buffer 10X	Tris Base	30.3 gr
	Glycine	144 gr
	SDS	10 gr
	ddH ₂ O	Bring up 800 mL
Transfer buffer 1X	Transfer buffer 10X	250 mL
	Methanol	500 mL
	ddH ₂ O	1750 mL
XF Seahorse assay media	DMEM	8.3 gr
	GlutaMax-1	10 mL
	Sodium Pyruvate	10 mL
	NaCl	1.85 gr
	ddH ₂ O	1000 mL

2.1.5 Primers

The primers used for PCR in the context of this thesis were found in Primer Bank (Harvard Medical School) and ordered from Integrated DNA Technologies. The list of these primers, with their sequences, is in the Table 5.

Table 5. List of primers

Primer	Sequence	T _m °C
CTSD-F	ATTCAGGGCGAGTACATGATCC	56.7

CTSD-R	CGACACCTTGAGCGTGTAG	55.6
CTSF-F	AGAGAGGCCCAATCTCCGT	58.1
CTSF-R	GCATGGTCAATGAGCCAAGG	56.8
GAA-F	TGCCCTCGCAGTATATCACAG	56.6
GAA-R	GAGACCCGTAGAGGTTTCGC	57.3
GAPDH-F	GGAGTCAACGGATTTGGTTCG	56
GAPDH-R	GACAAGCTTCCCGTTCTCAG	55.7
HPRT-F	ACCAGTCAACAGGGGACATAA	55.8
HPRT-R	CTTCGTGGGGTCCTTTTCACC	58.2
LAMP1-F	CAGATGTGTTAGTGGCACCCA	57.3
LAMP1-R	TTGGAAAGGTACGCCTGGATG	57.3
MITF-F	GCCTCCAAGCCTCCGATAAG	57.8
MITF-R	GCACTCTCTGTTGCATGAACT	55.5
TFEB-F	ACCTGTCCGAGACCTATGGG	58.2
TFEB-R	CGTCCAGACGCATAATGTTGTC	56.2
UQCRC1-F	GGGGCACAAGTGCTATTGC	57.1
UQCRC1-R	GTTGTCCAGCAGGCTAACC	56.1

2.1.6 Cell culture media and compounds

In the context of this thesis different media and compounds were used. The lists of cell culture media (Table 6) and compounds (Table 7) with the correspondent information are below.

Table 6. Cell culture media

Product	Supplier	Code	Compounds added
EBSS medium	House made	-----	1 mM Pyruvate 200 µM Uridine
DMEM high glucose	Gibco	41965-062	10% FBS 1% P/S

DMEM high glucose + pyruvate	Gibco	41966-029	10% FBS 1% P/S 200 µM Uridine
Dulbecco's Modified Eagle's Medium Base 8.3g/L	Sigma	D5030-1L	-----
Opti-MEM (1X)	Gibco	11058-021(6)	-----

Table 7. Cell culture compounds

Product	Supplier	Code
D(+)-Glucose	Carl Roth	275227941
Fetal Bovine Serum Heat Inactivated	Gibco	10500-064
GlutaMax-1 (100X)	Gibco	35050-061
PBS	Sigma	P44177-100TAB
Penicillin/Streptomycin	Gibco	15140-062
Sodium Pyruvate	Sigma	S8636
Triple ^t Express (1X)	Gibco	12605-010
Uridine	Sigma	U3003-56

2.1.7 Cell culture devices

In order to manipulate the cell cultures, different devices were used during the experiments performed in the context of this thesis. The list of devices with their supplier and code is below (Table 8).

Table 8. Cell culture devices

Product	Supplier	Code
60 x 20 mm TC dish	CytoOne	CC7682-3354
100 x 20 mm TC dish	CytoOne	CC7682-3394
150 x 20 mm TC dish	CytoOne	CC7682-3617
6-well TC plate	CytoOne	CC7682-7506

12-well TC plate	CytoOne	CC7682-7512
96-well TC plate	CytoOne	CC7682-7596
96-well TC plate black	Thermo Scientific	137104
Cell scraper	StartLab	CC7600-0202
Countess cell counting chamber slides	Invitrogen	C10283
Coverslips	Marienfeld	017580
Cryogenic vial 2 mL	Fisher Brand	1050026
Filter syringe 0.22 Ø Rotilabo CME	Carl Roth	SE2M35I07
Syringe Inject	Becton. Dickinson and Company	4606205
Trypan Blue 0.4%	Life Technologies	T10282

2.1.8 Plasmids and siRNA

The transfections were done with shRNA, pcDNA and siRNA listed below (Table9).

Table 9. Plasmids and siRNAs

Plasmid/siRNA	Supplier	Code
shRNA-UQCRC1	GE Dharmacon	TRCN0000046483
shRNA-UQCRC1	GE Dharmacon	TRCN0000046484
shRNA-UQCRC1	GE Dharmacon	TRCN0000046485
shRNA-UQCRC1	GE Dharmacon	TRCN0000046486
shRNA-UQCRC1	GE Dharmacon	TRCN0000046487
shRNA-TFEB	GE Dharmacon	TRCN0000013108
shRNA-TFEB	GE Dharmacon	TRCN0000013109
shRNA-TFEB	GE Dharmacon	TRCN0000013110
shRNA-TFEB	GE Dharmacon	TRCN0000013111
shRNA-TFEB	GE Dharmacon	TRCN0000013112
pEGFP-N1-TFEB	Addgene	38119

LAMP1-mGFP	Addgene	34831
pEGFP-LC3	Addgene	24920
pmRFP-LC3	Addgene	21075
pcDNA-mito-cyan	Gift from Dr. Ira Milosevic	Unpublished
pLKO.1-blast-scrambled	Addgene	26701
pcDNA-CnA	Gift from Prof. Luca Scorrano	Cereghetti et al. 2008
siRNA-MITF	Integrated DNA Technologies	69000547
siRNA-MITF	Integrated DNA Technologies	69000571
siRNA-MITF	Integrated DNA Technologies	69000568

2.1.9 Antibodies

Different primary and secondary antibodies were used for immunoblotting and immunocytochemistry (Table 10, 11).

Table 10. Primary antibodies for western blot and immunocytochemistry

Antibody	Company	Code	Applications
ATP6V0A1	SySy	109 002	Western blot
ATP6V1A	Novus	NBP1-33021	Western blot
GAPDH	Sigma Aldrich	G9545	Western blot
H4A3 (LAMP1)	DSHB	-----	Immunocytochemistry
Histone3 (96C10)	Cell Signaling	3638	Western blot
HPRT	Abcam	ab10479	Western blot
LAMP1	Abcam	ab24170	Western blot
LC3B (D11)	Cell Signaling	3868	Western blot
TFEB	Novus	NBP1-67872	Western blot
UQCRC1	Abcam	ab110252	Western blot

Table 11. Secondary antibodies for western blot and immunocytochemistry

Antibody	Company	Code	Applications
Goat anti-mouse IgG	Dianova	115-035-146	Western blot
Goat anti-mouse Alexa 488	Life Technologies	A-11001	Immunocytochemistry
Goat anti-rabbit IgG	Dianova	115-035-144	Western blot

2.1.10 Cell lines

In the context of this thesis, HeLa cells, provided by ATCC, were used as a mammalian cell model, which is a common practice in the field. HEK^{293T} cells, provided by ATCC, were used as packaging cells during the production of virus for the generation of stable UQCRC1 knock-downs.

2.1.11 Instruments

The instruments used in this thesis, their applications and the companies that produced them are listed in Table 12.

Table 12. Equipment

Instrument	Company	Applications
Ace Block Digital Dry Bath	Labnet	Incubate Eppendorf tubes with fixed temperature
Bio-Rad Power Pack HC Mini-Protean Tetra System	Bio-Rad	Run and transfer western blots
CAWOMAT 2000	CAWO	Develop film
Centrifuge 5415C	Eppendorf	Centrifuge Eppendorf tubes
Centrifuge 5415R	Eppendorf	Centrifuge Eppendorf tubes with controlled temperature
Centrifuge 5810R	Eppendorf	Centrifuge Falcon tubes

		with controlled temperature
Centrifuge Allegra X-15R	Beckman Coulter	Centrifuge plates with controlled temperature
Countess C10281	Invitrogen	Count cells
FACS Canto™II	BD Biosciences	Determination of lysosomal mass. mitochondrial membrane potential and ROS measurement
Gene Quant 1300	GE Healthcare	Measure protein concentration
Hood Herasafe	Thermo Scientific	Cell manipulation
Incubator Heracell 150i	Thermo Scientific	Grow cells at 37°C
Microscope Zeiss Axio Vert A1	Zeiss	Imaging cells
Multichannel pipette	Eppendorf Research	Pipette small volumes in 96-well plates
Nanodrop 2000C	Peqlab	Measuring of RNA concentration
Pipettes	Eppendorf Research	Pipette small volumes
Pipette gun accu-jet pro	BRAND	Pipette big volumes
pHmeter pH7110	WTW Inolab	Measuring pH
Precision balance Explorer	OHAUS	To weigh reagents
Quant Studio 6 Flex	Life Technologies	Real time quantitative PCR
Revolver wheel	Labnet	Rotate Eppendorf tubes
Scanner Epson Perfection V850 Pro	Epson	Scan films
Seahorse XF96	Agilent	Measure the oxygen

extracellular Flux Analyzer		consumption rate (OCR) of live cells
Spinning disk confocal microscope	Perkin Elmer	Fluoresce imaging
SYNERGYM1 microplate reader	BioTek	Determination of lysosomal mass and proteolytic capacity
Thermocycler UNO II	Biometra	cDNA synthesis
Vortex RS-VA10	Phoenix Instrument	Mix

2.1.12 Software

The software that was used in the realization of this thesis and the information about the companies that made them is listed in the table below (Table 13).

Table 13. Software

Software	Company	City/State	Country
FACS DIVA™ software	BD Biosciences	Heidelberg	Germany
GraphPad Prism 6	GraphPad Software Inc.	La Jolla. CA	USA
ImageJ	National Institutes of Health	Bethesda. MD	USA
Matlab	MathWorks	Natick, MA	USA
Mendeley	Mendeley Ltd.	London	UK
Microsoft Office	Microsoft Corporation	Redmond. WA	USA
Photoshop CS4	Adobe Systems	San Jose. CA	USA
Volocity	Perkin Elmer	Waltham. MA	USA

2.2 Methods

2.2.1 Cell work

2.2.1.1 Growth conditions

HeLa cells were grown in Dulbecco's Modified Eagle Medium high glucose medium (DMEM) supplemented with 10% fetal bovine serum (FBS) and 1% Penicillin/Streptomycin (P/S) at 37°C and 5% CO₂. HeLa UQCRC1kd and scrambled control cells were grown in DMEM high glucose medium with pyruvate supplemented with 10% FBS, 1% P/S and 200 µM uridine at 37°C and 5% CO₂. All media and solutions used for cell work were either autoclaved or filtered. Cells were counted using a cell counter, they were about 60-80% confluent when harvested for experiments and plated at least 24 hours before the experiment. The seeding cell number, which was changed according with the area of the plate, was:

10 cm plate → 1x10⁶ cells/plate

6 cm plate → 1x10⁵ cells/plate

6-well-plates → 120000 cells/well

12-well-plates → 35000 cells/well

96-well-plates → 12000 cells/well

2.2.1.2 Starvation treatment

HeLa cells were plated in 10 cm plates for RNA extraction. The cells were washed with PBS and the medium was replaced with EBSS medium. After the time of starvation ended, the medium was aspirated and the cells were washed with warm PBS and incubated with 1 mL of TrypLE Express Enzyme during 3 minutes at 37°C. After these 3 minutes, 2 mL of EBSS were added and cells were centrifuged for 5 minutes 800 x g at 4°C. The supernatant was aspirated and the pellets were kept at -80°C until the RNA was extracted.

2.2.1.3 Chemical treatments

HeLa cells were plated in 10 cm plates for protein/ RNA extraction or in coverslips placed in 12-well-plates for microscopy. They were treated with the following compounds: sodium azide

(NaN₃) 15 mM, carbonyl cyanide 3-chlorophenylhydrazone (CCCP) 10 μM, dorsomorphin (compound C) 10 μM, Torin1 250 nM, FK506 (Tacrolimus) 5 μM, ML-SA1 20nM, YM2010636 1 μM, A769662 100 μM. To treat the cells, the medium was aspirated and after the cells were washed with PBS, the medium was replaced with fresh DMEM medium plus the correspondent chemical. After 4 hours, the medium was aspirated and the cells were washed with warm PBS and depending on the use the samples could be:

- **Protein/RNA:** incubated with 1 mL of TrypLE Express Enzyme for 3 minutes at 37°C. After these 3 minutes, 2 mL of EBSS were added and cells were centrifuged for 5 minutes 800 x g at 4°C. The supernatant was aspirated and the pellets were kept at -80°C until the protein or the RNA was extracted.
- **Microscopy:** cells were fixed with 4% PFA overnight at 4°C. After, PFA was aspirated and the cells were washed twice with PBS and stored at 4°C in dark until use.

2.2.1.4 Transient knock-downs

HeLa cells were plated 24h before transfection in 6 cm plates for protein/RNA extraction or in a 12-well-plate with coverslips for microscopy and were transfected using FuGENE HD Transfection Reagent (1.5 μg DNA: 4.5 μl Fugene). The transfecting mix was prepared by adding in a microcentrifuge tube 50 μl of Opti-MEM medium and 4.5 μl of Fugene 6 directly into the medium. This was mixed and incubated for 5 minutes at room temperature (R/T). In the meanwhile, in another microcentrifuge tube with 50 μl of Opti-MEM medium 1.5 μg of DNA was added and mixed. During the incubation time the DMEM high glucose of the cells was replaced with DMEM high glucose with pyruvate, uridine, FBS and P/S. When the incubation was finished, the DNA dilution was added to the Fugene dilution, mixed and incubated for 15 minutes at R/T. After the incubation time was over, the total volume of transfecting mix was added to the plate/well dropwise and gently mixed. Between 4 to 6 hours post-transfection the medium was changed by fresh medium and cells were grown for at least 24 hours before they had to be collected for protein/RNA or used in microscopy according to the procedures previously explained.

2.2.1.5 Selection of stable knock-downs

The selection of stable knock-downs was done in DMEM with Puromycin (6 mg/mL). When the control HeLa cells were dead, the selection was completed and the cells were grown and stored in liquid nitrogen.

2.2.2 Molecular biology

2.2.2.1 RNA isolation from cells

Ribonucleic acid (RNA) isolation was done using CRYSTAL RNA Mini Kit BIOLAB. Cell pellets were in 2 mL Eppendorf tubes, where 400 μ L of Lysis Solution RL and 4 μ L of 2-Mercaptoethanol (β -SH) were added. After incubation at R/T for 2 minutes, the pellet was re-suspended with a pipette. The samples were incubated at room temperature for 3 minutes and later were transferred at Spin Filter D placed in Receiver Tubes 2 mL and centrifuged for 2 minutes at 10000 x g. The column was discarded and 400 μ L of 70 % ethanol were added to the flow-through and mixed gently by pipetting. The flow-through with ethanol was transferred to Spin Filter R in Receiver Tubes 2 mL and Centrifuged for 2 minutes at 10000 x g. After the column was placed and the flow-through was discarded, 500 μ L of Washing Solution HS were added to the Spin Filter R and the tubes were centrifuged for 1 minute at 10.000 x g. The column was shifted to a new collection tube and 700 μ L of Washing Solution LS were added to the Spin Filter R. After Centrifugation at 10000 x g for 1 minute, the flow-through was discarded and the Spin Filter R was placed in a new collection tube and it was centrifuged for 2 minutes at 10000 x g to dry the membrane. The Spin Filter R was moved in a new 1.5 mL collection tube and 20 μ L of RNAase-free water was added directly to the spin column membrane to elute the RNA. The tube was incubated for 1 minute at room temperature and was later centrifuged for 1 minute at 6000 x g to collect the RNA.

RNA quantification and quality control was done using the Nanodrop. Only samples with concentration >10 ng/ μ l were used for cDNA synthesis. RNA was stored at -80°C until it was used for cDNA synthesis.

2.2.2.2 cDNA synthesis

To continue with the analysis of RNA expression, the complementary Deoxyribonucleic Acid (cDNA) was generated from RNA extracted previously, using iScript cDNA synthesis kit. The

RNA samples and the components of the kit were thawed over the ice and later kept on it. A master mix was prepared for n+1 samples with these components:

Components	Volume/Reaction
5x iScript reaction mix	4 μ l
iScript reverse transcriptase	1 μ l

First the calculations to have 1 μ g of total RNA in 20 μ l of reaction were done per each sample. Later, in labeled PCR-tubes the following were added:

Components	Volume/Tube
Nuclease-free water	x μ l
RNA template	y μ l
Mastermix	5 μ l
Final volume	20 μ l

The complete reaction mix was mixed with a vortex and shortly centrifuged before it was incubated in a thermocycler with the following steps:

25°C	5 minutes
42°C	30 minutes
85°C	5 minutes
4°C	∞

After cDNA was synthesized it was 100 times diluted in double-distilled water ($_{dd}$ H₂O) and stored at -20°C until it was used in qPCR.

2.2.2.3 qPCR

The cDNA was used to perform quantitative real time polymerase chain reaction (qPCR), performed as at least technical triplicates. Mastermixes were prepared for each gene counting n+1 wells.

Components	Volume/Reaction
SYBR® Green	3.6 μ l
Reverse primer (25 μ M)	0.2 μ l
Forward primer (25 μ M)	0.2 μ l

In the 384-well-plate the 4 μ l/well cDNA were pipetted and later 4 μ l/well of mastermix were added. Before placing the plate in the qPCR machine, it was sealed and centrifuged for a short time. The reaction was performed following the qPCR protocol:

95°C	5 minutes	
95°C	30 seconds	} x 40
60°C	30 seconds	
72°C	30 seconds	
95°C	30 seconds	
60°C	30 seconds	
72°C	30 seconds	

Data were analyzed with QuantStudio™ Real-Time PCR Software.

2.2.2.4 DQ-BSA assay

The initial stock of DQ Green BSA was prepared fresh, by re-suspending 1 mg in 1 mL sterile PBS. The cells were plated in transparent 96 well-plate and the medium was changed by fresh DMEM with DQ Green BSA (10 μ L/mL) and incubated at 37°C for 1 hour. After incubation, the wells were washed 2 times with warm PBS and the medium replaced by 100 μ L/well of EBSS medium. The plate was placed in the plate reader and readings were taken every 5 minutes during 4 hours in the plate reader (excitation 505 nm and emission 515 nm). In order to normalize the data, when the assay was completed, the amount of protein per well was measured using Pierce assay.

2.2.2.5 Lysosomal quantification plate reader

Plate reader was used in order to determine lysosomal mass using LysoTracker Red DND-99. The cells were plated in a black 96-well-plate with at least 20 replicates for each condition. The cells were washed with warm PBS and the medium was replaced with DMEM with LysoTracker Red DND-99 200 nM and incubated for 30 minutes at 37°C. Later, cells were washed with warm PBS twice and fresh medium was added (100 μ L/well). The plate was placed in the plate reader and readings were taken every 5 minutes during 4 hours (excitation 494 nm and emission 521 nm). When the assay was completed, the amount of protein per well was measured using Pierce assay and used to normalize the data.

2.2.2.6 Protein concentration determination using Pierce BCA assay

Protein concentration determination using Pierce BCA Protein Assay Kit was done to help with the normalization using protein amount of assays in which the cells were plated in 96-well-plates.

After the assay was completed, the medium was aspirated and 125 μ L of d_4 H₂O was added. The plate was incubated for 1 hour at R/T with a mild shaking to lysate the cells. After the incubation, 100 μ L of double dye working mixture were added to each well (25 Pierce BCA buffer: 1 Pierce BCA dye). After 30 minutes of incubation at 37°, the plate was read at 562 nm in the plate reader. The results were analyzed using Microsoft Excel 2013 and protein concentration was calculated based on the calibration curve, obtained with the same kit and bovine serum albumin (BSA), and used to normalize other assays using plate reader.

2.2.2.7 FACS determinations

Flow cytometry (FACS) was used in order to determine lysosomal mass, mitochondrial superoxide and mitochondrial membrane potential. In order to perform these experiments, the cells were plated in 6-well-plate, triplicates for each condition plus the corresponding controls (not stained and stained in basal conditions). The cells were washed with warm PBS and the protocol to be followed varies depending on the results to be determined.

Lysosomal mass determination: The medium was replaced with DMEM with 200 nM LysoTracker® Green DND-26 and incubated for 10 minutes at 37°C.

Mitochondrial superoxide determination: In this case, the PBS always contains 0.5 µM Glucose. The medium was replaced with warm PBS containing 0.5 µM Glucose and 5 µM MitoSOX. Stained and non-stained control, were also prepared alongside positive controls with 100 µM H₂O₂ or 100 µM antimycin which were incubated for 20 minutes at 37°C.

Mitochondrial membrane potential determination: The medium was replaced with medium containing 70 nM Mitotracker Green FM and 90 nM Mitotracker Deep Red FM and the cells were incubated for 30 minutes at 37°C.

Once the incubation was over, cells were washed with warm PBS twice and 500 µL of TrypLE Express Enzyme were added before the cells were incubated for 3 minutes at 37°C. After cells were collected, 1 mL of PBS was added to the well and it was centrifuged for 5 minutes at 800 g and 4°C. The supernatant was aspirated, cells were re-suspended in 1mL of cold PBS and transferred to FACS tubes. The tubes were kept on ice until they could be read using a Calibur flow cytometer using GFP 530/30 (lysosomal mass), PI 585/42 (mitochondrial superoxide) and PE 585/42 (mitochondrial membrane potential). Data was analyzed using the DIVA software.

2.2.2.8 Mitochondrial oxygen consumption determination

Determination of mitochondrial oxygen consumption was performed using Seahorse XF96 extracellular Flux Analyzer in accordance to the manufacturer's instructions. HeLa stable UQCRC1kd and corresponding scrambled control cells were plated in a Seahorse plate (10000 cell/well) using DMEM high glucose with pyruvate, uridine, FBS and P/S. On the other hand 200µL/well of XF Calibrant Solution were added into each well of the cartridge for hydration of the Seahorse sensor microplate and the plate was incubated overnight at 37°C. Next day, the medium was replaced by XF assay medium (180 µL/well) and incubated in Seahorse incubator

at 37°C for 1 hour without CO₂. In the meanwhile, different compounds were pipetted in the corresponding wells of the sensor microplate according to the manufacturer's instructions:

- A – Oligomycin 10 μM (25 μL/well)
- B – FCCP 4 μM (28.5 μL/well)
- C – Antimycine / Rotenone 0.4 μM (32.5 μL/well)
- D – XF medium (30 μL/well)

When the assay was completed, the amount of protein per well was measured with Pierce assay. Data was normalized to protein amount shown by Pierce assay.

2.2.2.9 Nuclear isolation

The nuclear isolation was done starting with cells plated in 15 cm plates with 80% confluence. The cells were washed with ice-cold PBS twice, collected with scraper and ice-cold PBS and centrifuged for 5 minutes at 2000 x g at 4°C. The supernatant was removed and the pellets kept at -20°C. The cells were re-suspended in 3 volumes of hypotonic buffer of pH 7.9 and were transferred to Eppendorf tubes. Non-iod P-40 was added to the tubes with a final concentration of 0.6%. The tubes were mixed using a vortex and incubated for 30 minutes on ice. When the incubation is completed, the tubes were centrifuged for 5 minutes at 800 g at 4°C. The supernatants (cytoplasmic extract) were collected into new tubes and kept at -20°C until use. The pellet was re-suspended in 3 volumes of hypertonic buffer of pH 7.9 and the tubes were incubated in rotation at 4°C for 30 minutes. When the incubation was completed, the tubes were centrifuged for 30 minutes at 15000 g and 4°C. The supernatant (nuclear extract) was collected into new tubes and kept at -20°C until they were used for western blot.

2.2.3 Protein biochemistry

2.2.3.1 Sample preparation

The cell pellets were re-suspended in an appropriated volume of 1.5% N-dodecylmaltoside (50 – 100 μ L, depending on the amount of cells) by pipetting. Later, the cell suspensions were transferred to 1 mL Eppendorf tubes and mixed by rotation at 4°C for 30 minutes. At the end of the 30 minutes, the tubes were centrifuged at 4°C for 20 minutes at 15700 g. After the centrifugation, the supernatants (whole cell extracts) were transferred into new 1 mL Eppendorf. The protein concentration was determined by Bradford assay.

2.2.3.2 Protein concentration determination using Bradford assay

Protein concentration was determined using Protein Assay Dye Reagent Concentrate (Bio-Rad) according to manufacturer's instructions. First, the standard curve was established using bovine serum albumin (BSA). To determine the protein concentration in a glass tube, 1 μ L of sample was added to 800 μ L of d_4 H₂O and after 200 μ L of Protein Assay Dye Reagent Concentrate were added. The tubes were mixed using vortex and incubated in the dark at R/T for 5 minutes. The mix was transferred into a plastic cuvette and absorbance at 595 nm was measured using a GeneQuant 1300 spectrophotometer. Protein concentration was calculated based on the calibration curve using Microsoft Excel 2013. All the samples were measured in duplicates.

2.2.3.3 SDS-PAGE

Sodium dodecyl sulfate polyacrylamide gel electrophoresis (SDS-PAGE) was performed to separate denaturated proteins according to their molecular weight. Gels were prepared with 40% acrylamide solution. The resolving 12% gels were buffered with Tris/HCl of pH 8.8, and the stacking 4% gels were buffered with Tris/HCl of pH 6.8. The gels were prepared with 1mm thickness using the Bio-Rad system. After the resolving part was poured between the gel glasses, it was covered with 1mL of isopropanol to prevent air bubbles. When the gel was polymerized, isopropanol was removed, the stacking part was added and the 10-well comb was carefully inserted. The complete polymerized gel was stored in a box filled with running buffer at 4°C or used immediately.

In order to separate proteins from cellular extracts according to their molecular weight, samples were mixed with 6x SDS loading buffer and with the appropriate volume of $\text{d}_2\text{H}_2\text{O}$ to load the same amount of protein in each well and boiled for 5 minutes at 95°C . The electrophoresis run was performed in Mini-Protean Tetra System (Bio-Rad) with an initial voltage of 80 V until the samples got in the resolving gel, which was then changed to 180 V. As a standard of molecular weight, the Page Ruler plus Prestained was used. The markers appear at 250, 130, 100, 70, 55, 35, 25, 15 and 10 KDa.

2.2.3.4 Western blotting

The transfer of separated proteins from the SDS gel into a polyvinylidene fluoride membrane (PVDF) was done using a wet blotting system. The PVDF membranes were activated for 15 sec in pure methanol, washed with $\text{d}_2\text{H}_2\text{O}$ for 3 minutes and equilibrated on transfer buffer. Gels and western blot papers were equilibrated in transfer buffer too. Later, the gel and membrane were assembled together between 4 layers of western blot papers. The transfer was done from the gel to the PVDF membrane at 100 V during 80 minutes.

2.2.3.5 Immunostaining

After the transfer was completed, the PVDF membranes were blocking in 5% milk (blocking solution) for 1 hour with mild shaking. Following blocking, membranes were washed three times with Tris-buffered saline with Tween 20 (TBST) for 10 minutes and incubated in primary antibody (blocking solution) for 1 hour at R/T or overnight at 4°C . Before incubating the membrane with HRP-secondary antibodies, the membranes were washed with TBST three times for 10 minutes at R/T. The concentration of HRP-secondary antibodies was 1:5000 or 1:10000 in blocking solution and the incubation was 1 hour at room temperature. After three more washes with TBST buffer, the chemiluminescence was detected, after 3 minutes of incubation with Luminata Clasico Western HRP Substrate, using medical X-ray films and a Curix 60 processor. The films were scanned and the bands were quantified using ImageJ.

2.2.4 Microscopy

2.2.4.1 Mitochondria/lysosomes microscopy

To study mitochondria or lysosomes using dyes, cells were plated in coverslips placed in 12-well-plates. Later, the procedure varies depending on the kind of mitochondrial malfunction.

Acute mitochondrial malfunction: The cells were treated for 4 hours or transfected as it was previously described. After the treatment/transfection was done, the medium was replaced by DMEM high glucose with FBS and P/S with 12.5 nM Mitotracker Red/50 nM LysoTracker Green and incubated at 37°C for 15 minutes or transfected with plasmid that encodes a fluorescent protein. After the incubation, the coverslips were washed with PBS, mounted in a chamber with imaging buffer and imaging was performed using a spinning disk confocal microscope.

Chronic mitochondrial malfunction: The cells were transfected with plasmid that encodes a fluorescent protein and fixed with PFA. The coverslips were mounted on slides using Mowiol and when they were dry, sealed with nail polish and stored in dark at 4°C until imaging using a spinning disk confocal microscope.

2.2.4.2 Immunostaining in stable UQCRC1kd

The cells, plated in coverslips placed in 12-well-plates, were washed with PBS and fixed using PFA. After the PFA was removed, the coverslips were washed twice with PBS and 500 μ L of blocking solution was added and incubated for 1 hour at R/T with mild shake. In the meanwhile, the primary antibody was prepared in blocking solution (2 μ g/mL). When the blocking was completed, the coverslips were incubated overnight at 4°C with the primary antibody. The day after, the antibody was removed and the coverslips were washed with PBS for 10 minutes, thrice. After the wash, the coverslips were incubated with secondary antibody goat α -mouse Alexa 488 (1:200) for an hour at R/T in the dark. When the incubation was completed, the antibody was removed and the coverslips washed with PBS for 10 minutes, thrice, but in the second wash DAPI was added to the PBS (1:5000). The coverslips were mounted on slides using Mowiol, and when they were dry, sealed with nail polish and stored in dark at 4°C until that were imaged with the help of spinning disk confocal microscope. The images were analyzed using ImageJ.

2.2.4.3 Lysosomal pH determination with acridine orange

To determine if lysosomal pH is affected in cells with mitochondrial perturbations, the stable UQCRC1 knock-down and scrambled control cells were plated in coverslips placed in 12-well-

plates. The next day, the stable UQCRC1kd were treated for 4 hours with ML-SA1 20nM (Sigma) and scrambled and stable UQCRC1kd using DMSO as control. After the incubation, the cells were incubated for 20 minutes with acridine orange 20 μ M and then washed 3 quick times and later, 3 more times for 5 minutes with PBS. After the wash, the coverslips were mounted in a chamber with imaging buffer and imaging was performed with a spinning disk confocal microscope. Cells were imaged in time-lapse to capture signal in the red and green channels. Photodamage was induced by continuous illumination between images at 488 nm. The images were analyzed using a MatLab script (Stagi et al. 2014).

2.2.5 Statistical analysis

The data were analyzed using Microsoft Excel 2013 and normalized to loading control. All the values were represented in correlation to the corresponding control, which was set to 1 (except in microscopy experiments in which the total number was kept). Final graphs were done using GraphPad Prism 6.

3 Results

3.1 Acute mitochondrial malfunction

3.1.1 Effect of acute mitochondrial malfunction caused by chemicals on lysosomes and autophagy

To study acute mitochondrial malfunction there are several ways to induce it, like exercise or Ca^{2+} increase (Kwong et al. 2015; H. Li et al. 2016; Raimundo 2014). In addition, there are other approaches to trigger acute mitochondrial malfunction and in this thesis we decided to perturb the respiratory chain using inhibitors and an uncoupler.

In order to investigate the effects of acute mitochondrial malfunction on lysosomes, HeLa cells were treated with sodium azide (NaN_3) that inhibits complex IV and carbonyl cyanide m-chlorophenyl hydrazone (CCCP) which uncouples mitochondrial respiratory chain from oxidative phosphorylation (Ishii et al. 2014; Ivankovic et al. 2016) (Fig. 30).

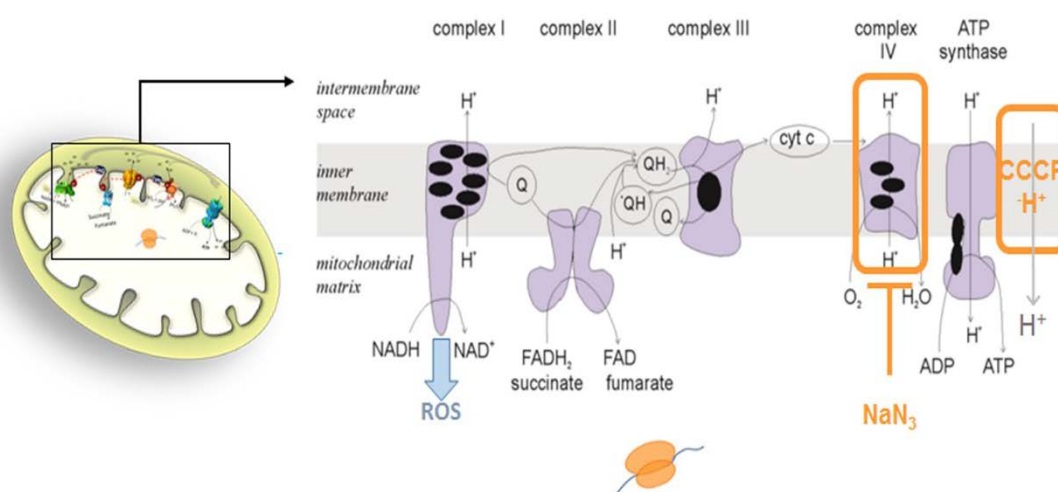


Figure 30. Induction of acute mitochondrial malfunction by chemicals - Scheme representing mitochondrial respiratory chain where NaN_3 and CCCP act to induce acute mitochondrial malfunction.

To study the effect of those acute mitochondrial malfunctions on mitochondrial shape and lysosomal number, HeLa cells were treated with NaN_3 and CCCP for 4 hours and stained with Mitotracker-Red and LysoTracker-Green. We assessed mitochondrial stress using microscopy. In the past, mitochondrial fission had been shown to be a phenotype of mitochondrial stress

(Cereghetti et al. 2008). Following these treatments, we observed mitochondria fragmented in cells treated with NaN_3 and even more in cells treated with CCCP (Fig. 31A). Also, a clear increase in the number of lysosomes was observed in cells treated with NaN_3 and the increase was stronger in cells treated with CCCP. Later, the lysosomes were quantified, using ImageJ, and the increase in the number of lysosomes was found to be significant (Fig. 31B).

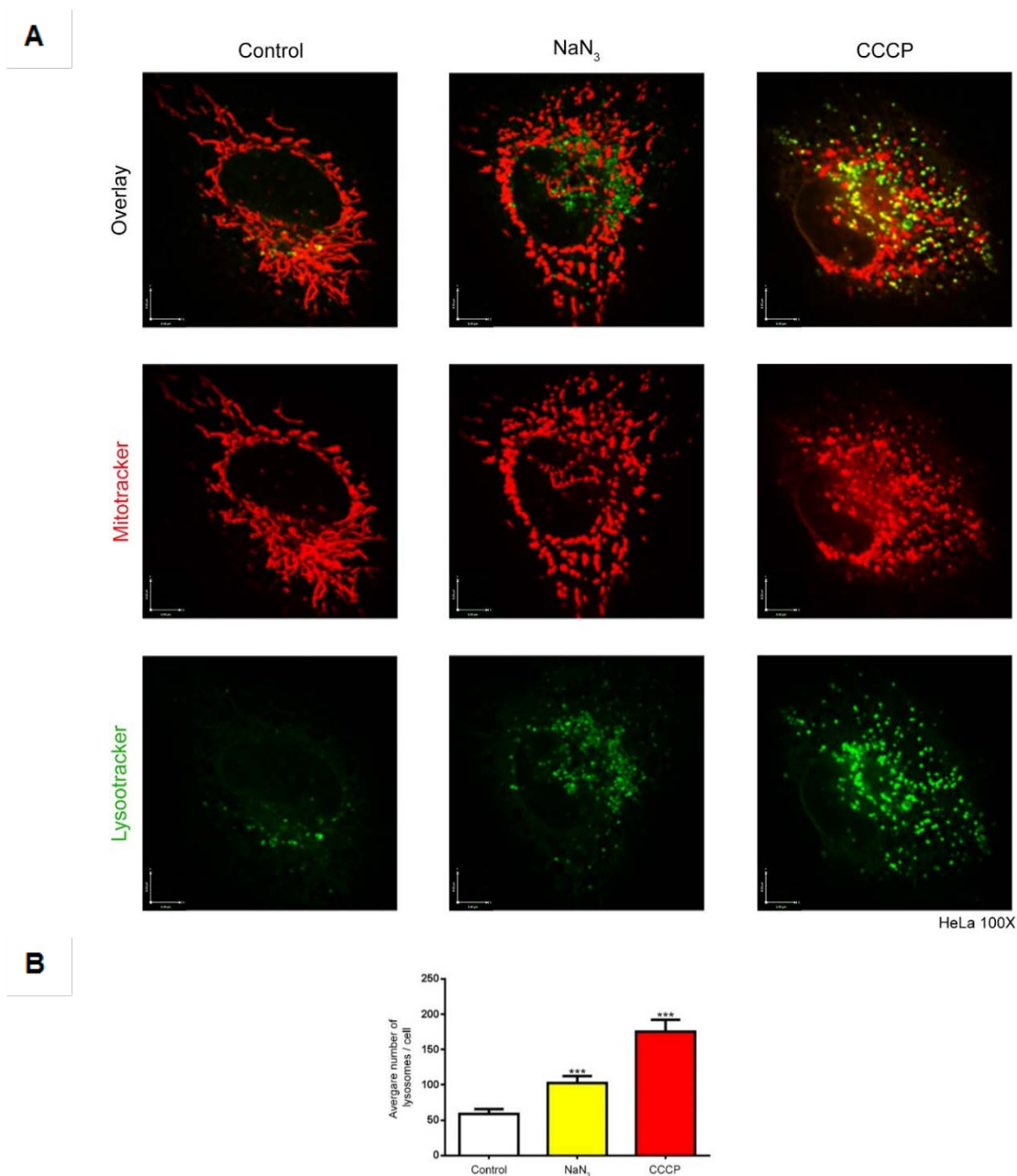


Figure 31. Representative images of mitochondria and lysosomes under acute mitochondrial malfunction triggered by chemicals – A) Microscopy in HeLa cells stained with Mitotracker Red and Lysotracker Green, showing that NaN_3 and CCCP

trigger mitochondrial fragmentation and increase in lysosomal number. B) Quantification showing an increase in the number of lysosomes per cell under acute mitochondrial malfunction

To verify that the increase in lysosomal number under acute mitochondrial malfunction was not an artifact related to the use of LysoTracker due to its reported pH sensitivity (Yapici et al. 2015), similar experiment was performed using HeLa cells previously transfected with GFP tagged lysosomal associated membrane protein 1 (LAMP1-GFP) (Fig 32A).

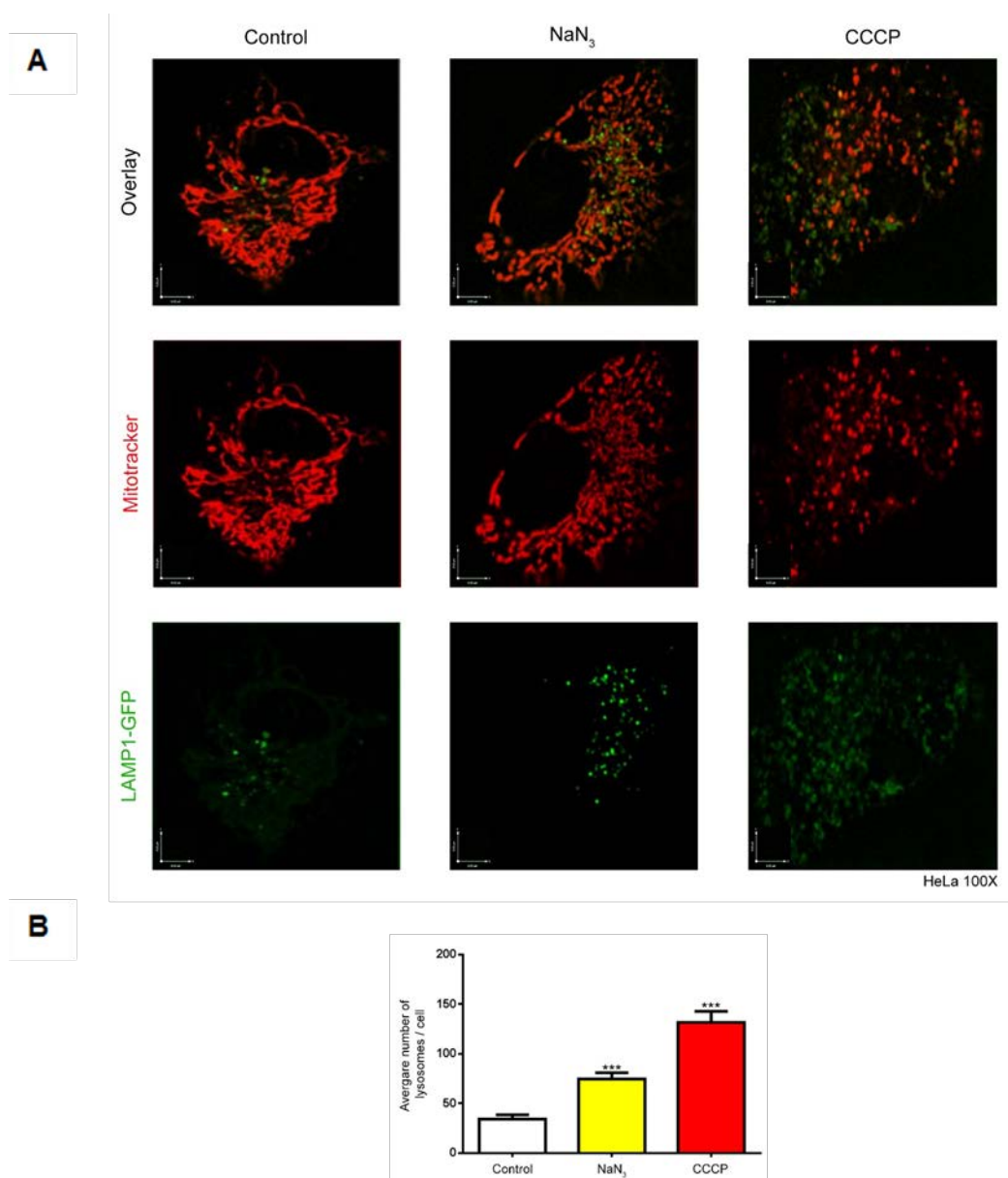


Figure 32. Representative images of mitochondria and lysosomes under acute mitochondrial malfunction triggered by chemicals, in cells with LAMP1-GFP – A) Microscopy, in HeLa cells tagged with Mitotracker Red and LAMP1-GFP, showing

that NaN_3 and CCCP trigger mitochondrial fragmentation and increase in lysosomal number. B) Quantification showing an increase in the number of lysosomes per cell under acute mitochondrial malfunction.

Again, the increase in lysosomal number was obvious in cells treated with NaN_3 and even more clear in cells treated with CCCP. Images were quantified using Image J, as it was done before. As expected, the result confirmed that the increase in lysosomal number was significant in both treatments (Fig. 32B).

With these results in mind, we decided to study the effects of acute mitochondrial malfunction on autophagy. To investigate those effects, the cells were treated again with NaN_3 and CCCP for 4 hours and an immunoblotting assay was performed with the whole cells extracts to detect microtubule-associated proteins 1B light chain 3B (LC3B). LC3B is in the cytoplasm but after a post-translational modification, it is translocated to the autophagosomal membrane where it is called LC3II (Tanida et al. 2005). The treated cells showed an increase in autophagy as indicated by the LC3II/LC3I ratio, meaning that there were more autophagosomes in stressed cells than in control cells (Fig. 33).

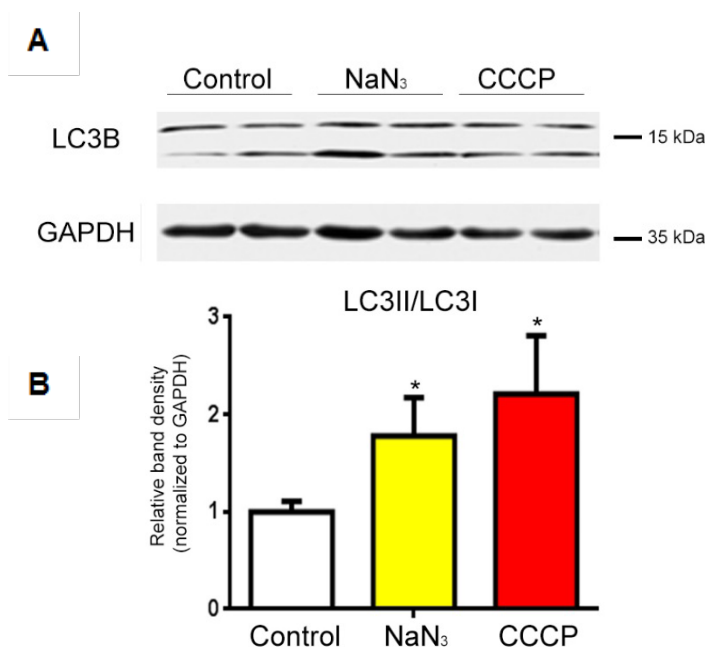


Figure 33. Autophagy under acute mitochondrial malfunction – A) Western blot of LC3 in HeLa cells treated with NaN_3 and CCCP during 4 hours. B) Quantification showing an increase in of LC3II/LC3I ratio corresponding with an increase in autophagy under acute mitochondrial malfunction caused by NaN_3 or CCCP.

These results indicate that acute mitochondrial malfunction, caused by inhibition of mitochondrial respiratory chain, induces an increase in lysosomal number and triggers autophagy.

3.1.2 Effects of acute mitochondrial malfunction caused by transient UQCRC1 knock-downs on lysosomes and autophagy.

With the aim of investigating the effects of acute mitochondrial malfunction on lysosomes and autophagosomes more extensively, we decided to use another kind of stress. This was aimed at elucidating whether the effects observed were not merely due to chemical treatment rather due to a mitochondrial stress response, as there could be concerns if the chemicals were not specific enough.

To achieve this goal, we used transient knock-downs, in this case, ubiquinol-cytochrome C reductase core protein 1 knock-downs (UQCRC1kd) in HeLa cells, which affects complex III of the mitochondrial respiratory chain (Fig. 34).

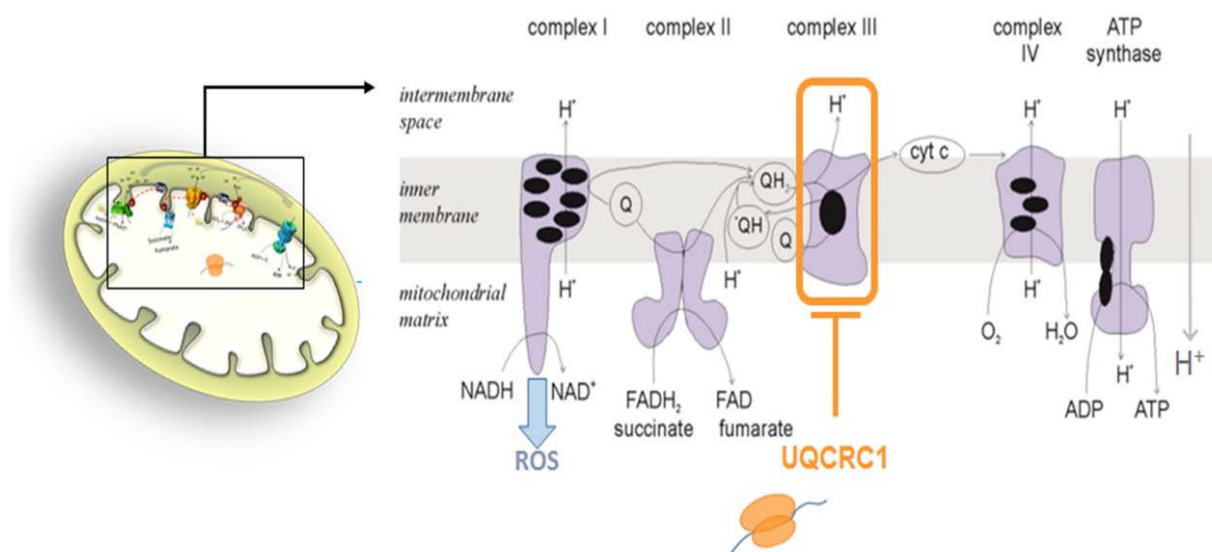


Figure 34. Induction of acute mitochondrial malfunction by transient knock-down - Scheme that represents mitochondrial respiratory chain and UQCRC1, which is a subunit of complex III.

These cells were transfected with shRNA, and 24 hours post-transfection the cells were stained using Mitotracker-Red and LysoTracker-Green. Also, the images were acquired using a spinning-disk confocal microscope and we observed, once again, a strong increase in the number of lysosomes and mitochondrial fragmentation (Fig 35).

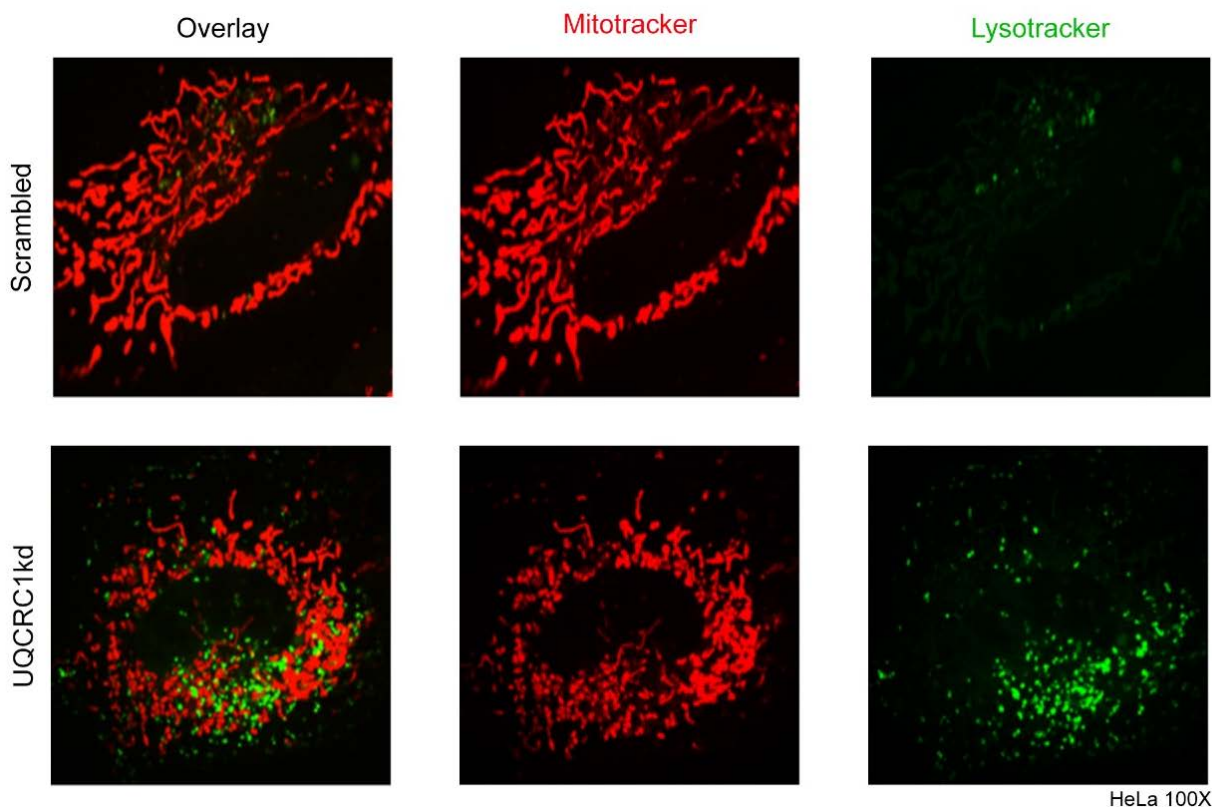


Figure 35. Representative images of mitochondria and lysosomes in cells under acute mitochondrial malfunction triggered by transient UQCRC1kd – Microscopy, in HeLa cells stained with Mitotracker Red and Lysotracker Green, showing mitochondrial fragmentation and increase in lysosomal number.

In order to confirm the increase of lysosomes in transient UQCRC1kd and at the same time check the effect of this acute response on autophagy, we double transfected UQCRC1kds with LAMP1-GFP and LC3-RFP (Fig. 36A). The result showed an expected increase in lysosomes in UQCRC1 and a correlated increased in autophagosome number and both corresponded with an increase in the number of autophagolysosomes as shown in the magnified image (Fig. 36B).

These results confirm that the previous observation, in which acute mitochondrial malfunction induced by chemicals triggered an increase in the number of lysosomes and autophagosomes, was due to the mitochondrial stress and not due to the system we used to induce the stress. We can therefore conclude that acute mitochondrial malfunction induces an increase in the number of lysosomes and autophagosomes regardless of the stress source.

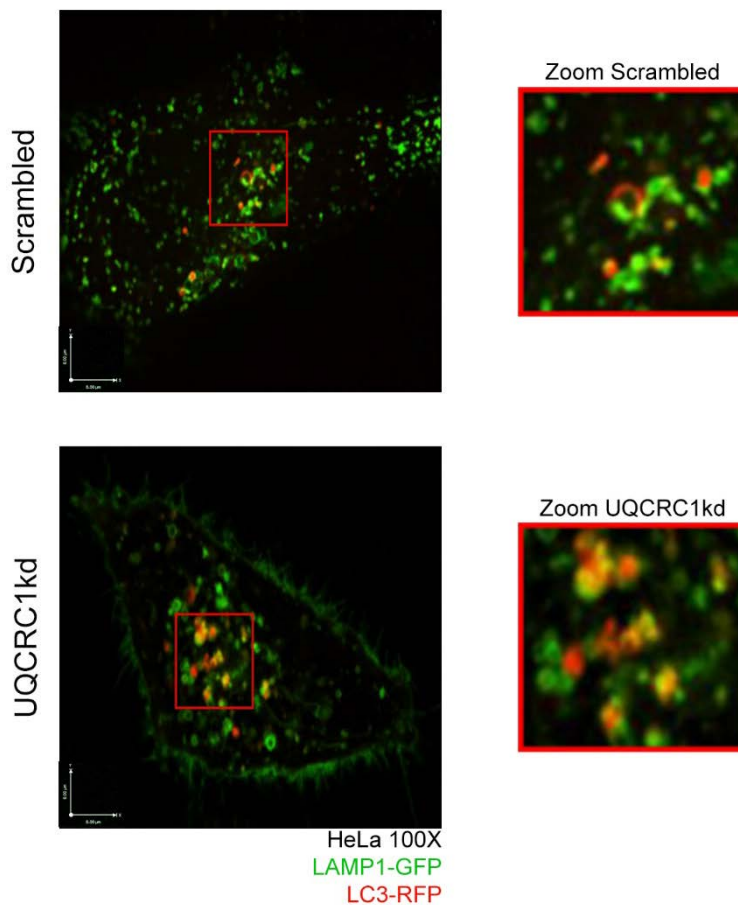


Figure 36. Representative image of lysosomes and autophagosomes in cells under acute mitochondrial malfunction triggered by transient UQCRC1kd – Microscopy, in HeLa cells tagged with LAMP1-GFP and LC3-RFP showing, in the left side, an increase in autophagosomes and lysosomes in UQCRC1kd. In the right side, there are zooms showing colocalization of LC3 and LAMP1 that represents an increase of autophagolysosomes in UQCRC1kd.

3.1.3 Effects of acute mitochondrial malfunction on lysosomal biogenesis

At this point, it was clear that acute mitochondrial malfunction was increasing the number of lysosomes. But what was not clear to us, was whether this increase was due to division of lysosomes or because mitochondrial stress was triggering lysosomal biogenesis.

With this in mind, we investigated if lysosomal biogenesis was affected by acute mitochondrial malfunction. In order to study how lysosomal-related genes were responding to the mitochondrial dysfunction, HeLa cells were treated with the mitochondrial uncoupler, CCCP, and the transcript levels of several genes encoding lysosomal proteins were measured using qPCR. It was observed that the transcript levels of lysosomal-related genes such as Lysosomal-associated membrane

protein 1 (LAMP1), Alpha Acid Glucosidase (GAA), Cathepsin D (CTSD) and Cathepsin F (CTSF) were increasing during the treatment (Fig. 37).

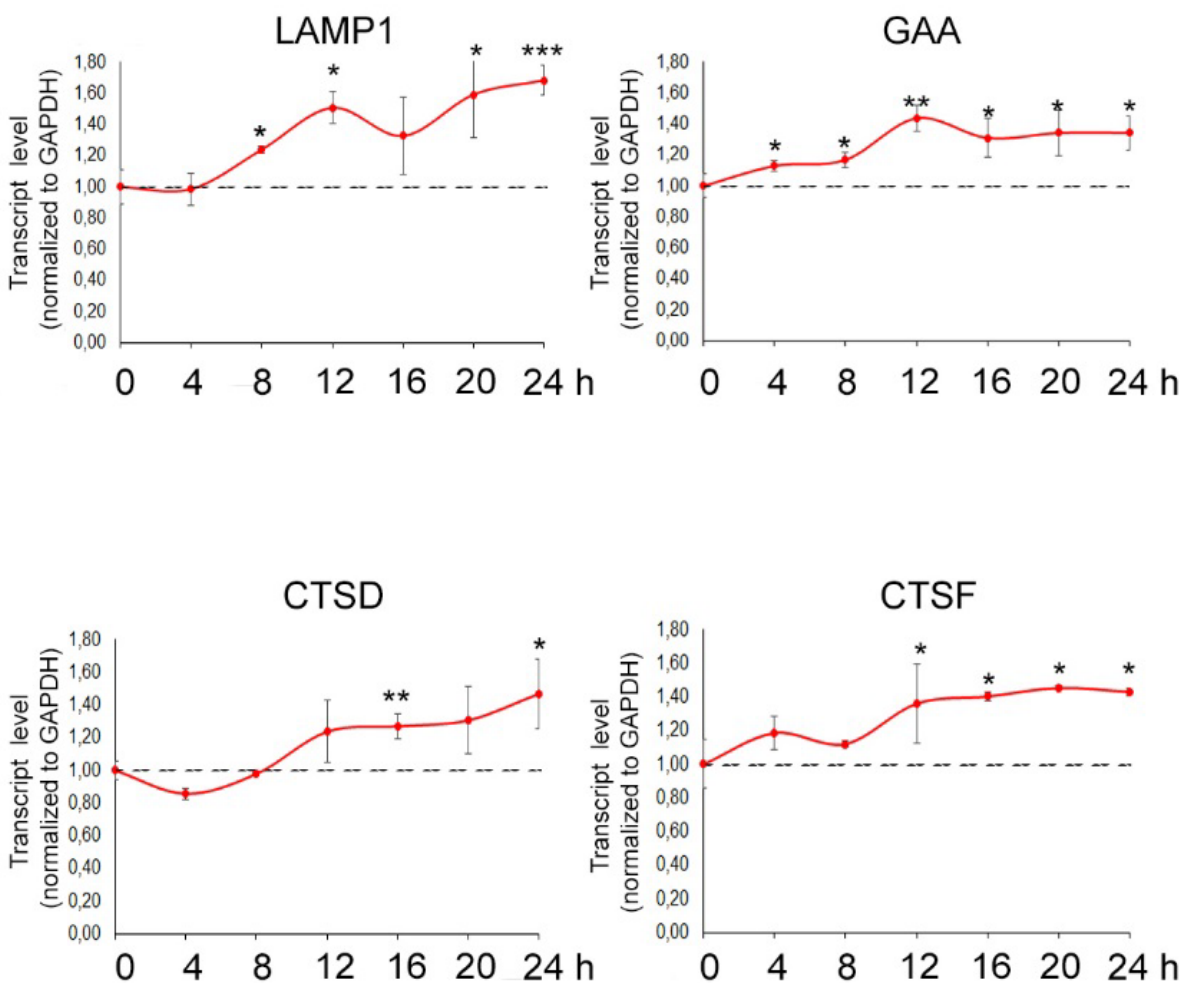


Figure 37. Effects on transcript levels of lysosomal-related genes caused by acute mitochondrial malfunction – Normalized transcript levels showing that increase along the time of LAMP1, GAA, CTSD and CTSF in cells the treated with CCCP.

This result shows that the increase in lysosomes due to acute mitochondrial dysfunction is likely to have been caused by an activation of lysosomal biogenesis.

3.1.4 Effects of acute mitochondrial malfunction on TFEB/MITF levels

Given the previously reported role of transcription factor EB (TFEB) in coordinated lysosomal biogenesis (Sardiello et al. 2009) and keeping our results in mind, we wanted to elucidate if TFEB

was involved in the lysosomal increase induced by acute mitochondrial malfunction. Again, HeLa cells were treated with CCCP and collected at different time points. A western blot analysis was performed and the results show that, under acute mitochondrial malfunction, there is an increasing trend in TFEB amount that reaches a maximum around 8-12 hours (Fig. 38A, B).

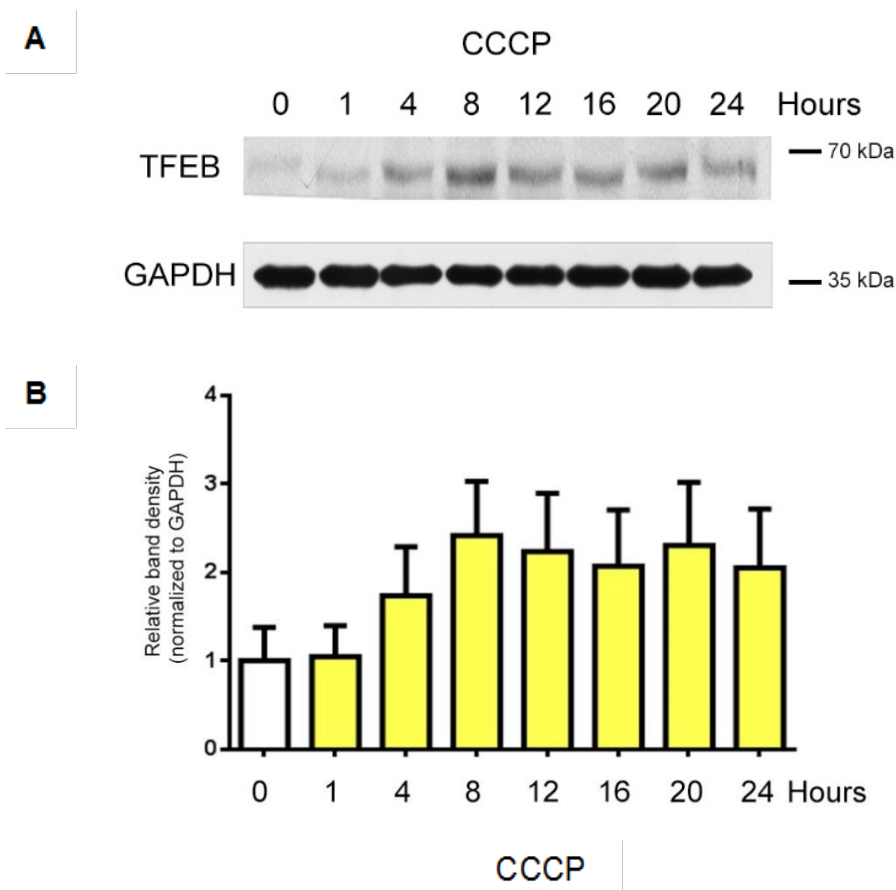


Figure 38. Effects on TFEB protein amount caused by acute mitochondrial malfunction – A) Western blot of TFEB in HeLa cells treated with CCCP and collected at different time points. B) Quantification of TFEB showing an increase in the protein amount during the treatment with CCCP.

However, it must be stated that TFEB belongs to the microphthalmia family that is formed by four members; TFEB, MITF, TFE3 and TFEC (Kuiper et al. 2004). Also, TFEB and MITF have been found to respond to similar stressors (Martina and Puertollano 2013) being translocated to the nucleus, where they can form homo- and hetero-dimers (Martina et al. 2014). To address the role of microphthalmia transcription factors TFEB and MITF and under acute mitochondrial malfunction, HeLa cells were treated with CCCP. We then monitored the transcript levels of TFEB and MITF over time. Both transcription factors show a similar response with an up-regulation in response to mitochondrial stress that is followed by a return to the baseline under both treatments (Fig. 39).

On the other hand, it was evident that they have different reaction times. While MITF was steeply upregulated and downregulated, TFEB had a more sustained expression returning to the basal line gently. (Fig. 39).

Since TFEB and MITF transcript levels increase strongly, initially in response to mitochondrial

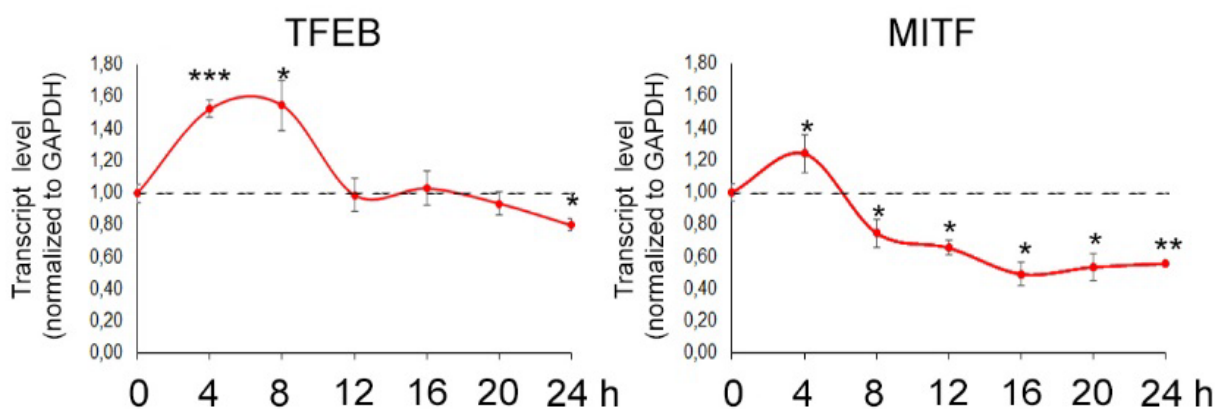


Figure 39. Effects TFEB and MITF transcript levels caused by acute mitochondrial malfunction – Normalized transcript levels showing that TFEB levels are and fast up-regulation with a mild turning to the base line during the treatment, while MITF has a fast up-regulation follow by a fast down-regulation.

stress, this could be the trigger for the observed lysosomal biogenesis:

In order to identify which transcription factor was responsible for the increase in lysosomal number, a set of stable TFEBkd were generated. The efficiency of the silencing was checked using western blot and the most efficient was used (Fig. 40A). Since MITF and TFEB are members of the same family and there is the possibility that the activity of one affects the activity of the other, MITF was silenced using siRNA in scrambled and stable TFEBkd (Fig. 40B). The efficiency of MITFkd was tested using qPCR. Also, it was checked that TFEBkd has no effect on MITF and that MITFkd has no effect over TFEB (Fig. 40C).

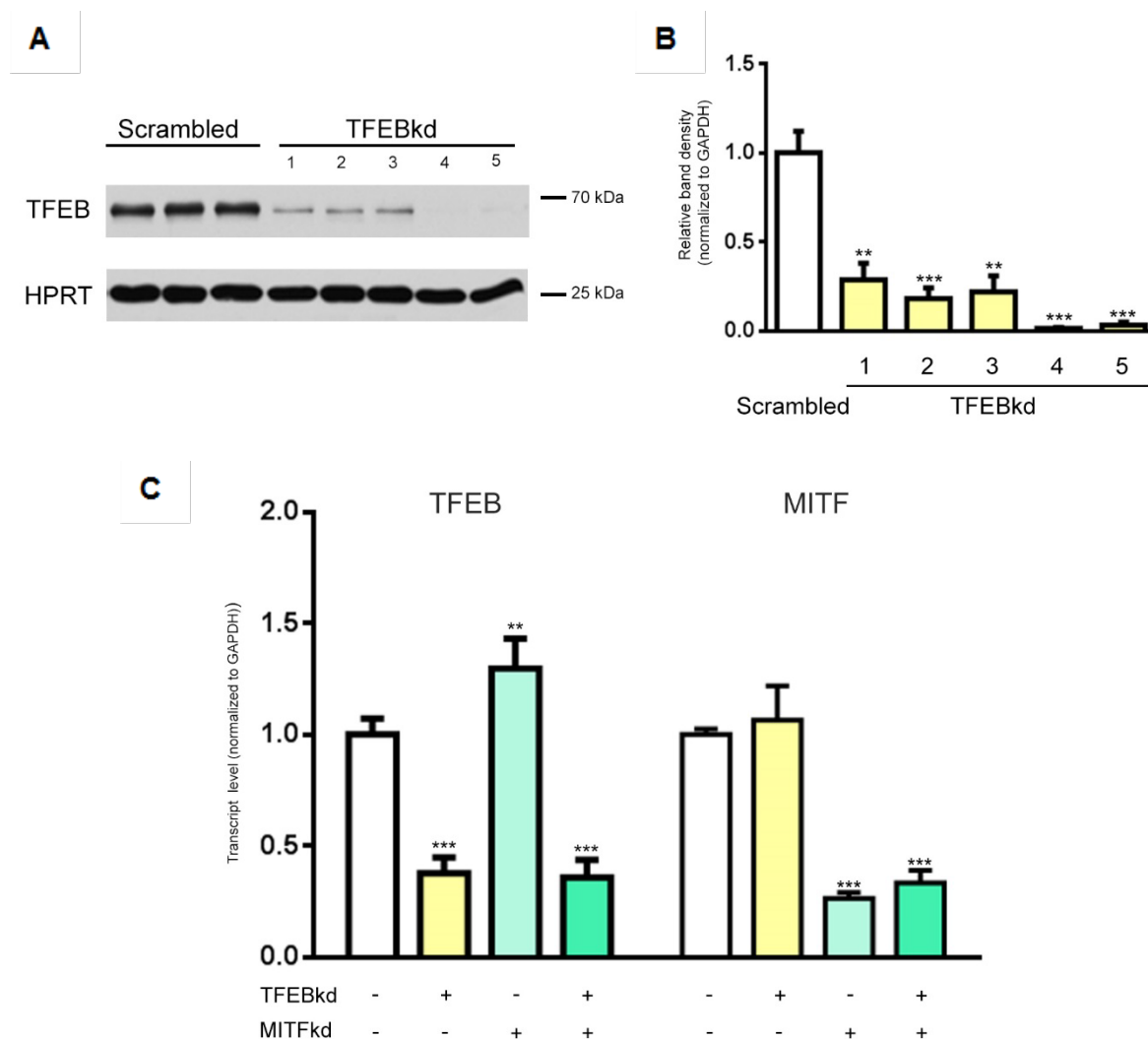


Figure 40. Effects of TFEB knock-down on MITF and of MITF knock-down on TFEB – A) Western blot of five different stable TFEBkds in HeLa. B) Quantification of stable TFEBkds. C) Graph showing that transcript levels of TFEB are not decreased by MITFkd and that transcript levels of MITF are not affected by TFEBkd.

Once the independency of TFEB and MITF was confirmed, the cells were treated with CCCP in order to verify which of the two transcription factors was related to lysosomal biogenesis under acute mitochondrial malfunction. As it was expected, CCCP treatment induced an increase in the expression levels of lysosomal-related genes tested in scrambled cells (Fig. 41). Although the TFEB/MITF knock-down cells were not able to mimic the changes in the transcription levels of almost all the lysosomal genes, like LAMP1 or CTSD, they could not inhibit the induction of GAA (Fig. 41). These results show that induction of lysosomal biogenesis caused by acute mitochondrial malfunction is, at least, partially dependent on TFEB/MITF.

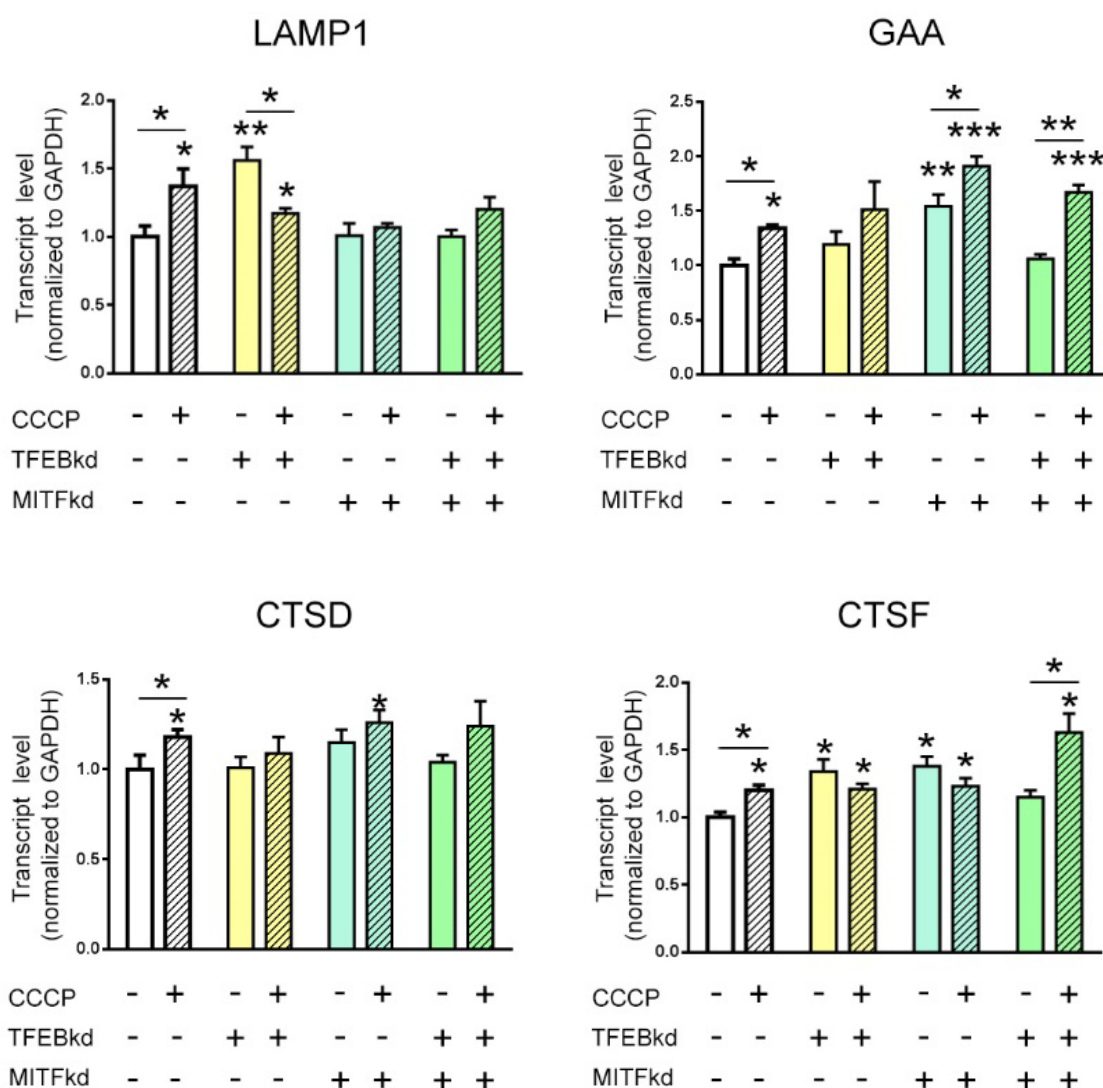


Figure 41. Effects on transcript levels of lysosomal-related genes caused by acute mitochondrial malfunction on TFEB and MITF knock-downs – Graphs showing that acute mitochondrial malfunction induces increase in the expression levels of lysosomal-related genes in scrambled cells. While the TFEB/MITF knock-down cells were not increasing transcription levels on almost all the lysosomal genes, like LAMP1 or CTSD, they could not inhibit the induction of GAA.

3.1.5 Acute mitochondrial malfunction and AMPK

Finally it was necessary to address the mechanism by which acute mitochondrial malfunction was driving lysosomal biogenesis. It was already shown that acute mitochondrial malfunction activated TFEB/MITF signaling (Fig 37), and this signaling resulted in increased lysosomal biogenesis (Fig. 31, 32). However, it was necessary to determine the connection between acute mitochondrial malfunction and TFEB/MITF. It is known that AMPK responds to mitochondrial stress (Raimundo

et al. 2012). At the same time, AMPK represses mTORC1 which in turn represses TFEB activity (Fig. 42). With this in mind, the next experiment was designed to define the role of AMPK in this response.

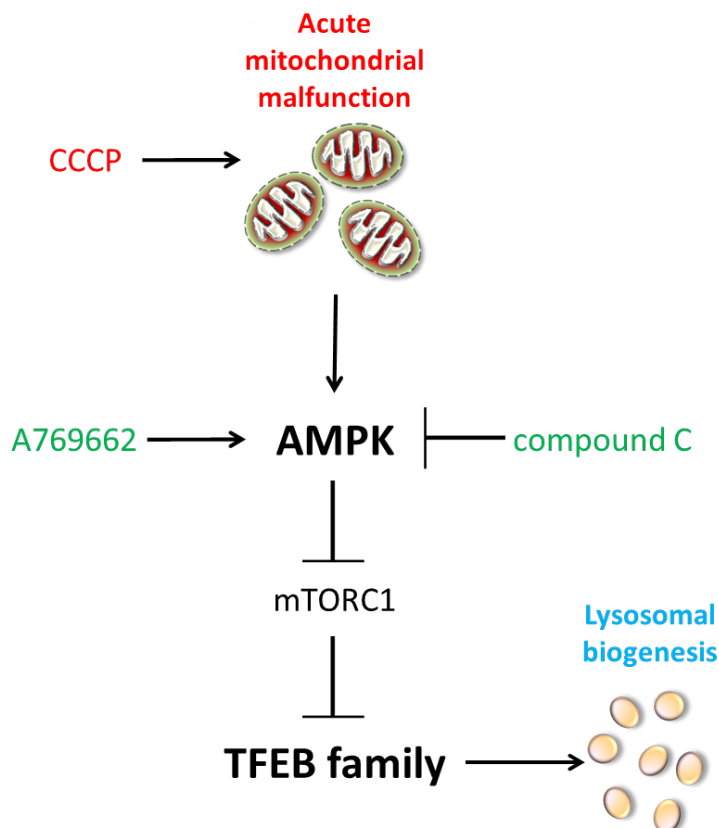


Figure 42. Pathway that connects acute mitochondrial malfunction with lysosomal biogenesis – Acute mitochondrial malfunction triggers TFEB-dependent lysosomal biogenesis via AMPK.

In order to determine the role of AMPK in lysosomal biogenesis under acute mitochondrial malfunction, HeLa cells were treated with CCCP and with dorsomorphine (compound C), which is a known inhibitor of AMPK (Zhou et al. 2001; Fryer et al. 2002). After 4 hours of treatment the transcript level of lysosomal-related genes such as LAMP1, GAA, CTSD or CTSF were strongly increased as it was expected. Despite of this, when the cells were treated simultaneously with CCCP and the AMPK inhibitor, compound C, the increase was blocked (Fig. 43A). These results suggest that AMPK signaling is needed for the activation of lysosomal biogenesis by acute mitochondrial malfunction. This activation is triggered through TFEB/MITF signaling as shown in Fig. 43B, in which treatment with CCCP increased the transpiration levels of TFEB family

members while when the cells were treated with compound C simultaneously, the response was ablated.

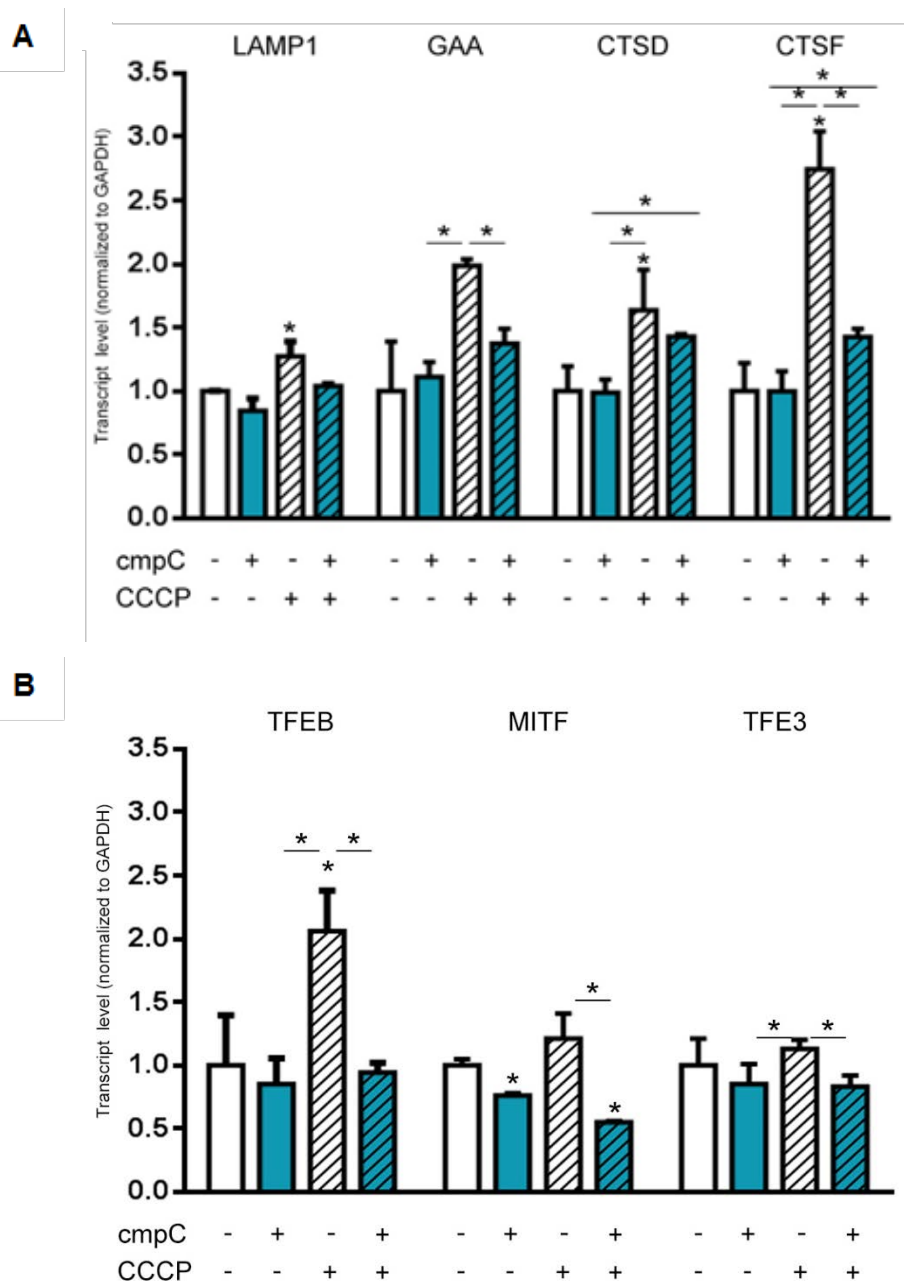


Figure 43. Effects on transcript levels of lysosomal-related genes and MITF family caused by acute mitochondrial malfunction in presence of an AMPK inhibitor – A) Normalized transcript levels showing that acute mitochondrial malfunction induces an increase of LAMP1, GAA, CTSD or CTSF that was blocked in the presence of AMPK inhibitor. B) Normalized transcript levels showing that acute mitochondrial malfunction induces increase of TFEB, MITF and TFE3 that was blocked in the presence of AMPK inhibitor.

Furthermore, we tested if the activation of AMPK alone, without any kind of mitochondrial stress, was enough to trigger lysosomal biogenesis. For this purpose, the cells were treated with A769662, a known activator of AMPK (Zhang et al. 2014), for 4 hours and the transcript levels of lysosomal-related genes were measured (Fig. 44). The qPCR showed that the transcript levels of lysosomal genes did not change. This implies that AMPK activation alone is not enough to trigger TFEB/MITF-dependent lysosomal biogenesis in the absence of mitochondrial stress.

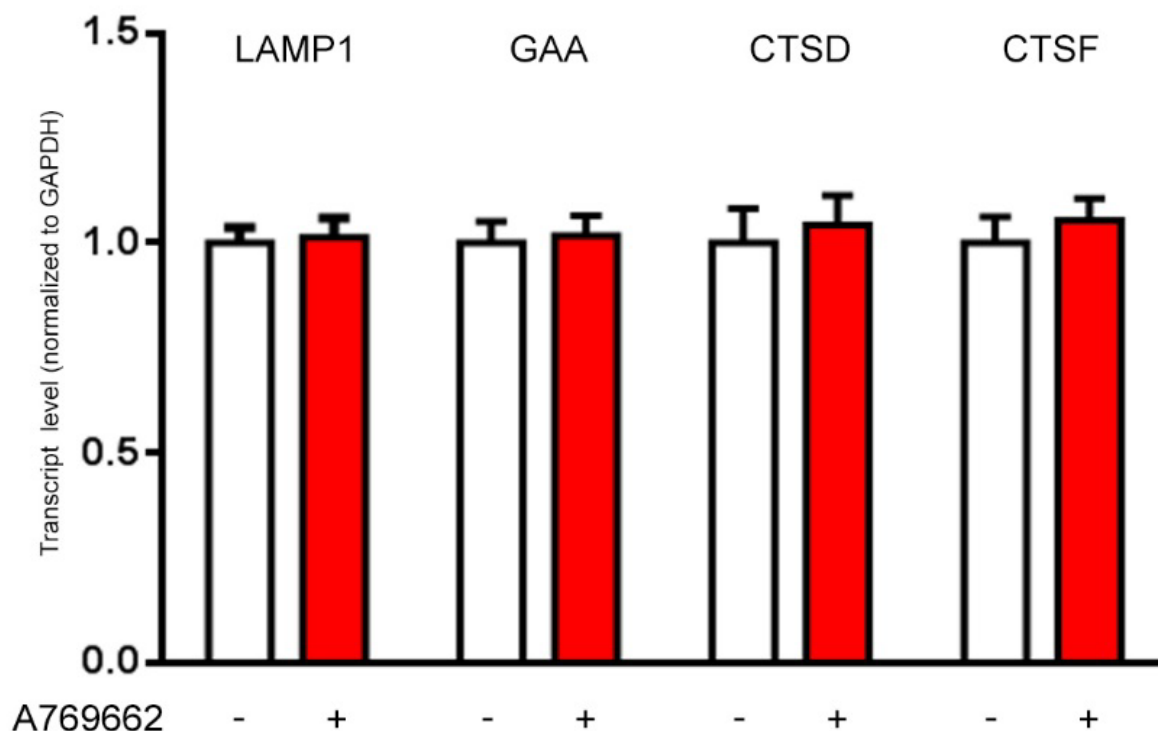


Figure 44. Effects on transcript levels of lysosomal-related genes by an AMPK activator – The graph shows the absence of changes in the transcript levels of lysosomal-related genes in the presence of AMPK activator.

3.1.5 Acute mitochondrial malfunction and calcineurin

Furthermore, TFEB is not only regulated by AMPK but the regulatory pathway of TFEB also involves calcineurin. (Medina et al. 2015) (Fig 45A). Our previous results showed the importance of AMPK, showing that it is necessary for the lysosomal biogenesis mediated by TFEB. However, it is important to also determine if calcineurin plays a role in this process.

In order to determine the role of calcineurin in TFEB regulated lysosomal biogenesis, during acute mitochondrial malfunction, HeLa cells were treated with CCCP and with FK506, a known inhibitor

of calcineurin (Cereghetti et al. 2008; Medina et al. 2015). The results showed that while the cells treated with CCCP had increased transcription levels of genes related to lysosomes, like LAMP1, GAA, CTSD or CTSF, in the cells treated simultaneously with CCCP and FK506, the increase was in general not ablated (Fig. 45B). From this result, we can conclude that the induction of lysosomal biogenesis under acute mitochondrial malfunction is mainly through AMPK and calcineurin-independent.

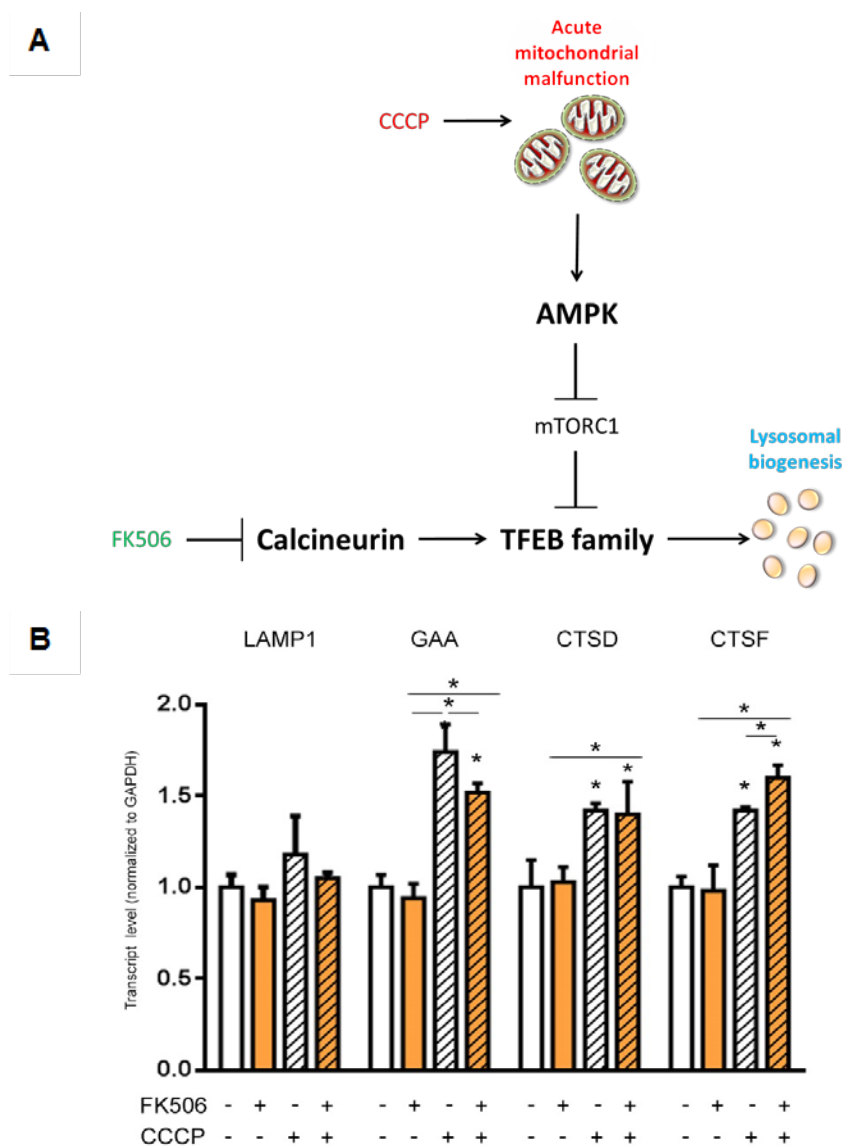


Figure 45. Acute mitochondrial malfunction and calcineurin – A) Pathway connecting acute mitochondrial malfunction with lysosomal biogenesis. B) Acute mitochondrial malfunction increases the transcription levels of LAMP1, GAA, CTSD or CTSF, while under calcineurin inhibition the increase in lysosomal-related genes in general was not ablated.

3.2 Chronic mitochondrial stress

3.2.1 Chronic mitochondrial malfunction model

In order to study chronic mitochondrial stress we generated a cellular model of stable UQCRC1kd in HeLa cells in which the expression of UQCRC1 is permanently reduced. Ubiquinol-cytochrome C reductase core protein 1 (UQCRC1) is the largest nuclear-encoded subunit of complex III of the mitochondrial respiratory chain (Hoffman et al. 1993). This core protein is involved in the electron transfer from ubiquinol (QH₂) to ferricytochrome c with the coupled translocation of protons across the mitochondrial inner membrane (Hoffman et al. 1993). UQCRC1 perturbations were described in relation with mitochondrial diseases such as myopathy, encephalomyopathy and cardiomyopathy (Kennaway 1988) or neurological disorders like the Rett syndrome (Kriaucionis et al. 2006).

Different regions of UQCRC1 gene were silenced using diverse shRNAs. The efficiency of the UQCRC1 knock-down was proven through western blot analysis to determine which short hairpin RNA (shRNA) led to the strongest silencing (Fig. 46) and the two strongest knock-downs were used in subsequent experiments.

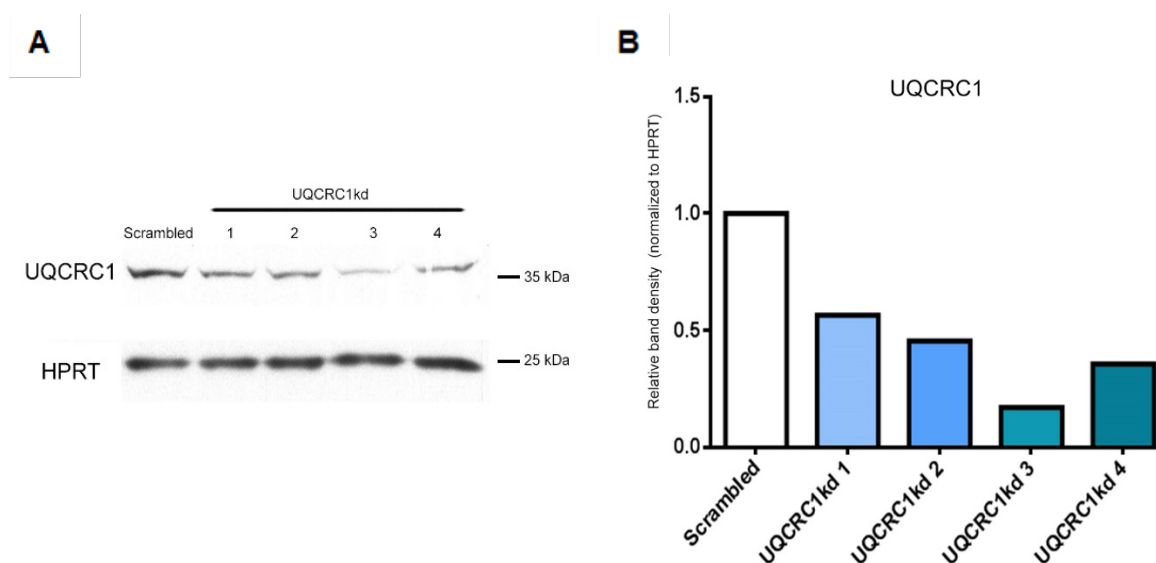


Figure 46. Western blot of stable UQCRC1 knock-down – A) Western blot of five different UQCRC1kds in HeLa. B) Graph showing the quantification of UQCRC1kds.

3.2.2 Effects of stable UQCRC1 knock-down on mitochondria

As UQCRC1 is a core subunit of complex III of the mitochondrial respiratory chain, we proposed that silencing it would perturb respiratory chain function and as a consequence affect the integrity of mitochondria. To determine the effect of UQCRC1 knock-down in mitochondria different methods were applied.

The stable UQCRC1kd cells were transfected with a cyan-fluorescence protein targeted to the mitochondria and fixed 24 hours post-transfection. The mitochondrial morphology was observed using a spinning-disk confocal microscope. Again, with mitochondrial fission as an indicator of mitochondrial stress (Cereghetti et al. 2008), we observed that chronic mitochondrial stress, caused by UQCRC1kd, resulted in a clear mitochondrial fragmentation (Fig 47).

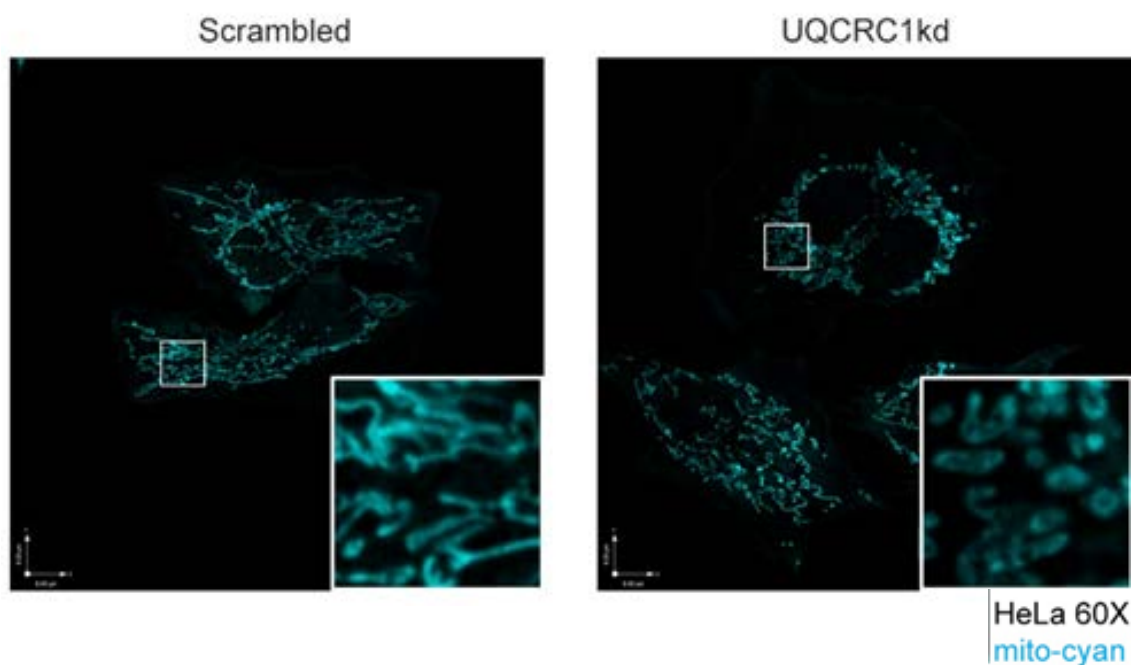


Figure 47. Representative images of cells with and without chronic mitochondrial malfunction – Microscopy of HeLa cells tagged with a cyan-fluorescence protein targeted to the mitochondria showing, in the left side, an increase in mitochondrial fragmentation in stable UQCRC1kd.

After this initial experiment in which stable UQCRC1kd showed a phenotype that corresponded to mitochondrial stress, it was necessary to study other parameters to confirm that mitochondria were actually affected.

It is well characterized that some defects in mitochondrial respiratory chain subunits perturb mitochondrial oxygen consumption rate (OCR) (Invernizzi et al. 2012) and we verified this using

the impact of UQCRC1kd on OCR. This effect was measured by Real Time Respirometry (Seahorse Biosciences). The results confirmed a decrease in OCR associated with UQCRC1kd (Fig.48A). On the other hand, mitochondrial stress is associated with the production of reactive oxygen species (ROS) (Raimundo et al. 2012), which we found to be significantly increased in UQCRC1kd compared to the control (Fig. 48B). Also, the mitochondrial membrane potential was measured using flow cytometry and as expected, the membrane potential was reduced in the stable UQCRC1kd in comparison to the scrambled cells (Fig. 48C).

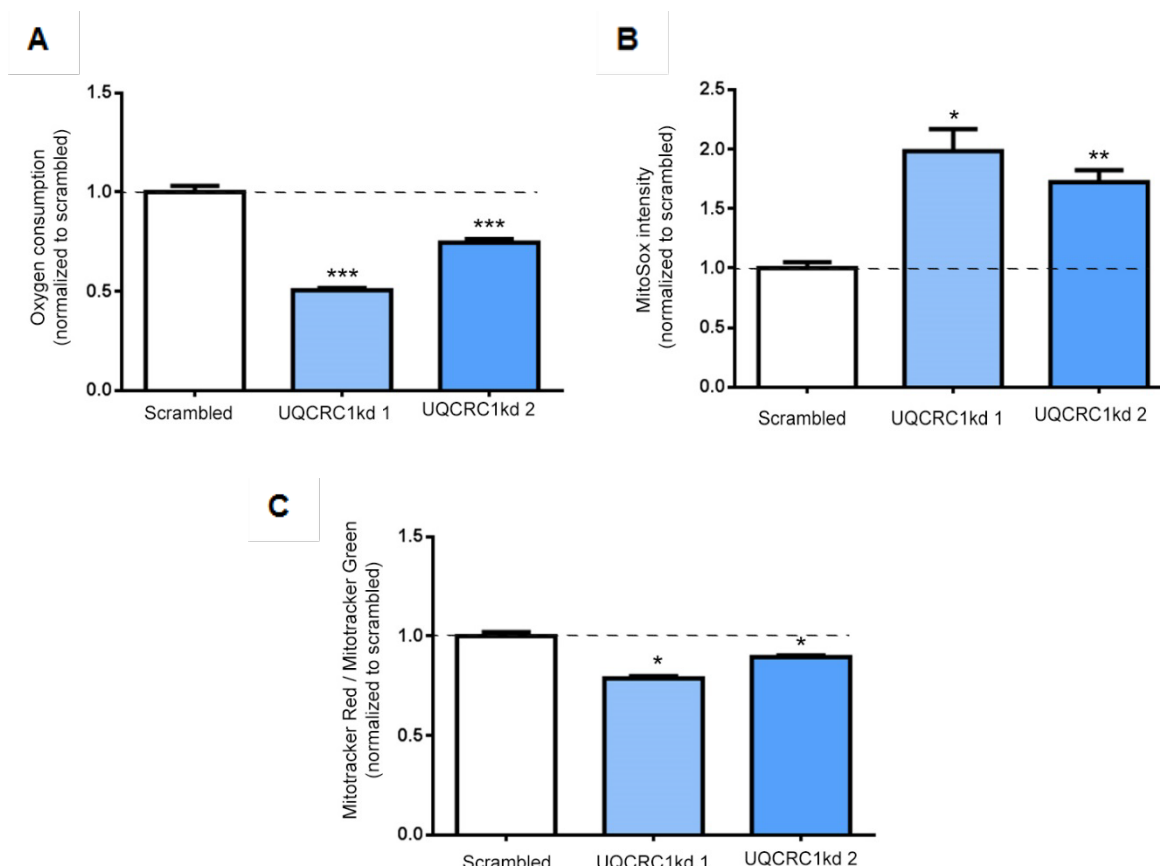


Figure 48. Effects on mitochondria caused by chronic mitochondrial malfunction – A) Stable UQCRC1kd showing a decrease in oxygen consumption rate. B) Stable UQCRC1kd showing an increase in reactive species production. C) Stable UQCRC1kd showing a decrease in mitochondrial membrane potential.

3.2.3 Effects of chronic mitochondrial malfunction on lysosomal morphology and function

Having shown the effects of stable UQCRC1kd on mitochondria, we studied the effect of chronic mitochondrial malfunction on lysosomes. With this aim, we first evaluated lysosomal mass in

stable UQCRC1kd and observed an increase in the amount of LAMP1 at protein level in the UQCRC1kds (Fig. 49A, B). This increase in lysosomal mass was confirmed using HeLa stable UQCRC1kd stained with LysoTracker Green. The intensity of LysoTracker was measured with two independent systems, plate reader (Fig. 49C) and fluorescence-activated cell sorting (Fig. 49D). As it was expected, in both cases, the increase of lysosomal mass in stable UQCRC1kds was confirmed.

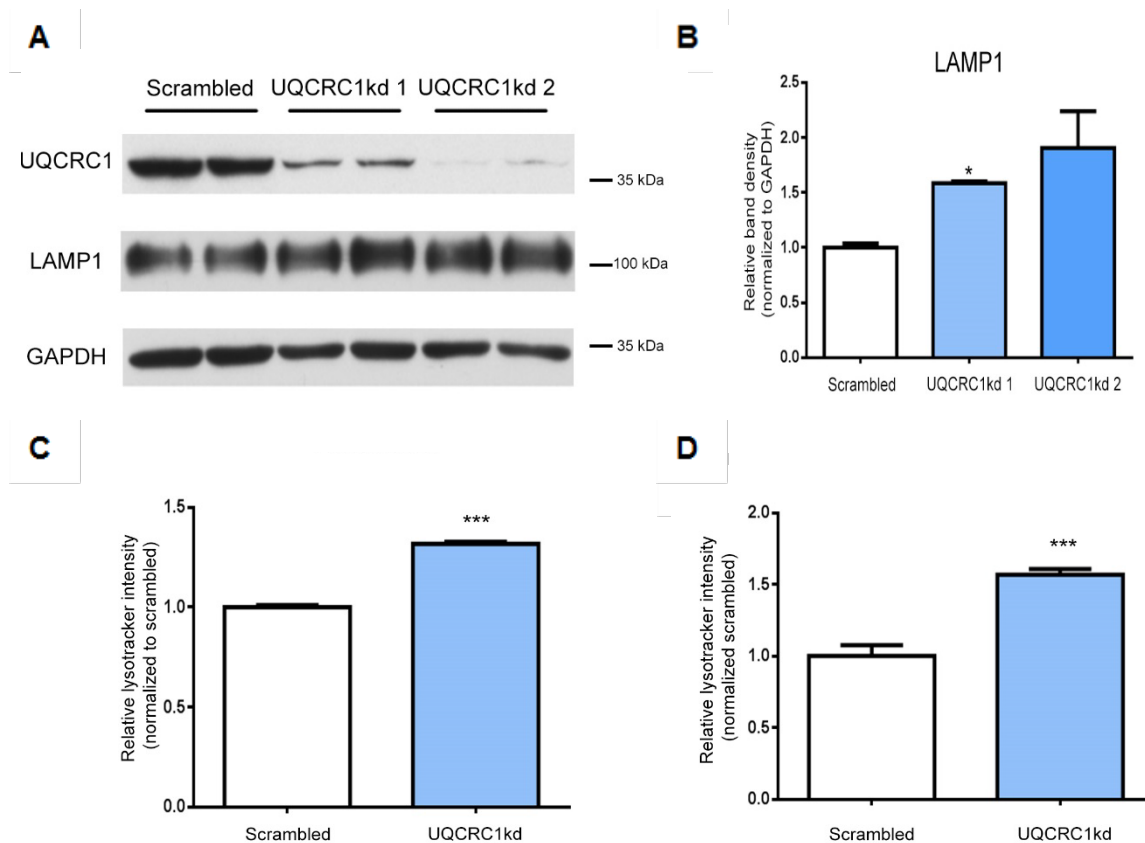


Figure 49. Effects on lysosomes caused by chronic mitochondrial malfunction – A) Western blot of LAMP1 in stable UQCRC1kd. B) Quantification of LAMP1 showing an increase under chronic mitochondrial malfunction. C) Graph showing an increase in relative LysoTracker intensity in stable UQCRC1kd determined by plate reader. D) Graph showing an increase in relative LysoTracker intensity in stable UQCRC1kd determined by flow cytometry.

Despite showing an increase in lysosomal mass using LAMP1 protein levels and LysoTracker intensity, we decided to further check the abundance of other lysosomal proteins. We observed increased amounts of v-ATPase Subunit A1 (ATP6V0A1) and v-ATPase Subunit V1 Subunit A

(ATP6V1A); subunits of the vacuolar proton pump (V-ATPase) (Fig. 50 A, B), which are in agreement with the data described above.

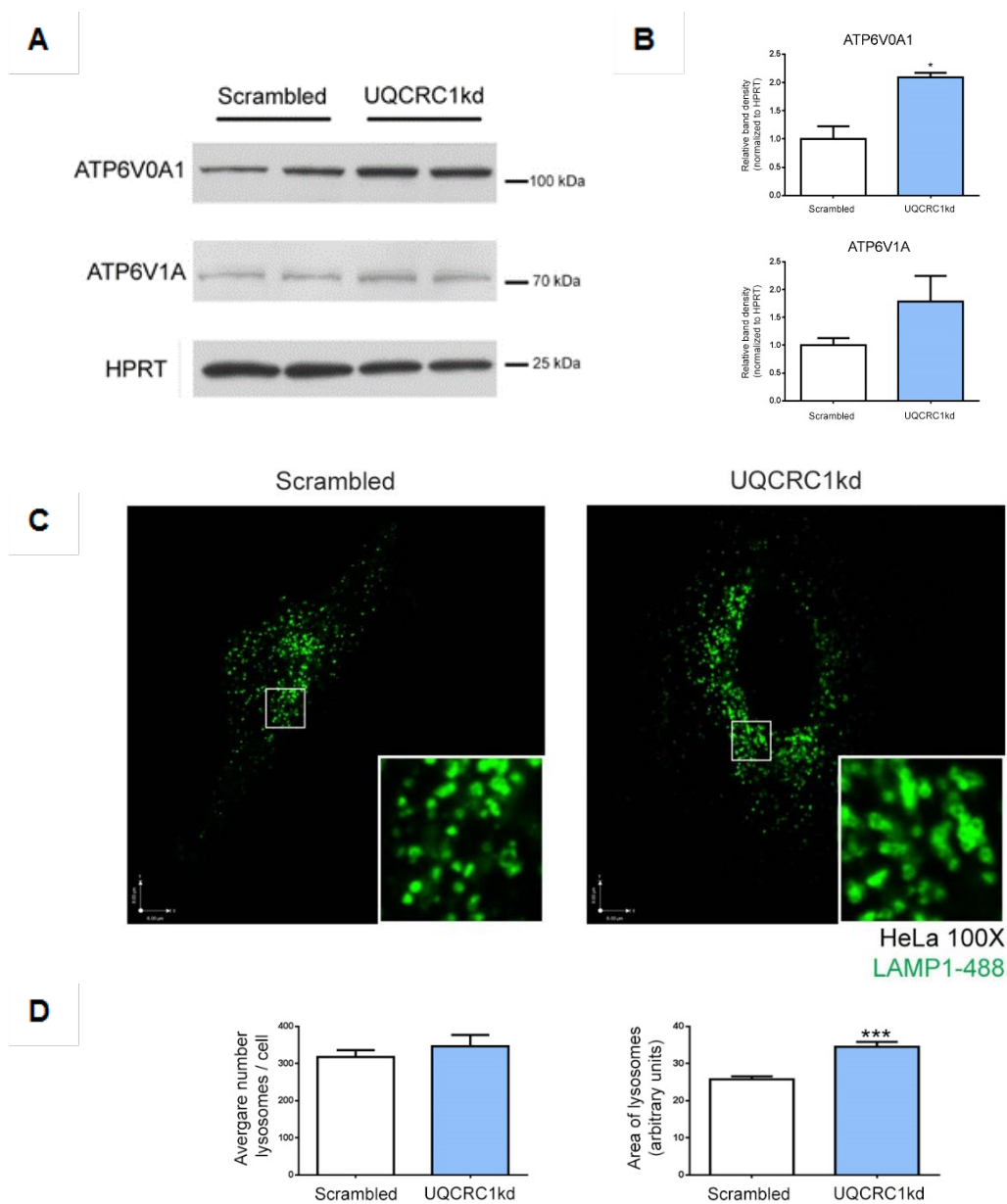


Figure 50. Effects on lysosomal mass caused by chronic mitochondrial malfunction – A) Western blot of ATP6V0E1 and ATP6V1A in stable UQCRC1kd. **B)** Quantification showing trend to increase of ATP6V0E1 and ATP6V1A under chronic mitochondrial malfunction. **C)** Microscopy images of HeLa cells stained with LAMP1 green showing an increase in lysosomal mass in stable UQCRC1kd. **D)** Quantifications showing that increase in lysosomal mass of UQCRC1kd was related to an increase in the lysosomal size.

We set out to determine whether the increase in lysosomal mass correlated with an increase in the number of lysosomes. We stained the lysosomes by immunocytochemistry using an antibody against the lysosomal protein LAMP1 on fixed HeLa UQCRC1kds and images were taken using a spinning-disk confocal microscope. Surprisingly, it became very clear that there was no increase in the number of the lysosomes (Fig. 50C). However, the lysosomes appeared larger in the UQCRC1kds and quantification, using ImageJ, confirmed a significant increase in the area of the lysosomes (Fig. 50D). We concluded from these results that chronic mitochondrial stress induced an increase in lysosomal mass, which was associated with an enlargement of the lysosomes.

Given that it has been widely shown that most LSDs present enlarged lysosomes, (Li et al. 2016), we found it necessary to evaluate the proteolytic capacity of these enlarged lysosomes using DQ-BSA. DQ-BSA is an assay in which a labeled derivative of bovine serum albumin (BSA) is driven to the lysosomes through phagocytosis. Once the DQ-BSA is in the lysosome, the proteolytic activity of the lysosomes releases the fluorophore thereby increasing the fluorescence that is measured by the plate reader. In the UQCRC1kds the proteolytic activity of the lysosomes was found to be compromised, even if there was an increase in lysosomal mass (Fig. 51).

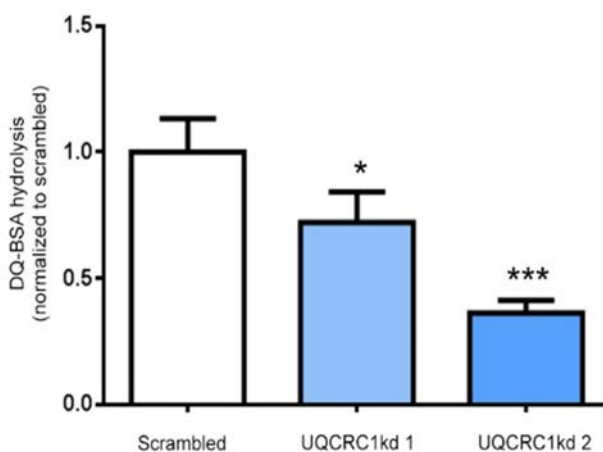


Figure 51. Effects on lysosomal proteolytic capacity caused by chronic mitochondrial malfunction – Chronic mitochondrial malfunction decreases the proteolytic capacity of the lysosomes measured by DQ-BSA assay.

These results show that long term mitochondrial malfunction induces an increase in lysosomal mass which is reflected as an increase in the size of the lysosomes but not as an augmented lysosomal number. These swollen lysosomes show a reduction in proteolytic activity which suggest that checking autophagy is relevant.

3.2.4 Effects of chronic mitochondrial malfunction on autophagy

Since there was an effect on lysosomes, caused by long term mitochondrial malfunction, the logical follow-up was to study how chronic mitochondrial malfunction affects autophagy.

Again, as a marker of autophagosomes, we determined the ratio LC3BII/LC3BI. In UQCRC1kd cells, we found an increase in LC3BII/LC3BI. This result means that in this model of chronic mitochondrial malfunction, there is an increase in autophagosomes (Fig. 52A, B).

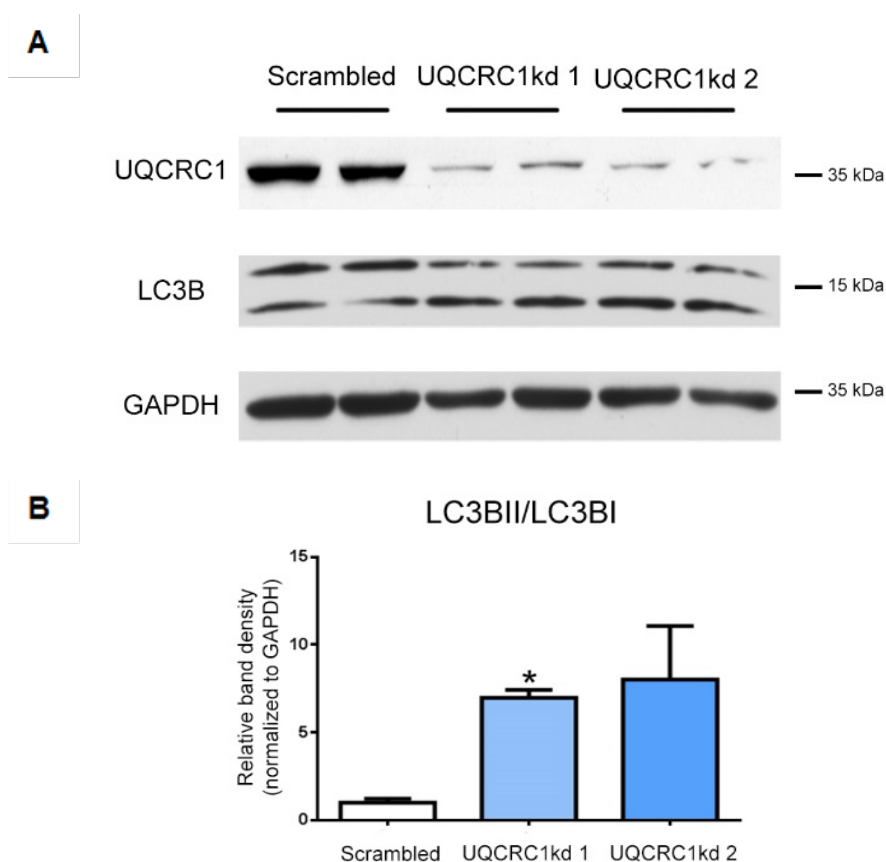


Figure 52. Effects of chronic mitochondrial malfunction on autophagy – A) Western blot of LC3B in stable UQCRC1kd. B) Graph showing an increase of LC3II/LC3BI ratio under chronic mitochondrial malfunction.

We investigated this result further by microscopy. UQCRC1kd and scrambled control cells were transfected with LC3-GFP. The images confirmed the previous result, showing clearly more autophagosomes in stable UQCRC1kds cells (Fig. 53A) and this was confirmed by quantification with ImageJ (Fig. 53B).

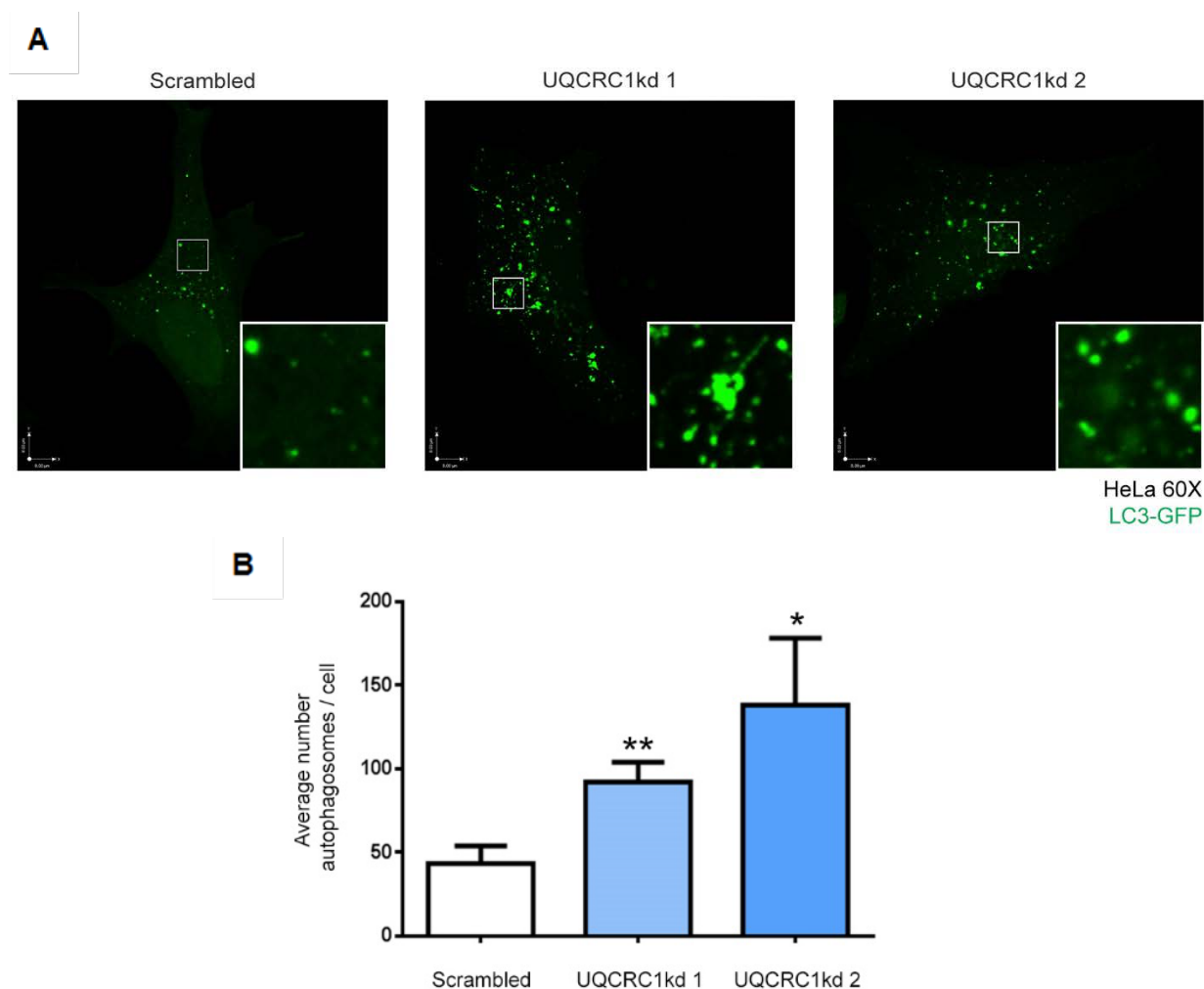


Figure 53. Effects of chronic mitochondrial malfunction on autophagosomes – A) Microscopy of HeLa cells tagged with LC3-GFP. B) Quantification showing an increase in number of autophagosomes in stable UQCRC1kd.

Given that chronic mitochondrial malfunction drives in an increase in autophagosomal number and in lysosomal mass, corresponding to lysosomal area but not number, it was logical to evaluate abundance of autophagolysosomes. Stable UQCRC1kds were transfected with LC3-RFP and LAMP1-GFP and imaged using the spinning disk confocal microscope. The images showed clearly more autophagolysosomes in UQCRC1kds cells, a phenotype that correlates

well with our previous observations of the effects of chronic mitochondrial malfunction on lysosomes and autophagy (Fig. 54).

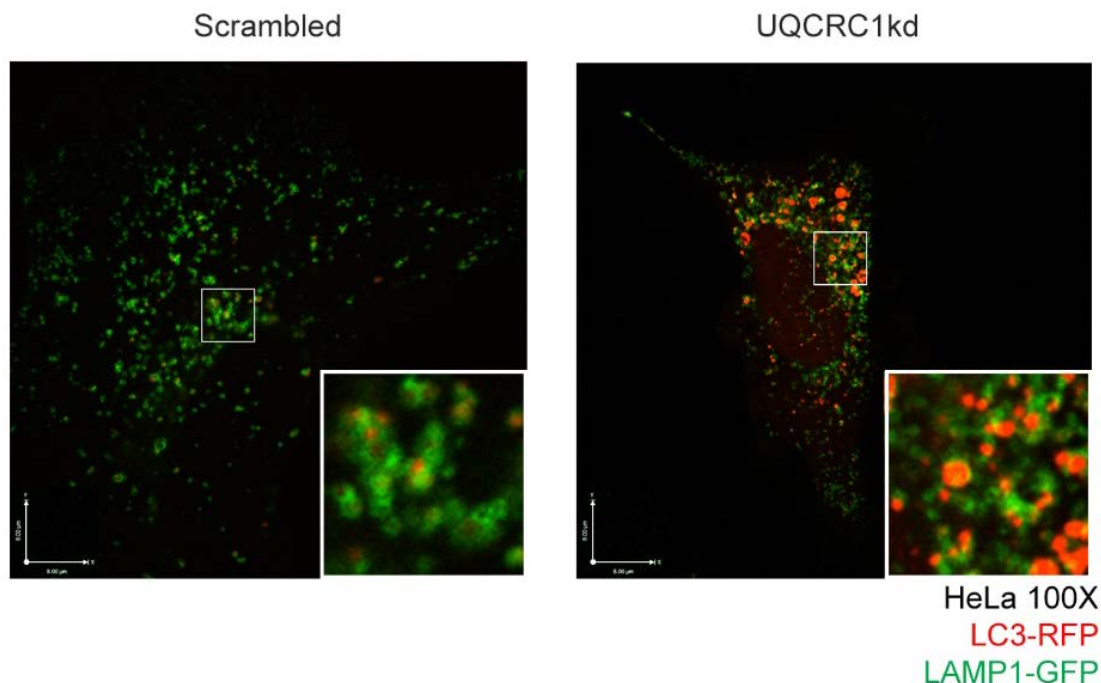


Figure 54. Representative image of autophagolysosomes in cells under chronic mitochondrial malfunction – Microscopy of HeLa cells tagged with LAMP1-GFP and LC3-RFP showing an increase in autophagolysosomes in stable UQCRC1kd.

3.2.5 Effect of chronic mitochondria malfunction on lysosomal biogenesis

Since chronic mitochondria malfunction seems to have an effect on lysosomal size and function, and our previous results showed an increase in lysosomal biogenesis in acute mitochondrial malfunction, we set to investigate the effect of chronic mitochondrial malfunction on lysosomal biogenesis. With this goal, the transcript levels of several lysosomal-related genes like LAMP1, GAA, CTSD and CTSF were measured, as described before. We also verified the transcript level of UQCRC1 as confirmation of the knock-down (Fig. 55B). The results showed an uncoordinated lysosomal biogenesis, with consistent downregulation and upregulation of LAMP1 and CTSF respectively. The expression levels of GAA and CTSD were as well inconsistent among biological replicates of UQCRC1kds (Fig 55A). This uncoordinated lysosomal biogenesis

signaling could be due to the fact that the transcription factors did not function as they normally do.

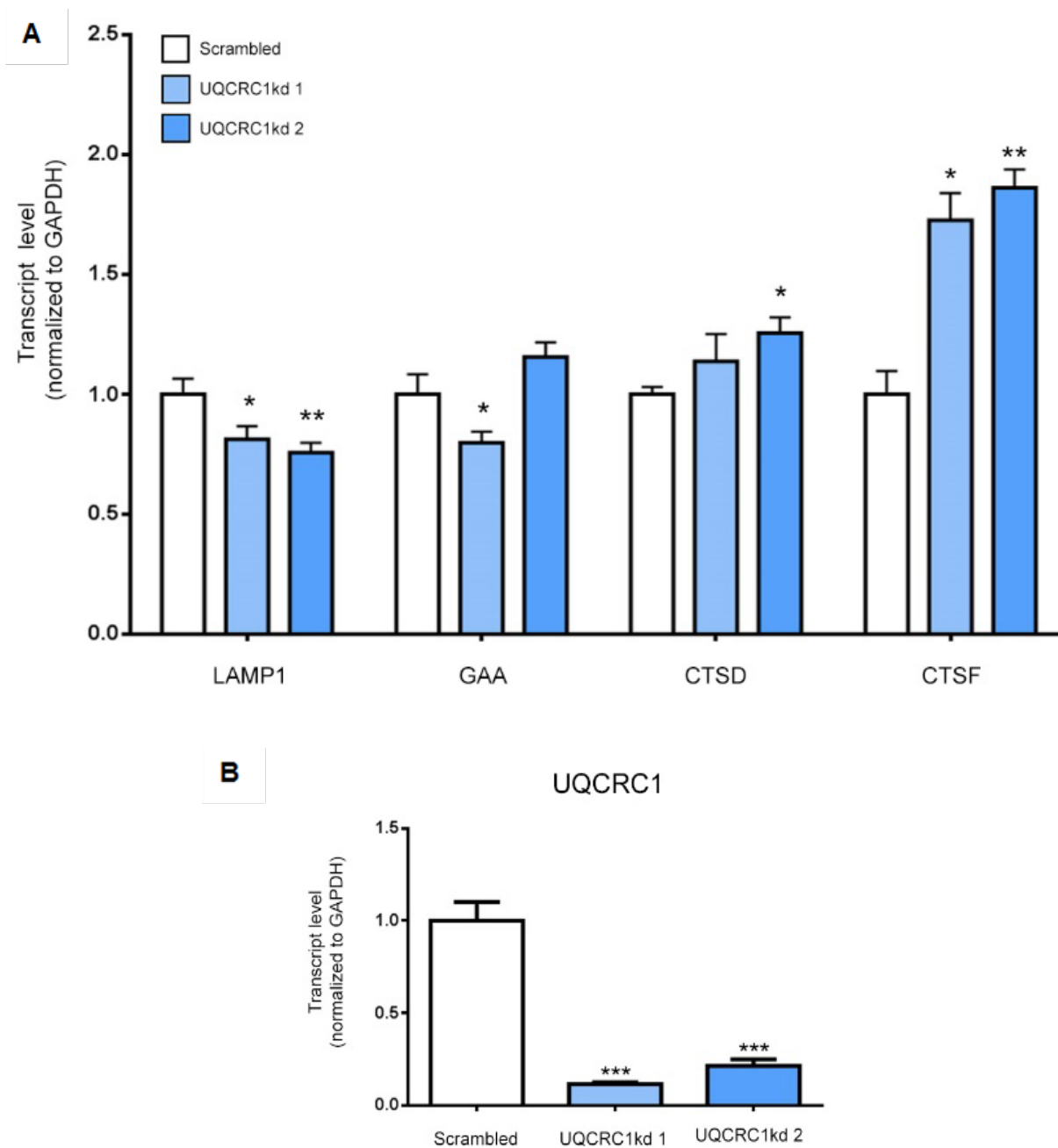


Figure 55. Effect of chronic mitochondrial malfunction on lysosomal biogenesis – A) Graph showing that chronic mitochondrial malfunction leads to an uncoordinated response of lysosomal-related genes. B) Graph showing that UQCRC1kds show a transcript level smaller than 40%.

3.2.6 Effect of chronic mitochondrial malfunction on TFEB localization

Having found an aberrant lysosome biogenesis in chronic mitochondrial malfunction, we investigated the role of TFEB in this response. The amount of TFEB was determined in stable UQCRC1kds and found to have increased in whole cell extracts (Fig. 56A, B).

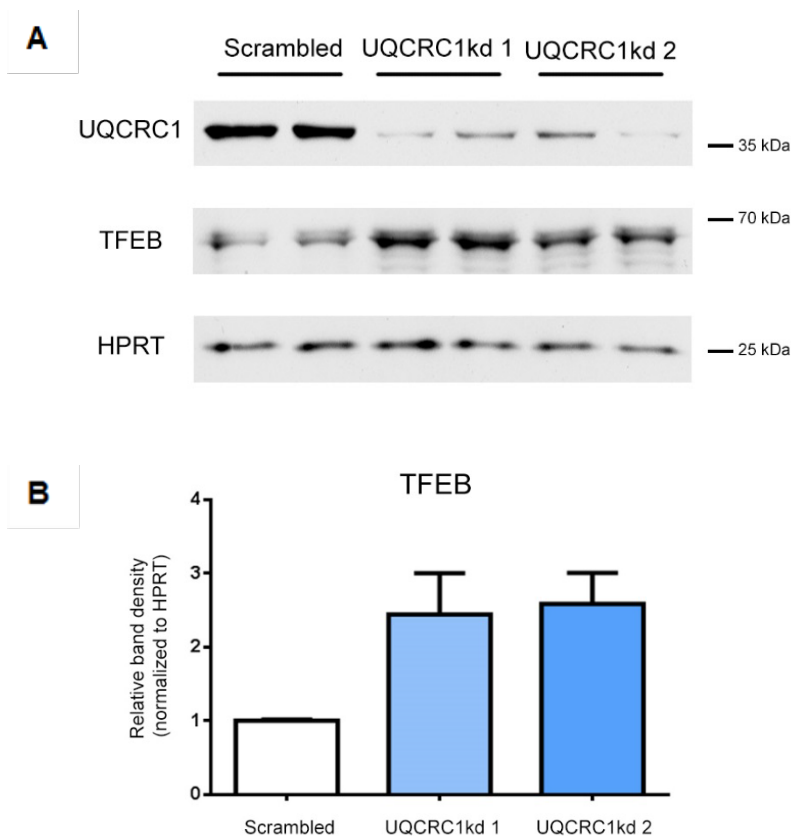


Figure 56. Effects of chronic mitochondrial malfunction on TFEB – A) Western blot of TFEB in stable UQCRC1kd. B) Graph showing an increase of TFEB under chronic mitochondrial malfunction.

However, the abundance of TFEB protein does not necessarily reflect its activity. TFEB, when localized in the cytoplasm, is inactive, but its nuclear translocation drives its activity and the transcription of lysosomal genes (Roczniak-ferguson et al. 2012; Settembre et al. 2012). In order to determine TFEB localization, we prepared nuclear and cytoplasmic extracts (Raimundo et al. 2008) and the nuclear extract was used to run a western blot. We found an increase in TFEB nuclear extracts of stable UQCRC1kds (Fig. 57A, B). To support this result, HeLa stable UQCRC1kd were transfected with TFEB-GFP and imaged with the spinning disk confocal microscope to determine the localization of TFEB. (Fig. 57C). The percentage of cells with nuclear TFEB was higher in UQCRC1kds (Fig. 57D) in agreement with the nuclear extract result.

The results of these experiments show that, in stable UQCRC1kds, TFEB is more abundant and it is nuclear localized despite not presenting normal activity. This is however inconsistent with the uncoordinated lysosomal biogenesis we found.

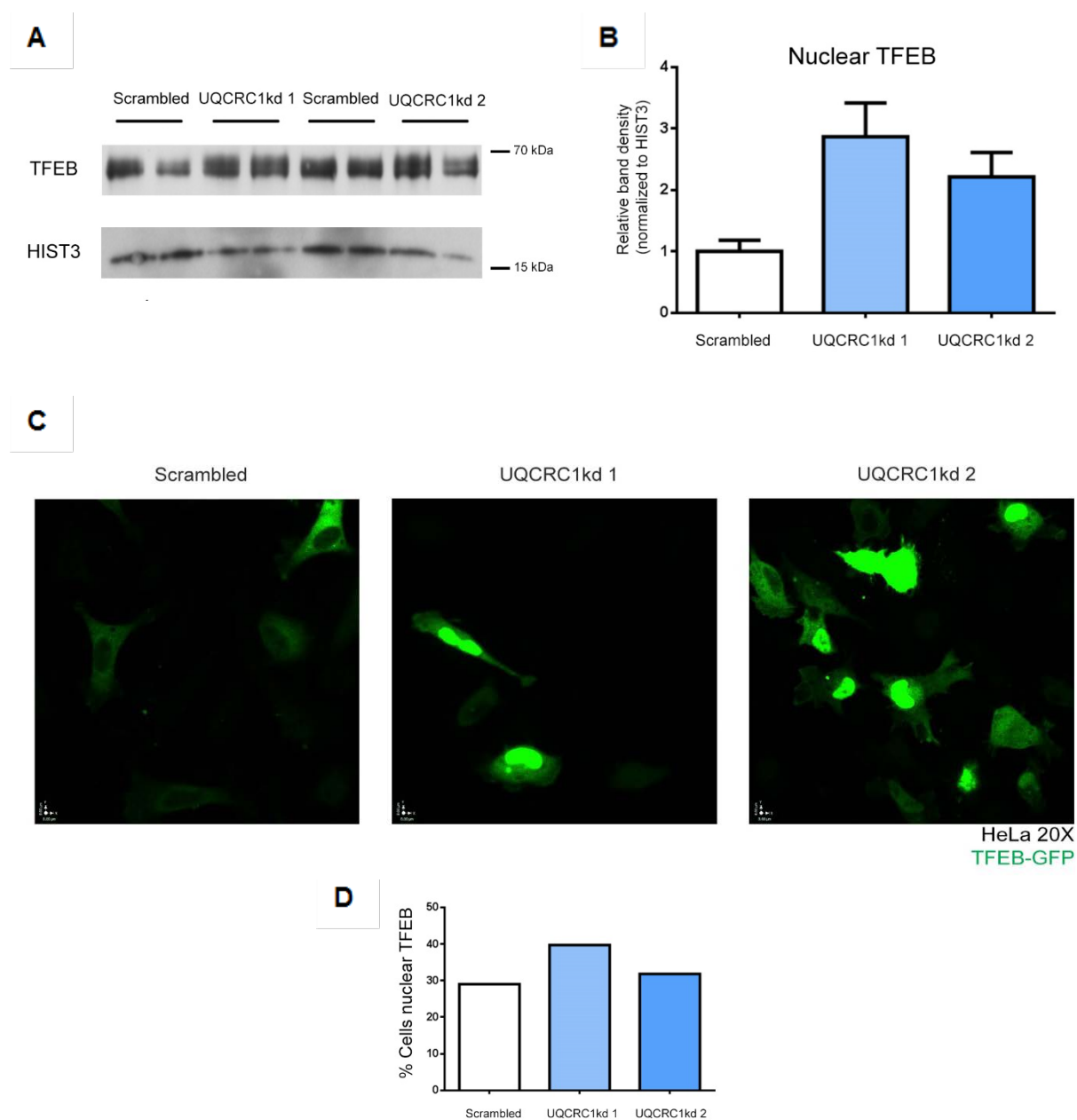


Figure 57. Effects of chronic mitochondrial malfunction on TFEB localization – A) Western blot of TFEB in nuclear extracts of stable UQCRC1kd. B) Graph showing an increase of TFEB under chronic mitochondrial malfunction in the nuclear extracts. C) Microcopy of stable UQCRC1kd HeLa cells tagged with TFEB-GFP. D) Graph showing an increase in the percentage of cells with nuclear TFEB in chronic mitochondrial stress.

3.2.7 Effect of chronic mitochondrial malfunction on TFEB regulation

Since in stable UQCRC1kds there was an uncoordinated lysosomal biogenesis, despite TFEB being nuclear, it is reasonable to assume that this chronic mitochondria deficiency does not trigger TFEB dependent lysosomal biogenesis in the canonical way. The canonical response to TFEB activation shows that under starvation, TFEB migrates to the nucleus and triggers lysosomal biogenesis (Sardiello and Ballabio 2009; Settembre et al. 2011). To elucidate if stable UQCRC1kds are able to trigger this canonical response, the cells were subjected to amino acid starvation with EBSS medium.

We monitored lysosomal biogenesis for expression of TFEB-dependent genes. Unlike in control cells, UQCRC1kd cells could not trigger the canonical TFEB response. In some cases, like CTSD or CTSD, the regulation of these genes was in the same direction, but in others like LAMP1 or GAA, it was in the direction opposite to the canonical response to TFEB activity (Fig. 58). These results suggest that even under amino acid starvation, the TFEB response in UQCRC1kds does not follow the canonical pathway.

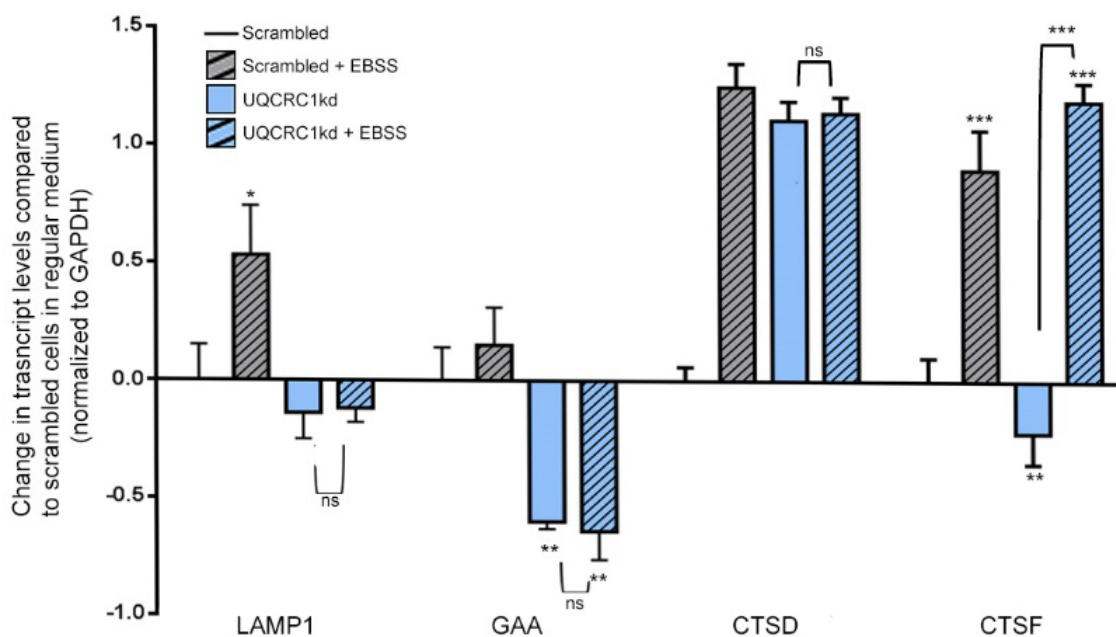


Figure 58. Effects of chronic mitochondrial malfunction on TFEB regulation – The graph shows increase in the transcript level of lysosomal-related genes in scrambled starved cells, while the stable UQCRC1kd still shows a misregulation in the transcription of lysosomal-related genes even under starvation.

3.2.8 Effects of chronic mitochondrial malfunction on lysosomal Ca²⁺ homeostasis

Since TFEB is not working as predicted, we focused on a mechanism known to regulate its activity. Lysosomal Ca²⁺ was reported to regulate calcineurin, a phosphatase that dephosphorylates TFEB and induces its nuclear translocation (Medina et al. 2015).

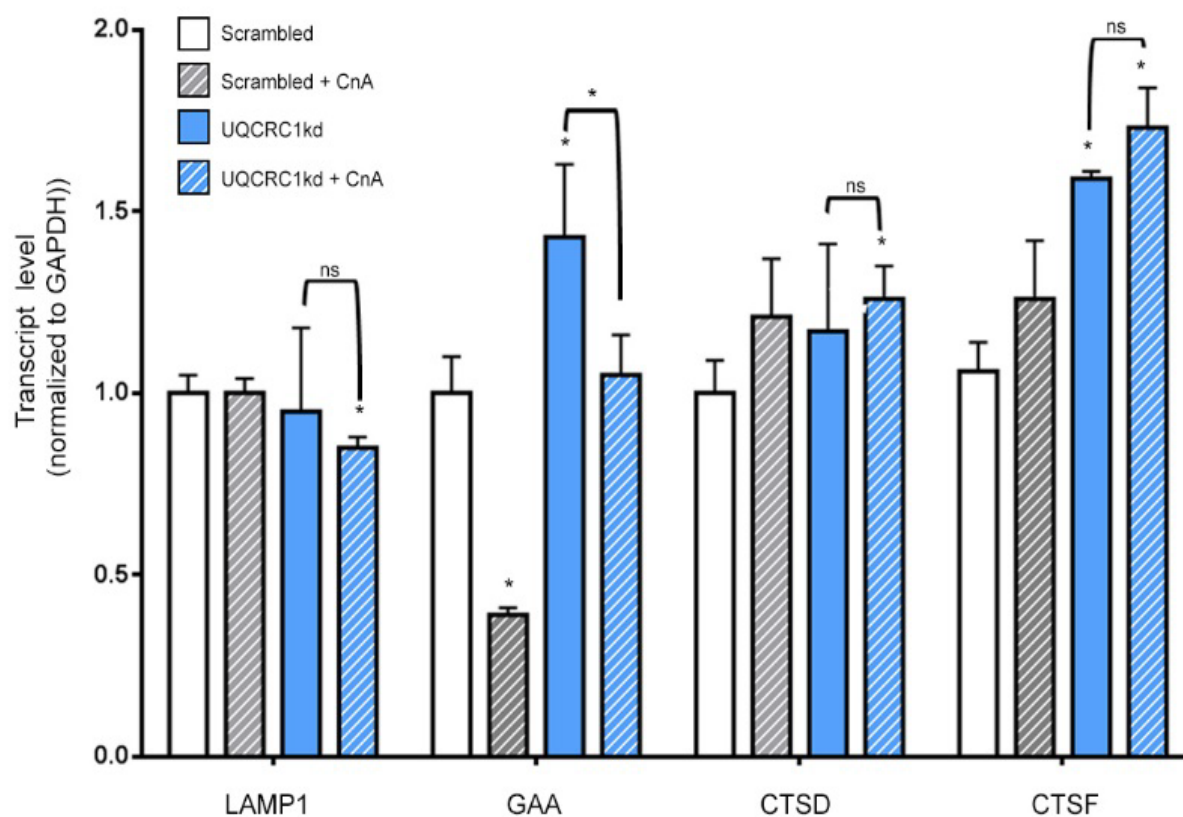


Figure 59. Effects of chronic mitochondrial malfunction on lysosomal Ca²⁺ homeostasis – The graph shows no global changes in lysosomal-related genes in calcineurin inhibited stable UQCRC1kd compared to changes in lysosomal-related genes in stable UQCRC1ks.

To study the effect of long term mitochondrial malfunction on lysosomal Ca²⁺ homeostasis, stable UQCRC1kd were transfected with a dominant negative calcineurin (CnA) (Cereghetti et al. 2008). The transcript levels of lysosomal-related genes were measured and in cells transfected with CnA, we observed no global changes in transcript levels of lysosomal-related genes compared to the transcription levels of lysosomal-related genes in stable UQCRC1kds. These results show that calcineurin repression has no effect suggesting that the effects that

were observed on lysosomal biogenesis under chronic mitochondrial malfunction are independent of calcineurin or that calcineurin was already repressed (Fig. 59).

The presence of enlarged lysosomes has been reported in lysosomal disorders like mucopolipidosis IV (Zou et al. 2015) (Dong et al. 2010). This increase in lysosomal size was related to the accumulation of Ca^{2+} inside the lysosomes (Dong et al., 2010).

With this in mind, we tested the hypothesis that Ca^{2+} trapped inside the lysosomes could be the cause of the swollen lysosomes that were shown in Fig. 50C. Since MCOLN1 channel is known to be an important point of Ca^{2+} release from the lysosomes, we decided to manipulate MCOLN1 channel to test if there was relation between lysosomal Ca^{2+} and swollen lysosomes (Fig. 60A).

In order to study how MCOLN1 manipulation affects lysosomal size in stable UQCRC1kd cells, they were treated with YM201636 and ML-SA1. It is known that YM201636 is an inhibitor of PIKFYVE, an enzyme needed to transform PI3P into PI(3, 5)P2 (Zolov et al. 2012); which in turn is an activator of MCOLN1 channel (Dong et al. 2010). On other hand, ML-SA1 is a synthetic activator of MCOLN1 channel (Zou et al. 2015). Following four hours of treatment, the cells were fixed, LAMP1 immunocytochemistry was performed and images were taken using a spinning-disk confocal microscope (Fig 60B). These results shows that while in the control cells the activation of MCOLN1 with ML-SA1 has no effect on the lysosomal size, in stable UQCRC1 the same treatment induced a clear reduction in the size of the lysosomes. On the other hand, the inactivation of MCOLN1 using YM201636 had no clear effect on the size of lysosomes in UQCRC1kd cells. However, there was an enlargement of lysosomes in the control cells treated with YM201636. These results imply that Ca^{2+} is involved in the appearance of swollen lysosomes in chronic mitochondrial malfunction.

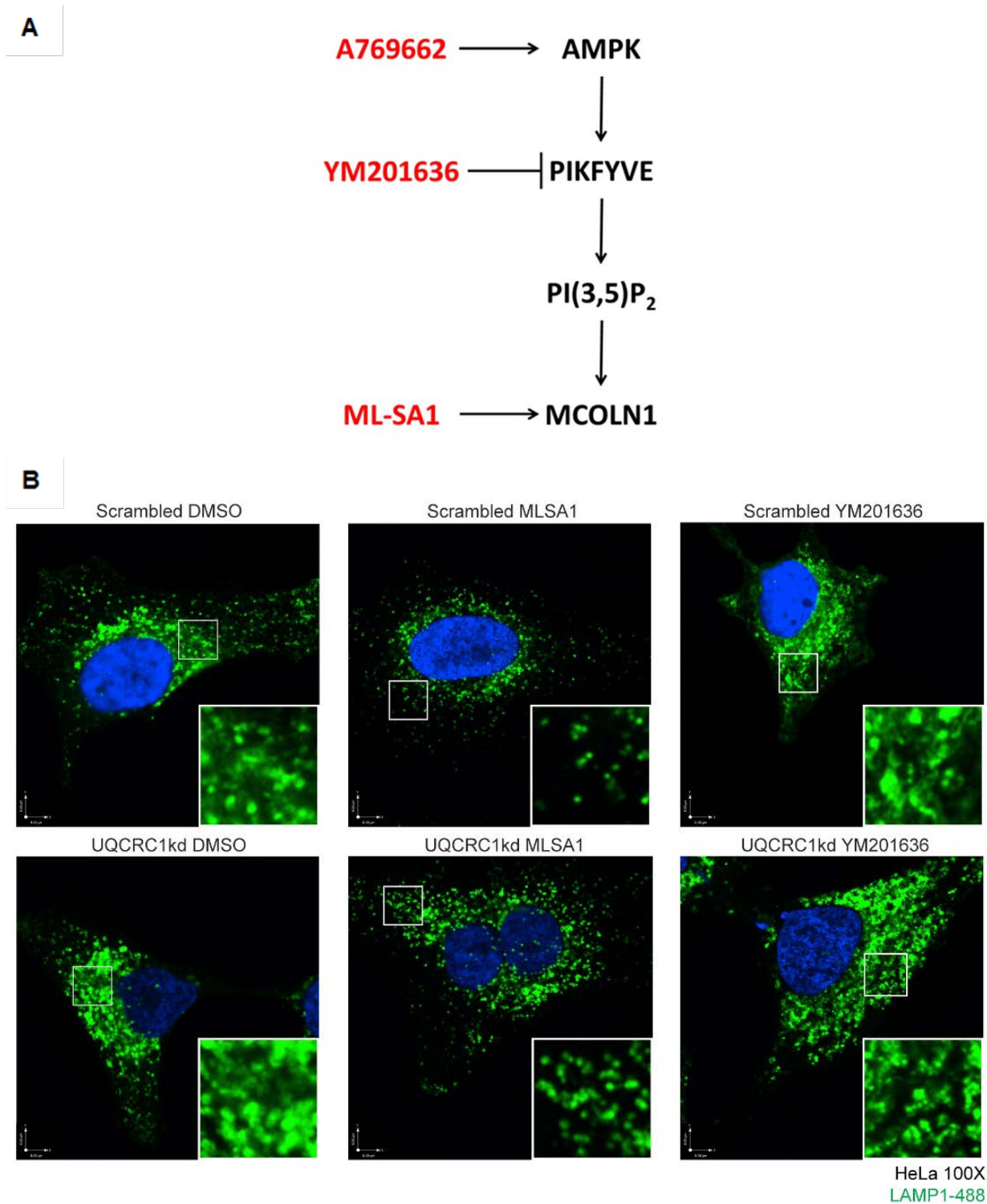


Figure 60. Representative images showing the effects of MCOLN1 manipulation on lysosomal size in chronic mitochondrial malfunction – A) Pathway that connects AMPK with MCOLN1 channel B) Microscopy of HeLa cells stained with LAMP1 green in which it is possible to appreciate that repression of MCOLN1 channel in scrambled cells induces an increase in lysosomal size while activation of MCOLN1 channel in stable UQCRC1kd leads to a diminution of lysosomal size.

2.2.9 Effects of chronic mitochondria malfunction on AMPK signaling

In order to study the relationship between chronic mitochondria deficiency and lysosomal biogenesis more deeply, it was necessary to investigate the pathway that mediates the communication between lysosomes and mitochondria. Following the pathway that we showed previously (Fig. 62A) along with our result in acute mitochondrial malfunction which demonstrated that AMPK was required for lysosomal biogenesis, we evaluated AMPK activity in stable UQCRC1kd cells. We found that AMPK activity decreased, as shown with the reduction in the ratio AMPK-P/AMPK (Fig. 62B). In our model of chronic mitochondrial stress, AMPK is repressed and at the same time AMPK is an upstream regulator of MCOLN1 which in turns regulates lysosomal Ca^{2+} homeostasis. As shown earlier, when MCOLN1 was activated in stable UQCRC1kd, the size of lysosomes was reduced. This result suggested that lysosomal size is probably influenced by AMPK activation. In order to test this, stable UQCRC1kd cells were treated with different chemicals that regulate parts of the hypothetical pathway (Fig. 61A). Following four hours of treatment with these chemicals, the cells were fixed and an immunocytochemistry of LAMP1 was performed. Images were taken using a spinning-disk confocal microscope (Fig. 61B).

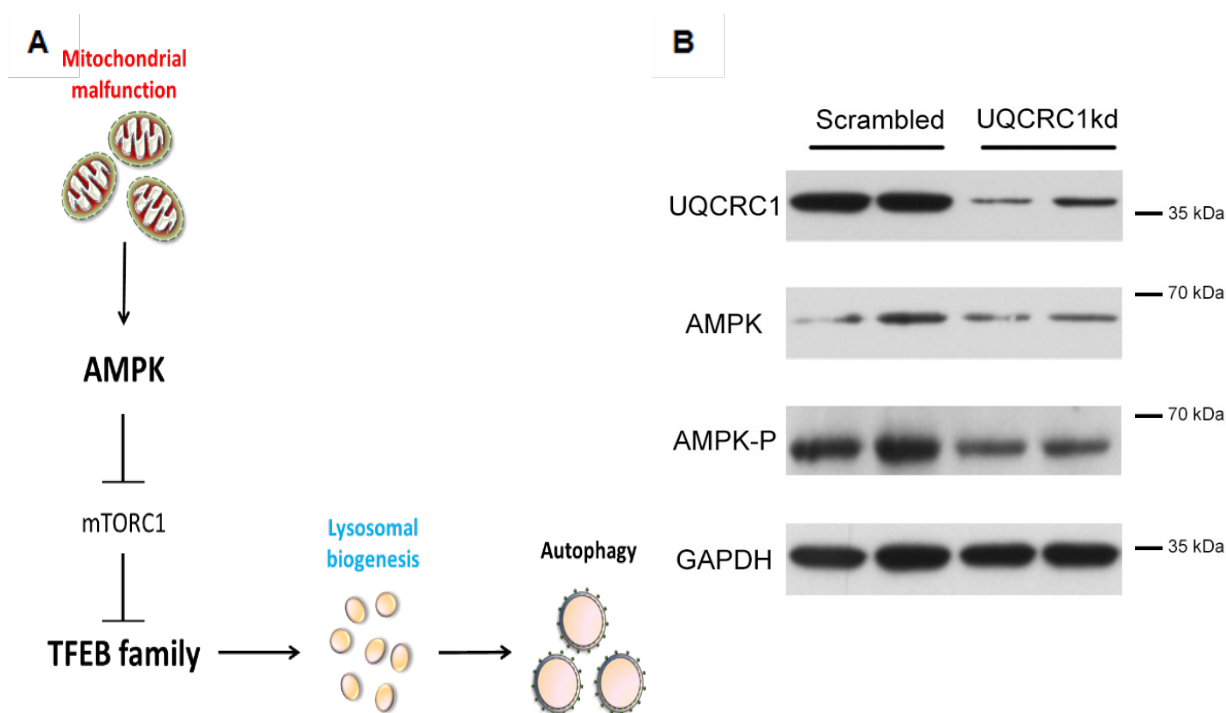


Figure 61. Effects of chronic mitochondrial malfunction on AMPK – A) Pathway that connects AMPK with autophagy via TFEB B) Western blot showing decrease in AMPK activity in stable UQCRC1kd.

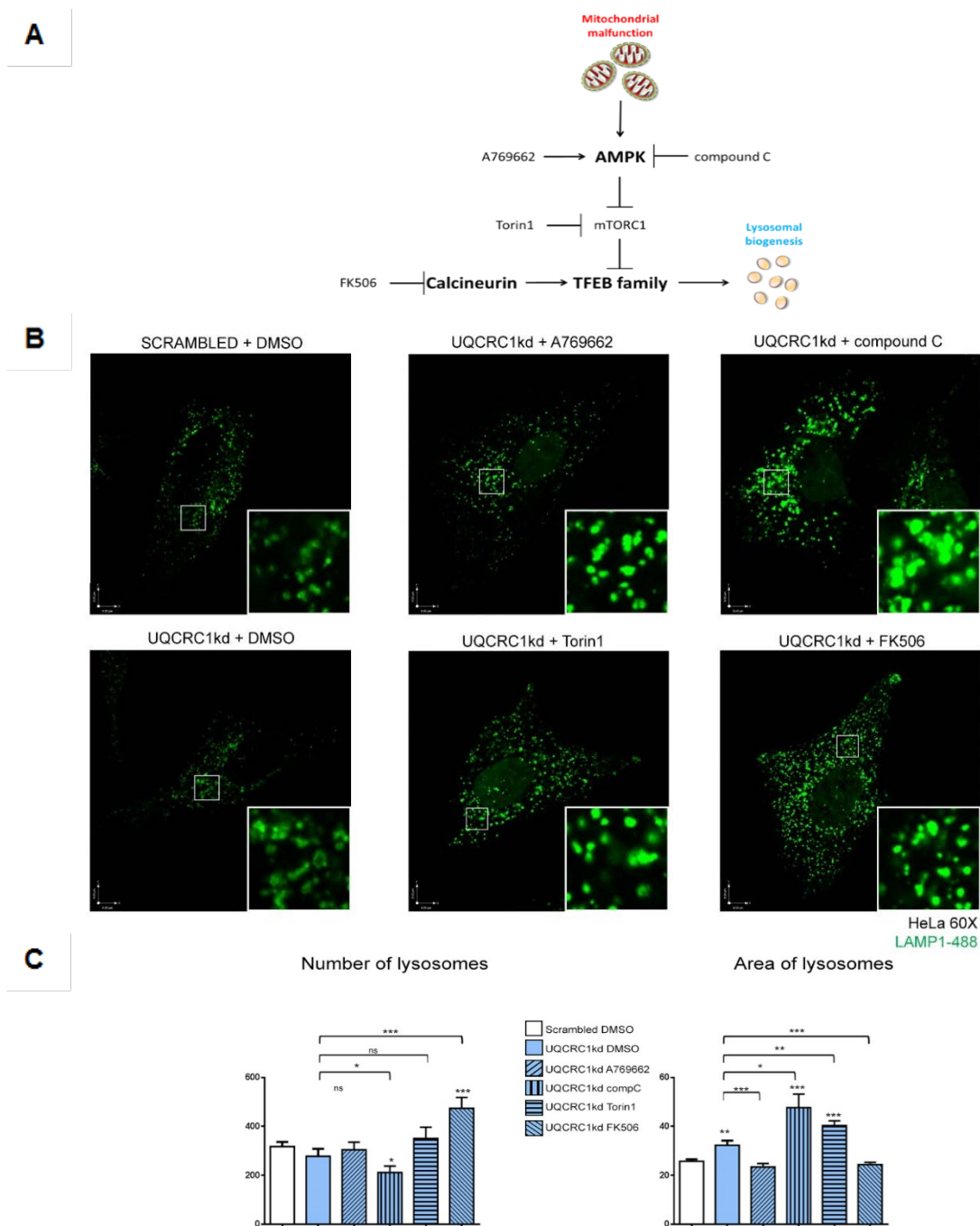


Figure 62. Representative images showing the effects of AMPK signaling manipulation on lysosomes in chronic mitochondrial malfunction – A) Pathway that connects mitochondrial malfunction with lysosomal biogenesis via AMPK B) Microscopy of HeLa cells stained with LAMP1 green in which it is possible to appreciate effects on lysosomes caused by AMPK signaling manipulation. C) Graphs showing how in stable UQCRC1kd, treatments with AMPK activator (A769662) and calcineurin inhibitor (FK506) rescued the lysosomal size. However, only the cells treated with AMPK activator retained the lysosomal number compared to the control cells.

As the compounds were dissolved in dimethyl sulfoxide (DMSO), the control in this case was UQCRC1kd treated DMSO. While in UQCRC1kd treated with A769662 (AMPK activator) (Zhang et al. 2014) and Torin1 (mTORC1 inhibitor) (Settembre et al. 2012) there was no change in the number of lysosomes; in UQCRC1kds treated with Tacrolimus (FK506) (calcineurin inhibitor) (Medina et al. 2015), there was an increase. Treatment with the AMPK inhibitor, compound C (Vingtdeux et al. 2010), resulted in a decrease in the number of lysosomes. With respect to the area of the lysosomes, there was a reduction in the knock-downs treated with A769662 and FK506 in comparison to the area in UQCRC1kd treated with DMSO. While in the other treatments (Torin-1 and compound C) the lysosomes were even bigger (Fig. 62B, C).

Despite the fact that AMPK activation was able to reduce the lysosomal size pointing to its role in regulating MCOLN1, we did not observe an increase in the number of lysosomes. In order to confirm that lysosomal biogenesis was not active, we monitored lysosomal biogenesis in UQCRC1kds cells supplemented with the AMPK activator A769662. The results showed an uncoordinated lysosomal biogenesis with consistent downregulation of LAMP1 and GAA in both treated and untreated UQCRC1kds and upregulation of CTSD and CTSF in both conditions of UQCRC1kds (Fig. 63).

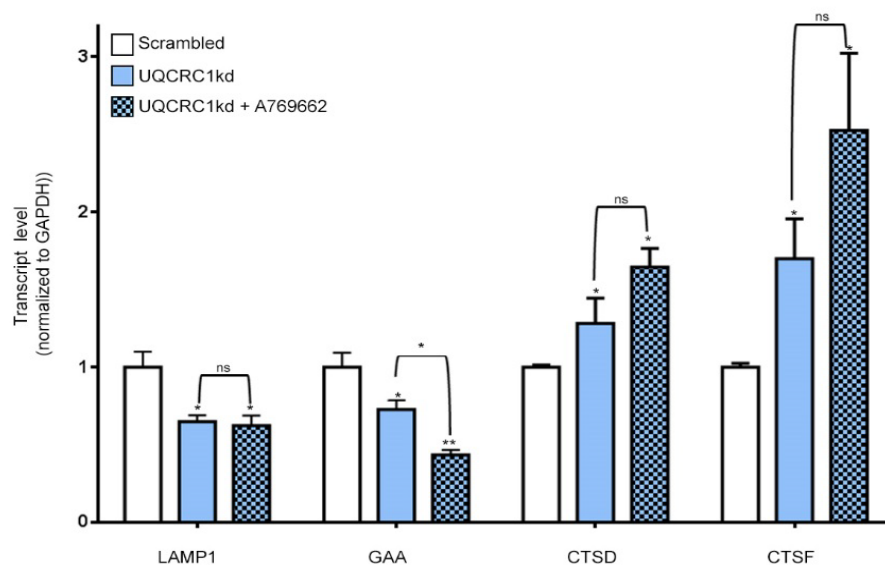


Figure 63. Effects of AMPK activation chronic on lysosomal biogenesis under mitochondrial malfunction – The graph shows an uncoordinated lysosomal biogenesis with downregulation of LAMP1 and GAA in UQCRC1kds with or without AMPK activation and upregulation of CTSD and CTSF in both conditions.

The results show that chronic mitochondrial malfunction unlike the acute case represses AMPK signaling which dysregulates lysosomal Ca^{2+} homeostasis thereby resulting in swollen lysosomes with reduced proteolytic capacity.

3.2.10 Effects of chronic mitochondria malfunction on lysosomal pH

Our data show that in chronic mitochondrial malfunction, the lysosomes present impaired proteolytic capacity (Fig.51) together with an increase in lysosomal area (Fig.50), which was also described in other studies (Demers-Lamarche et al. 2016). We therefore examined lysosomal pH, in stable UQCRC1kds and scrambled cells, using acridine orange (Zdolsek et al. 1990; Stagi et al. 2014). After triggering lysosomal photo-oxidative damage with blue light (Stagi et al. 2014), we found that stable UQCRC1kd lysosomes take longer to lose acridine orange fluorescence than the control cells (Fig. 64).

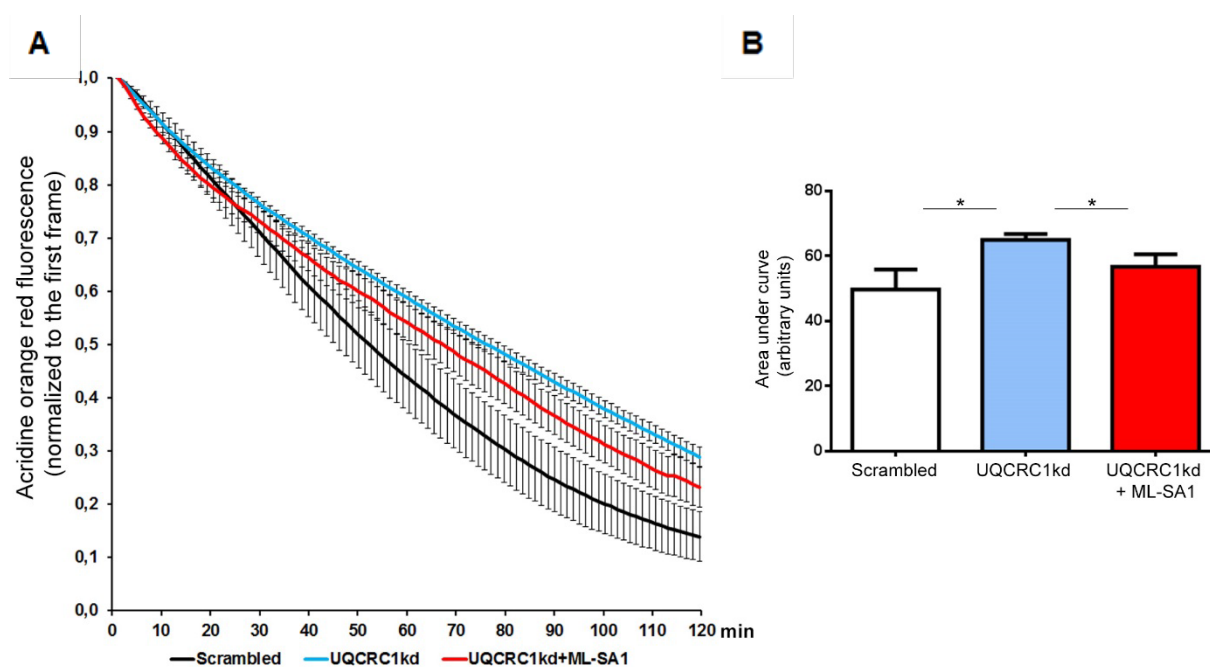


Figure 64. Effects of chronic mitochondrial malfunction on lysosomal pH – A) Graph showing the acridine orange red fluorescence in scrambled, stable UQCRC1kd and stable UQCRC1kd + ML-SA1 and its evolution along time. B) Bar charts representing the area under the curve, shown in graph A, and that shows the alkalization in stable UQCRC1kds and its rescue in stable UQCRC1kds treated with ML-SA1.

This result means that the pH in our model of chronic mitochondrial malfunction is less acidic than in the control. Moreover, we also monitored lysosomal pH in stable UQCRC1kds treated with ML-SA1, which we found causes a decrease in lysosomal size, and interestingly we the activation of MCOLN1 channel rescues the alkalization of lysosomes in chronic mitochondrial malfunction (Fig. 64). These results together with the previous one, in which direct and indirect MCOLN1 activation decreased lysosomal size, suggest that the function of this channel is closely related to the lysosomal dysfunction triggered by chronic mitochondrial malfunction.

4. Discussion

In recent years, numerous studies have addressed the influence of mitochondrial malfunction on the function of other organelles. It has been reported that mitochondrial malfunction can trigger endoplasmic reticulum stress and unfolded protein response (Haynes et al. 2013). Moreover, there are recent studies addressing the effect of mitochondrial malfunction on lysosomal biogenesis and function (Nezich et al. 2015; Baixauli et al. 2015; Demers-Lamarche et al. 2016).

This project is focused on the communication between mitochondria and lysosomes and particularly addresses the effects of mitochondrial malfunction on lysosomal biogenesis and function. We found that acute and chronic mitochondrial malfunction yields opposite effects on lysosomal biogenesis. Acute mitochondrial malfunction triggers TFEB/MITF-dependent lysosomal biogenesis via AMPK, while chronic mitochondrial malfunction actually results in lysosomal capacity saturation and repression of TFEB/MITF-dependent lysosomal biogenesis.

4.1 Acute mitochondrial malfunction triggers lysosomal biogenesis and autophagy

In this study, we induced acute mitochondrial malfunction with chemicals, like NaN_3 , to inhibit complex IV (Ishii et al. 2014) and CCCP to uncouple respiratory chain from oxidative phosphorylation (Ivankovic et al. 2016). On the other hand, we generated transient knock-down of UQCRC1, a core subunit of complex III (Hoffman et al. 1993)

In order to tackle the question of differential response of lysosomes to acute and chronic mitochondrial malfunction, we started by studying the lysosomal response to acute mitochondrial malfunction using imaging techniques. We observed that acute mitochondrial malfunction, chemically or genetically induced, causes mitochondrial fragmentation and also an increase in the number of lysosomes (Fig 31, 32 and 35). This demonstrates that acute mitochondrial malfunction leads to an increase in lysosomal number regardless of the source employed to induce the malfunction. Also, the analysis of lysosomal biogenesis showed that the increase in transcript levels of lysosome-related genes, like LAMP1, GAA, CTSD and CTSF was caused by acute mitochondrial malfunction (Fig. 37).

So far we have found that acute mitochondrial malfunction triggers lysosomal biogenesis, thereby increasing the number of lysosomes, independent of the stress source. However, lysosomes fuse with autophagosomes to continue with the autophagy (Kovacs et al. 1982;

Fengsrud et al. 1995), we have observed that under acute mitochondrial stress an increase in autophagy occurs, represented by an increase in autophagosomes, regardless of the stress source (Fig. 33, 36).

4.2 Acute mitochondrial malfunction triggers TFEB/MITF-dependent lysosomal biogenesis

TFEB has been reported as the master regulator of lysosomal biogenesis due to its ability to bind to the CLEAR region and regulate transcription of lysosome-related genes (Sardiello et al. 2009; Pastore et al. 2013). Also, there are studies showing that short-term mitophagy bursts affect the regulation of the microphthalmia transcription factor family (Nezich et al. 2015). With this in mind, together with our results indicating an increase in lysosomal biogenesis in response to acute mitochondrial stress, we decided to monitor TFEB/MITF activity finding an increase in TFEB and MITF. This increase corresponds to the first hour of induction of acute mitochondrial malfunction (Fig. 39).

It is known that the members of the microphthalmia family, that is a bHLH leucine zipper transcription factor, need to be homodimerized or heterodimerized to work correctly (Steingrimsson et al. 2002). We found that silencing of TFEB did not affect the MITF expression, whereas silencing of MITF results in an increase in TFEB expression (Fig. 40), suggesting the possibility of a compensatory mechanism and pointing to the cooperation of both transcription factors in acute mitochondrial stress induced lysosomal biogenesis. This was confirmed after monitoring lysosome-related genes, under acute mitochondrial malfunction, with combinations of TFEB and MITF deletions. We show that deletion of TFEB, MITF or both, decreases the expression of majority of the tested lysosome-related genes. However, some of the genes were still responding to the stress, suggesting that other members of the MITF family, like TFE3, could be compensating for the absence of TFEB and MITF. Additionally, these results are in accordance to the work presented by Nezich et al. in which it was necessary to perform the ablation of multiple MIT/TFE transcription factors to cause defects in mitophagy (Nezich et al. 2015).

4.3 TFEB/MITF-dependent lysosomal biogenesis is AMPK-dependent

In order to address the pathway connecting acute mitochondrial malfunction and TFEB/MITF-dependent lysosomal biogenesis, we turned to AMPK due to its known involvement in response to mitochondrial stress (Raimundo 2014). While the exact mechanism leading to AMPK activation in acute mitochondrial malfunction is still not clear, several AMPK activators are already known, for example ROS (Raimundo et al. 2012; Emerlinga et al. 2009), Ca^{2+} (Sinha et al. 2015; Mungai et al. 2011) and decreased energy (Hardie & Ashford 2014). These AMPK activators are signals of acute mitochondrial malfunction. We found that while acute mitochondrial malfunction triggers transcription of lysosome-related and MITF family genes, such a response was absent under AMPK inhibition (Fig. 43), suggesting that AMPK is required for the activation of MITF gene family and therefore to trigger lysosomal biogenesis. On the other hand, we found that AMPK activation alone is not enough to trigger TFEB/MITF-dependent lysosomal biogenesis in the absence of mitochondrial malfunction stimuli (Fig. 44). AMPK has broad roles in cellular signaling, for example, in the regulation of compensatory mitochondrial biogenesis by upregulation of the transcription coactivator peroxisome proliferator-activated receptor gamma, coactivator 1 alpha (PGC1- α) (Yan et al. 2013); activation of autophagy through ULK1/2 activation resulting in formation of autophagosomes (Egan et al. 2010); as well as the regulation of mTORC1 activity (Gwinn et al. 2008). Furthermore, AMPK was recently shown to have the ability to regulate TFEB activity in embryonic stem cells through mTORC1 regulation (Young et al. 2016). With all this in mind, we can suggest a model in which acute mitochondrial malfunction triggers TFEB/MITF-dependent lysosomal biogenesis that is also AMPK-dependent. The activation of AMPK can thus be triggered by mitochondrial signaling like ROS or Ca^{2+} and at the same time AMPK can regulate TFEB/MITF through mTORC1 activity.

4.4 TFEB/MITF-dependent lysosomal biogenesis is calcineurin-independent

mTORC1 has been well characterized as a TFEB/MITF regulator. When mTORC1 is present at the lysosomal surface, it is active and it phosphorylates TFEB and MITF allowing them to bind the 14-3-3 proteins and keeping them in the cytoplasm where they are inactive. However, when mTORC1 is inactive, it cannot phosphorylate TFEB and MITF and they are translocated to the nucleus where they can bind to the CLEAR region on the promoters of lysosome-related genes and trigger their transcription (Settembre et al. 2012; Martina et al. 2012; Martina & Puertollano 2013). mTORC1 is not the only regulator of TFEB activity. Recently, calcineurin has been reported as TFEB regulator, wherein it can dephosphorylate S211 of TFEB rendering it unable to bind 14-3-3 proteins and it is translocated to the nucleus where it can trigger transcription of

lysosome-related genes (Medina et al. 2015). However, we found that under acute mitochondrial malfunction, TFEB/MITF-dependent lysosomal biogenesis is calcineurin-independent (Fig. 45); the increase in the transcript levels of lysosome-related genes triggered by acute mitochondrial stress is still present when calcineurin is inhibited.

A summary of all this information allowed us to propose the pathway that connects acute mitochondrial stress with TFEB/MITF-dependent lysosomal biogenesis (Fig. 65). In the proposed pathway, mitochondrial malfunction leads to a modification in the release of a signaling molecule, for example ROS, which activates AMPK, a known repressor of mTORC1. mTORC1 repression allows nuclear translocation of TFEB/MITF and the nuclear localization of TFEB/MITF would allow the transcription of lysosome-related genes like LAMP1, GAA, CTSD and CTSF.

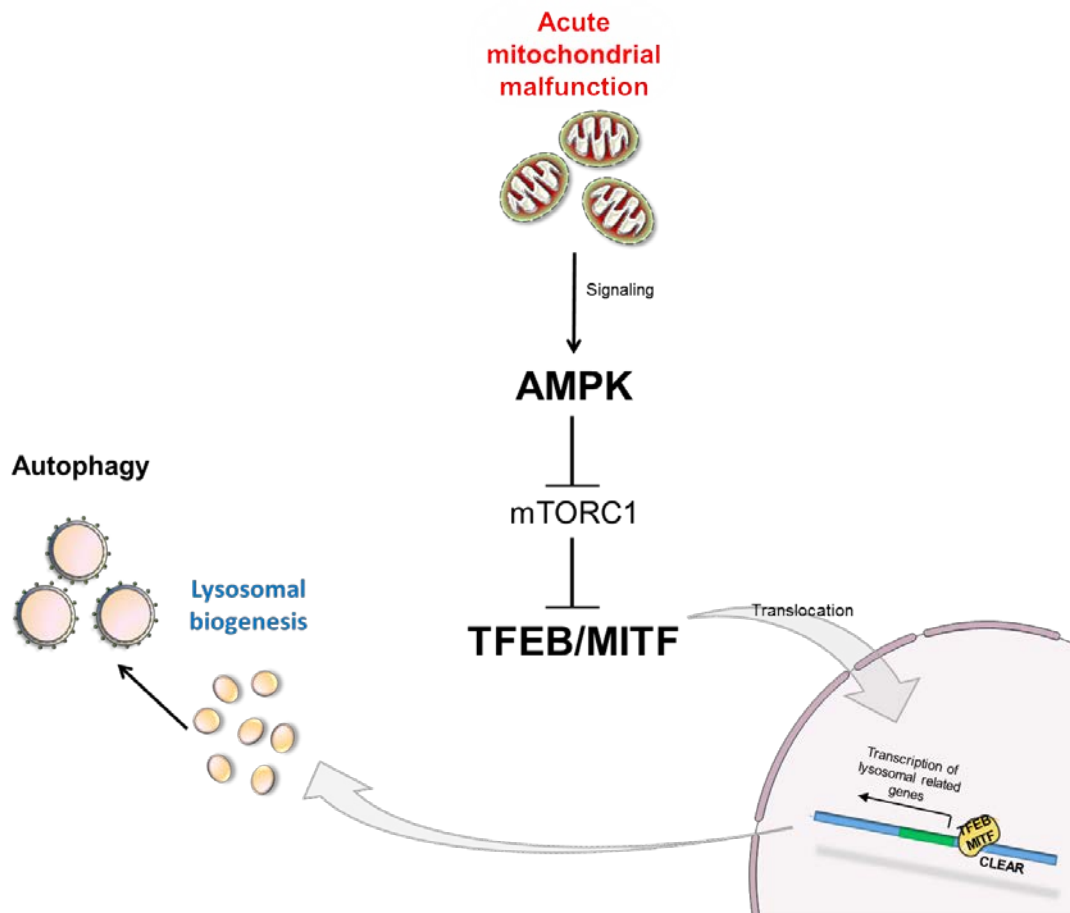


Figure 65. Lysosomal biogenesis pathway in acute mitochondrial malfunction - This pathway shows how acute mitochondrial malfunction triggers lysosomal biogenesis. Acute mitochondrial malfunction releases signaling that triggers TFEB/MITF-dependent lysosomal biogenesis via AMPK activation, increasing lysosomal number and autophagy.

4.5 Chronic mitochondrial malfunction triggers uncoordinated lysosomal biogenesis and dysfunctional lysosomes

Previously, in this thesis, it was shown that acute mitochondrial malfunction triggers TFEB/MITF-dependent lysosomal biogenesis and now we will focus on how mitochondrial malfunction affects lysosomal biogenesis in chronic mitochondrial malfunction. Recently, two studies addressed the effect of long term mitochondrial malfunction on lysosomal function and biogenesis. Impairment of mitochondrial respiration due to deletion of the mitochondrial transcription factor A (TFAM) triggers a program of incomplete lysosomal biogenesis and causes a perturbation of lysosomal function in mouse T cells upon activation (Baixauli et al. 2015). On the other hand, induction of long term mitochondrial malfunction by deletion of mitochondrial proteins like AIF, OPA1 or PINK1 caused the appearance of large lysosomes with compromised functionality in MEFs (Demers-Lamarche et al. 2016). In agreement with those studies, we show that chronic mitochondrial malfunction, caused by the repression of a core subunit of the complex III of mitochondrial respiratory chain, triggers an uncoordinated lysosomal biogenesis (Fig. 55). This uncoordinated response is characterized by an inconsistent expression of the lysosome-related genes, in which some of them are upregulated like CTSE and others downregulated like LAMP1. Interestingly, this uncoordinated response in lysosomal genes correlates with an increase in lysosomal mass (Fig. 49), which can in its entirety be attributed to an increase in lysosomal size and not in their number (Fig. 50). Using imaging techniques, we found that the cells with chronic mitochondrial malfunction are characterized by the presence of huge vesicles denoted as lysosomes. Remarkably, we also found that chronic mitochondrial malfunction leads to enhanced autophagy, resulting in an increase of LC3II/LC3I ratio, pointing to the presence of more autophagosomes (Fig. 52). In this case, using imaging techniques we have confirmed that under chronic mitochondrial stress there is an increase in the number of autophagosomes (Fig. 53) and that this correlates with an increase in autophagolysosomes (Fig. 54).

In summary, chronic mitochondrial malfunction leads to an uncoordinated response of lysosome-related genes response (Fig. 55), the appearance of swollen lysosomes without increase in their number (Fig. 49, 50), the increase in autophagosome number (Fig 53), and other phenotypes like the loss of mobility in the big lysosomes. Therefore, our finding that chronic mitochondrial malfunction leads to a decrease in lysosomal proteolytic capacity was expected (Fig. 51).

These results together point to the fact that chronic mitochondrial malfunction triggers uncoordinated lysosomal biogenesis that leads to accumulation of morphologically altered

lysosomes with an impaired function. Our findings are in agreement with the studies of Demers-Lamarche and Baixauli. However, the mechanisms underlying the impairment of lysosomal function under chronic mitochondrial malfunction are not yet fully understood.

4.6 Chronic mitochondrial malfunction triggers a non-canonical TFEB pathway

Since we found an uncoordinated response in lysosome-related genes whose transcription was reported to be dependent on TFEB (Settembre et al. 2012), it was not surprising to find that TFEB amount was increased in chronic mitochondrial malfunction (Fig. 56). However, it is known that TFEB activity depends on its localization: under normal conditions, TFEB is in the cytoplasm where it is inactive but can be active upon its translocation to the nucleus (Settembre et al. 2012). In this thesis, we show that chronic mitochondrial malfunction not only leads to an increase in TFEB but it also triggers an increase in the nuclear localization of TFEB (Fig. 57). Previous studies have connected TFEB nuclear translocation with activation of lysosome-related genes transcription (Sardiello & Ballabio 2009; Baixauli et al. 2015), however our results do not support that observation. Therefore, we explored the possibility that chronic mitochondrial malfunction is able to trigger a TFEB-dependent lysosomal biogenesis in a canonical way. We found that even under amino acid starvation, which is the system initially used to trigger TFEB-dependent lysosomal response (Sardiello et al. 2009), our model of chronic mitochondrial malfunction was not able to activate the canonical TFEB response (Fig. 58). This implies that chronic mitochondrial malfunction triggers an uncoordinated lysosomal biogenesis via a non-canonical TFEB pathway.

4.7 Chronic mitochondrial malfunction caused dysfunctional calcium lysosomal homeostasis AMPK-dependent

Given that TFEB did not display the same behavior, as proposed in the case of amino acid-dependent activation (Sardiello et al. 2009; Settembre et al. 2013), we have focused on calcineurin, another reported inductor of TFEB nuclear translocation (Medina et al. 2015). Interestingly, we did not find global changes in the expression of lysosome-related genes suggesting that calcineurin repression has no effect on non-canonical TFEB pathway (Fig. 59). One possible reason for this could be that calcineurin is not involved in this alternative TFEB pathway or alternatively, because TFEB was already repressed by a lack of lysosomal Ca^{2+} release. Medina et al. reported that it is the release of Ca^{2+} from the lysosomes, through the

MCOLN1 channel, that serves as a trigger for another way to induce TFEB nuclear translocation via calcineurin activation. On the other hand, there are reports of swollen lysosomes in mitochondrial and lysosomal disorders that have been connected to Ca^{2+} accumulation in lysosomes (Dong et al. 2010; Zou et al. 2015). With all this in mind, we decided to check how MCOLN1 manipulation affects lysosomal morphology and we found that upon activation of MCOLN1 channel in chronic mitochondrial malfunction, the lysosomes displayed smaller size while the inhibition of MCOLN1 channel regulators in the control scrambled gave rise to a further increase in lysosomal size (Fig. 60), corroborating our idea of Ca^{2+} being trapped in the lysosomes. Furthermore, AMPK activity, supposedly activated by increased mitochondrial ROS level (Fig. 48), is repressed in chronic mitochondrial malfunction (Fig. 61), and is located upstream of the activation of MCOLN1 channel that in our model seems to be inactive. We further tried to elucidate if a connection exists between the AMPK deficiency and lysosomal size and we found that AMPK and mTORC1 repression aggravate the phenotype of swollen lysosomes, while AMPK activation and calcineurin repression were rescuing the phenotype (Fig. 62). However, since AMPK activation was rescuing the lysosomal size without an increase in the lysosomal number, supporting our previous results that pointed towards a misregulation of lysosomal Ca^{2+} , it was natural to monitor expression of lysosome-related genes. We have found that the uncoordinated response was still present (fig. 63), suggesting that AMPK activation was acting through MCOLN1, thereby reducing the lysosomal size.

4.8 Chronic mitochondrial malfunction increases lysosomal pH misregulating lysosomal calcium homeostasis

Our data point towards the accumulation of Ca^{2+} in the lysosomes (Fig. 60, 62) as the cause of the swollen lysosomes present in chronic mitochondrial malfunction (Fig.50), supported by studies showing changes in lysosomal pH associated with chronic mitochondrial stress (Demers-Lamarche et al. 2016; Baixauli et al. 2015), correlation between lysosomal size and pH (Stagi et al. 2014) or correlation between alterations in lysosomal pH and dysfunctional Ca^{2+} homeostasis (Christensen et al. 2002; Zou et al. 2015). Therefore, we investigated lysosomal integrity after photo-oxidative damage triggered by blue light of the lysosomal dye acridine orange (Stagi et al. 2014; Zdolsek et al. 1990) in our model of chronic mitochondrial malfunction. Interestingly, we found that in stable UQCRC1kd, lysosomes were protected from membrane disruption and leakage of the dye (Fig.64) that is correlated with an increase in the fluorescence, suggesting

that under chronic mitochondrial malfunction there is an increase in lysosomal pH (e.g. less acidic).

This result is in agreement with the observations of Demers-Lamarche and could explain the observed accumulation of dysfunctional lysosomes (Fig. 50) and of autophagosomes (Fig. 52, 53), since lysosomal enzymes need to be at acidic pH for an optimal function (Ballabio 2016; Perera & Zoncu 2016).

Furthermore, we found that misregulation of lysosomal pH in cells with chronic mitochondrial malfunction is connected to Ca^{2+} accumulation in lysosomes: after activation of MCOLN1 channel, triggering Ca^{2+} release from lysosomes, the lysosomal integrity after photo-oxidative damage by orange acridine is rescued and it is comparable to lysosomal integrity in control cells (Fig. 64). This result suggests that in chronic mitochondrial malfunction pH and Ca^{2+} regulation of lysosomes are connected, and that lysosomal Ca^{2+} homeostasis is dependent of AMPK activity allowing us to propose an alternative pathway (Fig. 66)

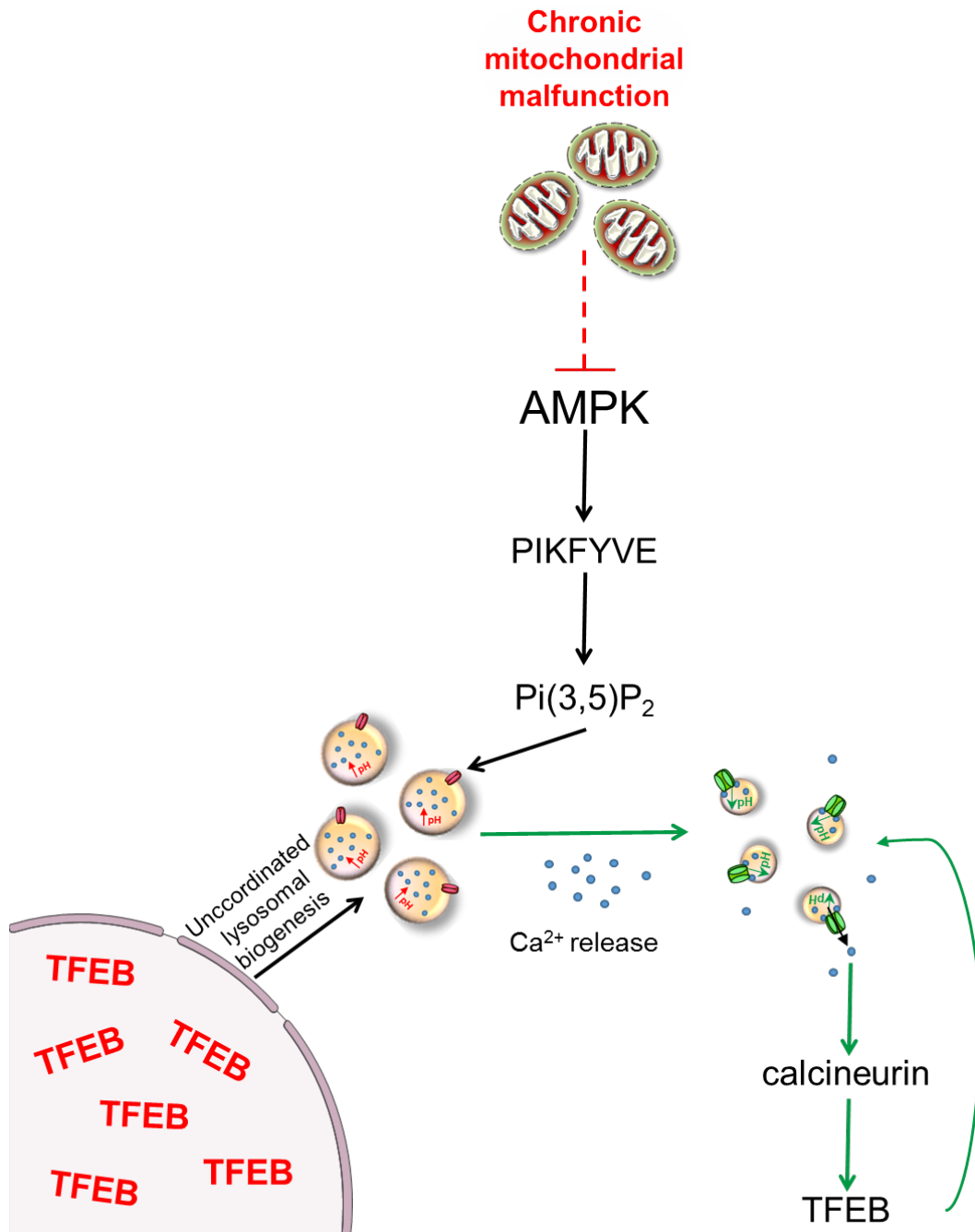


Figure 66. Lysosomal biogenesis pathway in chronic mitochondrial malfunction – Pathway representing how chronic mitochondrial malfunction triggers uncoordinated lysosomal biogenesis and accumulation of Ca²⁺ in swollen lysosomes. Chronic mitochondrial malfunction represses AMPK activity, needed to activate PIKfyve, which in turn transforms PI(3)P to PI(3,5)P₂, an activator of MCOLN1 channel. MCOLN1 activation will release Ca²⁺ from the lysosomes accompanied by a decrease of lysosomal pH. Simultaneously Ca²⁺ release will activate calcineurin that relocates TFEB to the nucleus and triggers canonical lysosomal biogenesis.

Summary and conclusions

In recent years there has been a growing interest in studying the role of mitochondrial malfunction in cellular function. However, studies about the impact of mitochondrial defects on other organelles have received less attention.

This thesis addresses the effect of mitochondrial malfunction, mainly originating from respiratory chain stress on lysosomal biogenesis and function. In the context of this thesis, it was shown that acute and chronic mitochondrial malfunction have different effects on the lysosomes. While acute mitochondrial malfunction triggers TFEB/MITF-dependent lysosomal biogenesis via AMPK, chronic mitochondrial malfunction results in an alternative TFEB signal trigger and uncoordinated lysosomal biogenesis with the appearance of swollen dysfunctional lysosomes. Moreover, we show that in chronic mitochondrial malfunction, a relationship exists between the formation of aberrant lysosomes with the accumulation of Ca^{2+} and pH increase inside those lysosomes. Furthermore, we propose that AMPK downregulation can be responsible for the calcium dysregulation and we show that MCOLN1 channel activation, direct or via AMPK activation, can rescue the accumulation of swollen lysosomes. We also show that MCOLN1 channel activation can rescue the alkalization of the lysosomes in chronic mitochondrial malfunction.

To conclude, this thesis contributes to a more comprehensive understanding of the communication between mitochondria and lysosomes and highlights the importance of distinguishing between acute and chronic mitochondrial malfunction, presenting a different perspective in the context of dealing with different kinds of mitochondrial stresses and their effects on other organelles.

References

- Abada, A. & Elazar, Z., 2014. Getting ready for building: signaling and autophagosome biogenesis. *EMBO reports*, 15(8), pp.839–852.
- Addink, A.D.F. et al., 1972. Enzyme Localization in Beef-Heart Mitochondria: A Biochemical and Electron-Microscopic Study. *European Journal of Biochemistry*, 29(1), pp.47–59.
- Andreyev, A.Y., Kushnareva, Y.E. & Starkov, A.A., 2005. Mitochondrial metabolism of reactive oxygen species. *Biochemistry*, 70(2), pp.200–214.
- Appelqvist, H. et al., 2013. The lysosome: From waste bag to potential therapeutic target. *Journal of Molecular Cell Biology*, 5(4), pp.214–226.
- Axe, E.L. et al., 2008. Autophagosome formation from membrane compartments enriched in phosphatidylinositol 3-phosphate and dynamically connected to the endoplasmic reticulum. *Journal of Cell Biology*, 182(4), pp.685–701.
- Baixaui, F. et al., 2015. Mitochondrial respiration controls lysosomal function during inflammatory t cell responses. *Cell Metabolism*, 22(3), pp.485–498.
- Ballabio, A., 2016. The awesome lysosome. *EMBO Molecular Medicine*, 8(2), pp.73–76.
- Bar-Peled, L. & Sabatini, D.M., 2014. Regulation of mTORC1 by amino acids Liron. *Trends Cell Biology*, 100(2), pp.130–134.
- Barrientos, A. et al., 2002. Cytochrome oxidase in health and disease. *Gene*, 286(1), pp.53–63.
- Bennett, M.C. et al., 2002. Chronic In Vivo Sodium Azide Infusion Induces Selective and Stable Inhibition of Cytochrome c Oxidase. *Journal of Neurochemistry*, 66(6), pp.2606–2611.
- Bénil, P., Lebon, S. & Rustin, P., 2009. Respiratory-chain diseases related to complex III deficiency. *Biochimica et Biophysica Acta - Molecular Cell Research*, 1793(1), pp.181–185.
- Benz, R., 1994. Permeation of hydrophilic solutes through mitochondrial outer membranes: review on mitochondrial porins Roland. *Biochimica et Biophysica Acta*, 1197, pp.167–196.
- Bernardi, P. & Azzone, G.F., 1981. Cytochrome c as an electron shuttle between the outer and inner mitochondrial membranes. *The Journal of Biological Chemistry*, 256(14), pp.7187–7192.

- Bratic, A. & Larsson, N., 2013. Review series The role of mitochondria in aging. *The Journal of Clinical Investigation*, 123(3), pp.951–957.
- Braulke, T. & Bonifacino, J.S., 2009. Sorting of lysosomal proteins. *Biochimica et Biophysica Acta - Molecular Cell Research*, 1793(4), pp.605–614.
- Brunori, M. et al., 1987. Cytochrome-c oxidase. Subunit structure and proton pumping. *European Journal of Biochemistry*, 169, pp.1–8.
- Budzińska, M. et al., 2009. The TOM complex is involved in the release of superoxide anion from mitochondria. *Journal of Bioenergetics and Biomembranes*, 41(4), pp.361–367.
- Cantalupo, G. et al., 2001. Rab-interacting lysosomal protein (RILP): the Rab7 effector required for transport to lysosomes. *The EMBO Journal*, 20(4), pp.683–693.
- Cantó, C. et al., 2010. Interdependence of AMPK and SIRT1 for Metabolic Adaptation to Fasting and Exercise in Skeletal Muscle. *Cell Metabolism*, 11(3), pp.213–219.
- Cao, S.S. & Kaufman, R.J., 2014. Endoplasmic Reticulum Stress and Oxidative Stress in Cell Fate Decision and Human Disease. *Antioxidants & Redox Signaling*, 21(3), pp.396–413.
- Cereghetti, G.M. et al., 2008. Dephosphorylation by calcineurin regulates translocation of Drp1 to mitochondria. *Proceedings of the National Academy of Sciences of the United States of America*, 105(41), pp.15803–15808.
- Chacinska, A. et al., 2010. Distinct Forms of Mitochondrial TOM-TIM Supercomplexes Define Signal-Dependent States of Preprotein Sorting. *Molecular and Cellular Biology*, 30(1), pp.307–318.
- Chacinska, A. et al., 2009. Importing Mitochondrial Proteins: Machineries and Mechanisms. *Cell*, 138(4), pp.628–644.
- Chandel, N.S. et al., 1998. Mitochondrial reactive oxygen species trigger hypoxia-. *Cell Biology*, 95, pp.11715–11720.
- Chandel, N.S. et al., 2000. Reactive oxygen species generated at mitochondrial Complex III stabilize hypoxia-inducible factor-1 α during hypoxia: A mechanism of O₂ sensing. *Journal of Biological Chemistry*, 275(33), pp.25130–25138.
- Charman, M. et al., 2010. MLN64 mediates egress of cholesterol from endosomes to mitochondria in the absence of functional Niemann-Pick Type C1 protein. *Journal of Lipid*

- Research*, 51(5), pp.1023–1034.
- Christensen, K. a, Myers, J.T. & Swanson, J. a, 2002. pH-dependent regulation of lysosomal calcium in macrophages. *Journal of Cell Science*, 115(Pt 3), pp.599–607.
- Chu, C.T. et al., 2013. Cardiolipin externalization to the outer mitochondrial membrane acts as an elimination signal for mitophagy in neuronal cells. *Nature Cell Biology*, 15(10), pp.1197–1205.
- Cuervo, A.M., 2008. Autophagy and aging: keeping that old broom working. *Trends in Genetics*, 24(12), pp.604–612.
- Demers-Lamarche, J. et al., 2016. Loss of mitochondrial function impairs Lysosomes. *Journal of Biological Chemistry*, 291(19), pp.10263–10276.
- DiCiccio, J.E. & Steinberg, B.E., 2011. Lysosomal pH and analysis of the counter ion pathways that support acidification. *The Journal of general physiology*, 137(4), pp.385–390.
- DiMauro, S. & Schon E.A. 2008. Mitochondrial disorders in the nervous system. *Annual Review of Neuroscience*, 31, pp.91–123.
- Dolezal, P. et al., 2006. Evolution of the Molecular Machines for Protein Import into Mitochondria. *Science*, 313(5785), pp.314–318.
- Dong, X. et al., 2010. PI(3,5)P₂ Mucolipin Ca²⁺ Controls Membrane Traffic by Direct Activation of Release Channels in the Endolysosome. *Nature Communications*, 1(4), pp.1–21.
- de Duve, C., 2005. The lysosome turns fifty. *Nature cell biology*, 7(9), pp.847–9.
- De Duve, C. & Wattiaux, R., 1966. Functions of lysosomes. *Annual review of physiology*, 28(September), pp.435–492.
- Egan, D.F. et al., 2010. Phosphorylation of ULK1 (hATG1) by AMP-Activated Protein Kinase Connects Energy Sensing to Mitophagy. *Science*, 331(2011), pp.456–461.
- Elbaz-Alon, Y. et al., 2014. A dynamic interface between vacuoles and mitochondria in yeast. *Developmental Cell*, 30(1), pp.95–102.
- Elbaz-Alon, Y. et al., 2015. Lam6 Regulates the Extent of Contacts between Organelles. *Cell Reports*, 12(1), pp.7–14.
- Emerlinga, B.M. et al., 2009. Hypoxic activation of AMPK is dependent on mitochondrial ROS

- but independent of an increase in AMP/ATP ratio. *Free Radical Biology and Medicine*, 46(10), pp.1386–1391.
- Enríquez, J.A., 2016. Supramolecular Organization of Respiratory Complexes. *Annual review of physiology*, 78(December 2015), pp.533–61.
- Fengsrud, M. et al., 1995. Ultrastructural and immunocytochemical characterization of autophagic vacuoles in isolated hepatocytes: Effects of vinblastine and asparagine on vacuole distributions. *Experimental Cell Research*, 221, pp.504–519.
- Frezza, C. et al., 2006. OPA1 Controls Apoptotic Cristae Remodeling Independently from Mitochondrial Fusion. *Cell*, 126(1), pp.177–189.
- Fry, M. & Green, D.E., 1978. Resolution of complex III of the mitochondrial electron transfer chain into two component complexes. *Proceedings of the National Academy of Sciences*, 75(11), pp.5377–5380.
- Fryer, L.G., Parbu-Patel, A. & Carling, D., 2002. Protein kinase inhibitors block the stimulation of the AMP-activated protein kinase by 5-amino-4-imidazolecarboxamide riboside. *FEBS Letters*, 531(2), pp.189–192.
- Galione, A., 2011. NAADP Receptors. In *Cold Spring Harbor Perspectives in Biology*. pp. 1–17.
- Gandre-Babbe, S. & Blik, A.M. van der, 2008. The Novel Tail-anchored Membrane Protein Mff Controls Mitochondrial and Peroxisomal Fission in Mammalian Cells. *Molecular biology of the Cell*, 19(1), pp.2402–2412.
- Geisler, S. et al., 2010. PINK1/Parkin-mediated mitophagy is dependent on VDAC1 and p62/SQSTM1. *Nature Cell Biology*, 12(2), pp.119–131.
- Gwinn, D.M. et al., 2008. AMPK phosphorylation of raptor mediates a metabolic checkpoint. *Molecular Cell*, 30(2), pp.214–226.
- Hailey, D.W. et al., 2010. Mitochondria supply membranes for autophagosome biogenesis during starvation. *Cell*, 141(4), pp.656–667.
- Hamasaki, M. et al., 2013. Autophagosomes form at ER-mitochondria contact sites. *Nature*, 495(7441), pp.389–393.
- Han, D. et al., 2003. Voltage-dependent anion channels control the release of the superoxide anion from mitochondria to cytosol. *Journal of Biological Chemistry*, 278(8), pp.5557–5563.

- Hardie, D.G., 2015. AMPK: Positive and negative regulation, and its role in whole-body energy homeostasis. *Current Opinion in Cell Biology*, 33, pp.1–7.
- Hardie, D.G. & Ashford, M.L.J., 2014. AMPK: Regulating Energy Balance at the Cellular and Whole Body Levels. *Physiology (Bethesda)*, 29(2), pp.99–107.
- Haynes, C.M., Fiorese, C.J. & Lin, Y.-F., 2013. Evaluating and responding to mitochondrial dysfunction: The UPRmt and beyond. , 100(2), pp.130–134.
- Hoffman, G.G. et al., 1993. Complete coding sequence, intron/exon organization, and chromosomal location of the gene for the core I protein of human ubiquinol- cytochrome c reductase. *The Journal of Biological Chemistry*, 268(28), pp.21113–21119.
- Hönscher, C. et al., 2014. Cellular metabolism regulates contact sites between vacuoles and mitochondria. *Developmental Cell*, 30(1), pp.86–94.
- Hu, Y.-B. et al., 2015. The endosomal-lysosomal system: from acidification and cargo sorting to neurodegeneration. *Translational Neurodegeneration*, 4(1), pp.1–10.
- Hurley, R.L. et al., 2005. The Ca²⁺/calmodulin-dependent protein kinase kinases are AMP-activated protein kinase kinases. *Journal of Biological Chemistry*, 280(32), pp.29060–29066.
- Invernizzi, F. et al., 2012. Microscale oxygraphy reveals OXPHOS impairment in MRC mutant cells. *Mitochondrion*, 12(2), pp.328–335.
- Isaacs, J.S. et al., 2005. HIF overexpression correlates with biallelic loss of fumarate hydratase in renal cancer: Novel role of fumarate in regulation of HIF stability. *Cancer Cell*, 8(2), pp.143–153.
- Ishihara, N. et al., 2006. Regulation of mitochondrial morphology through proteolytic cleavage of OPA1. *Embo J*, 25(13), pp.2966–2977.
- Ishihara, N., Eura, Y. & Mihara, K., 2004. Mitofusin 1 and 2 play distinct roles in mitochondrial fusion reactions via GTPase activity. *Journal of cell science*, 117(Pt 26), pp.6535–46.
- Ishii, H. et al., 2014. Mitochondrial inhibitor sodium azide inhibits the reorganization of mitochondria-rich cytoplasm and the establishment of the anteroposterior axis in ascidian embryo. *Development Growth and Differentiation*, 56(2), pp.175–188.
- Itakura, E., Kishi-Itakura, C. & Mizushima, N., 2012. The hairpin-type tail-anchored SNARE

- syntaxin 17 targets to autophagosomes for fusion with endosomes/lysosomes. *Cell*, 151(6), pp.1256–1269.
- Ivankovic, D. et al., 2016. Mitochondrial and lysosomal biogenesis are activated following PINK1/parkin-mediated mitophagy. *Journal of Neurochemistry*, 136(2), pp.388–402.
- Iwata, S. et al., 1998. Complete structure of the 11-subunit bovine mitochondrial cytochrome bc(1) complex. *Science*, 281(5373), pp.64–71.
- James, D.I. et al., 2003. hFis1, a novel component of the mammalian mitochondrial fission machinery. *Journal of Biological Chemistry*, 278(38), pp.36373–36379.
- Jeon, S.-M., 2016. Regulation and function of AMPK in physiology and diseases. *Experimental & molecular medicine*, 48(7), p.e245.
- Jin, S.M. & Youle, R.J., 2012. PINK1- and Parkin-mediated mitophagy at a glance. *Journal of cell science*, 125(Pt 4), pp.795–799.
- Kadenbach, B. et al., 2000. Mitochondrial energy metabolism is regulated via nuclear-coded subunits of cytochrome c oxidase. *Free Radical Biology and Medicine*, 29(3–4), pp.211–221.
- Kaelin Jr. W.G. & McKnight, S.L., 2013. Influence of Metabolism on Epigenetics and Disease. *Cell*, 153(1), pp.56–69.
- Kaushik, S., Massey, A.C. & Cuervo, A.M., 2006. Lysosome membrane lipid microdomains: novel regulators of chaperone-mediated autophagy. *The EMBO journal*, 25(17), pp.3921–3933.
- Kennaway, N.G., 1988. Defects in the cytochrome bc1 complex in mitochondrial diseases. *Journal of bioenergetics and biomembranes*, 20(3), pp.325–52.
- Kesidou, E. et al., 2013. Autophagy and neurodegenerative disorders. *Neural Regeneration Research*, 8(24), pp.2275–2283.
- Kessler, R.J., Tyson, C.A. & Green, D.E., 1976. Mechanism of uncoupling in mitochondria: uncouplers as ionophores for cycling cations and protons. *Proceedings of the National Academy of Sciences of the United States of America*, 73(9), pp.3141–3145.
- Khaminets, A., 2016. Ubiquitin-dependent and independent signals in selective autophagy. *Trends Cell Biology*, 26, pp.1–11.

- Kiffin, R. et al., 2004. Activation of Chaperone-mediated Autophagy during Oxidative Stress. *Molecular Biology of the Cell*, 15, pp.4829–4840.
- Koehler, C.M., 2000. Protein translocation pathways of the mitochondrion. *FEBS Letters*, 476(1–2), pp.27–31.
- Korla, K. & Mitra, C.K., 2013. Modelling the Krebs cycle and oxidative phosphorylation. *Journal of biomolecular structure & dynamics*, 32(2), pp.242–56.
- Korolchuk, V.I. et al., 2011. Lysosomal positioning coordinates cellular nutrient responses. *Nature cell biology*, 13(4), pp.453–60.
- Kovacs, L., Reith, A. & Seglez, P. O., 1982. Accumulation of autophagosomes after inhibition of hepatocytic protein degradation by vinblastine. Leupeptin or a lysosomotropic amine. *Experimental Cell Research*, 137, pp.191–201.
- Krebs, H.A. & Johnson, W.A., 1937. Metabolism of ketonic acids in animal tissues. *The Biochemical journal*, 31(4), pp.645–60.
- Kriaucionis, S. et al., 2006. Gene Expression Analysis Exposes Mitochondrial Abnormalities in a Mouse Model of Rett Syndrome. *Molecular and Cellular Biology*, 26(13), pp.5033–5042.
- Kuiper, R.P. et al., 2004. Regulation of the MiTF/TFE bHLH-LZ transcription factors through restricted spatial expression and alternative splicing of functional domains. *Nucleic Acids Research*, 32(8), pp.2315–2322.
- Kwong, J.Q. et al., 2015. The Mitochondrial Calcium Uniporter Selectively Matches Metabolic Output to Acute Contractile Stress in the Heart. *Cell Reports*, 12(1), pp.15–22.
- Lang, B.F. et al., 1997. An ancestral mitochondrial DNS resembling a eubacterial genome in miniature. *Nature*, 387(29), pp.493–497.
- Laplante, M. & Sabatini, D.M., 2009. mTOR signaling at a glance. *Journal of Cell Science*, 122(Pt 20), pp.3589–3594.
- Laukka, T. et al., 2016. Fumarate and succinate regulate expression of hypoxia-inducible genes via TET enzymes. *Journal of Biological Chemistry*, 291(8), pp.4256–4265.
- Lazarou, M. et al., 2015. The ubiquitin kinase PINK1 recruits autophagy receptors to induce mitophagy. *Nature*, 524(7565), pp.309–14.
- Li, H. et al., 2016. Acute exercise-induced mitochondrial stress triggers an inflammatory

- response in the myocardium via nlrp3 inflammasome activation with mitophagy. *Oxidative Medicine and Cellular Longevity*, 2016, pp.1–11.
- Li, W.W., Li, J. & Bao, J.K., 2012. Microautophagy: Lesser-known self-eating. *Cellular and Molecular Life Sciences*, 69(7), pp.1125–1136.
- Li, X. et al., 2016. A molecular mechanism to regulate lysosome motility for lysosome positioning and tubulation. *Nature Cell Biology*, 18(4), pp.404–417.
- Li, Y. et al., 2006. Cytochrome c oxidase subunit IV is essential for assembly and respiratory function of the enzyme complex. *Journal of Bioenergetics and Biomembranes*, 38(5–6), pp.283–291.
- Lightowers, R.N., Taylor, R.W. & Turnbull, D.M., 2015. Mutations causing mitochondrial disease: What is new and what challenges remain? *Science*, 349(6255), pp.1494–1499.
- Lim, C.-Y. & Zoncu, R., 2016. The lysosome as a command-and-control center for cellular metabolism. *The Journal of Cell Biology*, 214(6), pp.653–664.
- Lim, J.A. et al., 2015. Defects in calcium homeostasis and mitochondria can be reversed in Pompe disease. *Autophagy*, 11(2), pp.385–402.
- Lim, M.L., Minamikawa, T. & Nagley, P., 2001. The protonophore CCCP induces mitochondrial permeability transition without cytochrome c release in human osteosarcoma cells. *FEBS Letters*, 503(1), pp.69–74.
- Liu, L. et al., 2012. Mitochondrial outer-membrane protein FUNDC1 mediates hypoxia-induced mitophagy in mammalian cells. *Nature Cell Biology*, 14(2), pp.177–185.
- Liu, X. et al., 1996. Induction of apoptotic program in cell-free extracts: Requirement for dATP and cytochrome c. *Cell*, 86(1), pp.147–157.
- Losón, O.C. et al., 2012. Fis1, Mff, MiD49, and MiD51 mediate Drp1 recruitment in mitochondrial fission. *Molecular Biology of the Cell*, 24(5), pp.659–67.
- Lou, P.-H. et al., 2007. Mitochondrial uncouplers with an extraordinary dynamic range. *The Biochemical journal*, 407(1), pp.129–140.
- Luzio, J.P. et al., 2000. Lysosome-endosome fusion and lysosome biogenesis. *Journal of Cell Science*, 113 (Pt 9, pp.1515–1524.
- Luzio, J.P. et al., 2003. Membrane dynamics and the biogenesis of lysosomes. *Molecular*

- Membrane Biology*, 20(2), pp.141–154.
- Luzio, J.P., Pryor, P.R. & Bright, N.A., 2007. Lysosomes: fusion and function. *Nature reviews. Molecular cell biology*, 8(8), pp.622–32.
- Maranzana, E. et al., 2013. Mitochondrial respiratory supercomplex association limits production of reactive oxygen species from complex I. *Antioxidants & redox signaling*, 19(13), pp.1469–80.
- Martina, J.A. et al., 2012. MTORC1 functions as a transcriptional regulator of autophagy by preventing nuclear transport of TFEB. *Autophagy*, 8(6), pp.903–914.
- Martina, J.A. et al., 2014. Novel roles for the MITF/TFE family of transcription factors in organelle biogenesis, nutrient sensing, and energy homeostasis. *Cellular and Molecular Life Sciences*, 71(13), pp.2483–2497.
- Martina, J.A. et al., 2014. The Nutrient-Responsive Transcription Factor TFE3 Promotes Autophagy , Lysosomal Biogenesis , and Clearance of Cellular Debris. , 7(309), pp.1–16.
- Martina, J.A. & Puertollano, R., 2013. Rag GTPases mediate amino acid-dependent recruitment of TFEB and MITF to lysosomes. *Journal of Cell Biology*, 200(4), pp.475–491.
- Martina, J.A. & Puertollano, R., 2013. RRAG GTPases link nutrient availability to gene expression, autophagy and lysosomal biogenesis. *Autophagy*, 9(6), pp.928–930.
- Medina, D.L. et al., 2015. Lysosomal calcium signalling regulates autophagy through calcineurin and TFEB. *Nature Cell Biology*, 17(3), pp.288–299.
- Van Meel, E. & Klumperman, J., 2008. Imaging and imagination: Understanding the endo-lysosomal system. *Histochemistry and Cell Biology*, 129(3), pp.253–266.
- Merkulova, M. et al., 2015. Mapping the H(+) (V)-ATPase interactome: identification of proteins involved in trafficking, folding, assembly and phosphorylation. *Scientific Reports*, 5, pp.1–15.
- Miles, B., 2003. Inhibitors & Uncouplers. *Free Radical Biology & Medicine*, 52, pp.1075–1085.
- Mindell, J.A., 2012. Lysosomal acidification mechanisms. *Annual Review Physiology*, 74, pp.69–86.
- Mitchell, P. & Moyle, J., 1969. Estimation of Membrane Potential and pH Difference across the Cristae Membrane of Rat Liver Mitochondria. *European Journal of Biochemistry*, 7(4),

pp.471–484.

Mizushima, N., Ohsumi, Y. & Yoshimori, T., 2002. Autophagosome Formation in Mammalian Cells. *Cell Structure and Function*, 27, pp.421–429.

Mungai, P.T. et al., 2011. Hypoxia Triggers AMPK Activation through Reactive Oxygen Species-Mediated Activation of Calcium Release-Activated Calcium Channels. *Molecular and cellular biology*, 31(17), pp.3531–3545.

Murphy, M.P., 2009. How mitochondria produce reactive oxygen species. *The Biochemical journal*, 417(1), pp.1–13.

Nakamura, T. et al., 2013. Aberrant Protein S-Nitrosylation in Neurodegenerative Diseases. *Neuron*, 78(4), pp.596–614.

Neupert, W. & Herrmann, J.M., 2007. Translocation of Proteins into Mitochondria. *Annual Review of Biochemistry*, 76(1), pp.723–49.

Nezich, C.L. et al., 2015. MiT/TFE transcription factors are activated during mitophagy downstream of Parkin and Atg5. *Journal of Cell Biology*, 210(3), pp.435–450.

Ni, H.M., Williams, J.A. & Ding, W.X., 2015. Mitochondrial dynamics and mitochondrial quality control. *Redox Biology*, 4, pp.6–13.

Nisoli, E., 2003. Mitochondrial Biogenesis in Mammals: The Role of Endogenous Nitric Oxide. *Science*, 299(5608), pp.896–899..

Novak, I. et al., 2010. Nix is a selective autophagy receptor for mitochondrial clearance. *EMBO reports*, 11(1), pp.45–51.

Nunnari, J. & Suomalainen, A., 2012. Mitochondria: In sickness and in health. *Cell*, 148(6), pp.1145–1159.

Ohsumi, Y., 2014. Historical landmarks of autophagy research. *Cell research*, 24(1), pp.9–23.

Olichon, A. et al., 2003. Loss of OPA1 perturbs the mitochondrial inner membrane structure and integrity, leading to cytochrome c release and apoptosis. *Journal of Biological Chemistry*, 278(10), pp.7743–7746.

Osellame, L.D. et al., 2013. Mitochondria and quality control defects in a mouse model of gaucher disease - Links to parkinson's disease. *Cell Metabolism*, 17(6), pp.941–953.

- Pastore, N., Ballabio, A. & Brunetti-Pierri, N., 2013. Autophagy master regulator TFEB induces clearance of toxic SERPINA1/a-1-antitrypsin polymers. *Autophagy*, 9(7), pp.1094–1096.
- Patten, D.A. et al., 2010. Reactive oxygen species: Stuck in the middle of neurodegeneration. *Journal of Alzheimer's Disease*, 20.
- Pellegrino, M.W., Nargund, A.M. & Haynes, C.M., 2012. Signaling the Mitochondrial Unfolded Protein Response. *Biochim Biophys Acta*, 1833(2), pp.410–416.
- Perera, R.M. & Zoncu, R., 2016. The Lysosome as a Regulatory Hub. *Annual Review of Cell and Developmental Biology*, 32(1), p.annurev-cellbio-111315-125125.
- Pernas, L. & Scorrano, L., 2015. Mito-Morphosis: Mitochondrial Fusion, Fission, and Cristae Remodeling as Key Mediators of Cellular Function. *Annual review of physiology*, 78(1), p.annurev-physiol-021115-105011.
- Platt, F.M., Boland, B. & van der Spoel, A.C., 2012. Lysosomal storage disorders: The cellular impact of lysosomal dysfunction. *Journal of Cell Biology*, 199(5), pp.723–734.
- Porstmann, T. et al., 2008. SREBP Activity Is Regulated by mTORC1 and Contributes to Akt-Dependent Cell Growth. *Cell Metabolism*, 8(3), pp.224–236.
- Pu, J. et al., 2015. BORC, a Multisubunit Complex that Regulates Lysosome Positioning. *Developmental Cell*, 33(2), pp.176–188.
- Quintero, M. et al., 2006. Mitochondria as signaling organelles in the vascular endothelium. *Proceedings of the National Academy of Sciences of the United States of America*, 103(14), pp.5379–5384.
- Raffaello, A. et al., 2016. Calcium at the Center of Cell Signaling: Interplay between Endoplasmic Reticulum, Mitochondria, and Lysosomes. *Trends in Biochemical Sciences*, xx, pp.1–15.
- Raimundo, N. et al., 2008. Differential metabolic consequences of fumarate hydratase and respiratory chain defects. *Biochimica et Biophysica Acta*, 1782(5), pp.287–294.
- Raimundo, N., Fernández-Mosquera, L., et al., 2016. Mechanisms of communication between mitochondria and lysosomes. *The International Journal of Biochemistry & Cell Biology*, 79, pp.345–349.
- Raimundo, N., 2014. Mitochondrial pathology: Stress signals from the energy factory. *Trends in*

- Molecular Medicine*, 20(5), pp.282–292.
- Raimundo, N. et al., 2012. Mitochondrial stress engages E2F1 apoptotic signaling to cause deafness. *Cell*, 148(4), pp.716–726.
- Raimundo, N., Fernandez-Mosquera, L. & Yambire, K.F., 2016. Mitochondrial Signaling. In D. M. Hockenbery, ed. *Mitochondria and Cell Death*. Seattle , WA , USA: Springer Science+Business Media New York, pp. 169–186.
- Ravikumar, B. et al., 2011. Plasma membrane contributes to the formation of pre-autophagosomal structures. *Cell*, 12(8), pp.747–757.
- Reczek, C.R. & Chandel, N.S., 2015. ROS-dependent signal transduction Colleen. *Current Opinion in Cell Biology Opin Cell Bio*, 33(4), pp.8–13.
- Rieske, J.S., 1976. Composition, structure and function of complex III of the respiratory chain. *Biochimica et Biophysica Acta*, 456, pp.195–247.
- Rizzuto, R. et al., 2012. Mitochondria as sensors and regulators of calcium signalling. *Nature Reviews Molecular Cell Biology*, 13(9), pp.566–578. Available at: <http://dx.doi.org/10.1038/nrm3412>.
- Roczniak-ferguson, A. et al., 2012. The Transcription Factor TFEB Links mTORC1 Signaling to Transcriptional Control of Lysosome Homeostasis. *Science Signaling*, 5(228).
- Rosen, D. et al., 1993. Mutations in Cu/Zn superoxide dismutase gene are associated with familial amyotrophic lateral sclerosis. *Nature*, 363, pp.59–62.
- Rosignol, R. et al., 2004. Energy Substrate Modulates Mitochondrial Structure and Oxidative Capacity in Cancer Cells. *Cancer Research*, 64(3), pp.985–993.
- Rubinsztein, D.C., Shpilka, T. & Elazar, Z., 2012. Mechanisms of autophagosome biogenesis. *Current Biology*, 22(1), pp.R29–R34.
- Sakai, Y. et al., 1998. Peroxisome Degradation by Microautophagy in *Pichia pastoris* : Identification of Specific Steps and Morphological Intermediates. *The Journal of Cell Biology*, 141(3), pp.625–636.
- Sancak, Y. et al., 2010. Ragulator-Rag complex targets mTORC1 to the lysosomal surface and is necessary for its activation by amino acids. *Cell*, 141(2), pp.290–303.
- Sandalio, L.M. et al., 2013. Peroxisomes and their Key Role in Cellular Signaling and

- Metabolism. In *Sub-cellular biochemistry*. pp. 117–120.
- Santel, A. & Fuller, M.T., 2001. Control of mitochondrial morphology by a human mitofusin. *Journal of Cell Science*, 114(Pt 5), pp.867–874.
- Saraste, M., 1999. Oxidative phosphorylation at the fin de siècle. *Science*, 283(5407), pp.1488–1493.
- Sardiello, M. et al., 2009. A Gene Network Regulating Lysosomal Biogenesis and Function. *Science*, 325, pp.473–477.
- Sardiello, M. & Ballabio, A., 2009. Lysosomal enhancement: A CLEAR answer to cellular degradative needs. *Cell Cycle*, 8(24), pp.4021–4022.
- Sardiello Marco et al., 2009. A Gene Network Regulating Lysosomal Biogenesis and Function. *Science*, 325, pp.473–477.
- Scalettar, B.A., Abney, J.R. & Hackenbrock, C.R., 1991. Dynamics, structure, and function are coupled in the mitochondrial matrix. *Proceedings of the National Academy of Sciences*, 88(18), pp.8057–8061.
- Schäfer, E. et al., 2006. Architecture of active mammalian respiratory chain supercomplexes. *Journal of Biological Chemistry*, 281(22), pp.15370–15375.
- Schägger, H. & Pfeiffer, K., 2000. Supercomplexes in the respiratory chains of yeast and mammalian mitochondria. *The EMBO journal*, 19(8), pp.1777–1783.
- Scheffler, I.E., 2008. *Mitochondria* 2nd ed. I. E. Scheffler, ed., Hoboken, New Jersey: John Wiley & Sons, Inc.
- Schieke, S.M. et al., 2006. The mammalian target of rapamycin (mTOR) pathway regulates mitochondrial oxygen consumption and oxidative capacity. *Journal of Biological Chemistry*, 281(37), pp.27643–27652.
- Schleiff, E. & Becker, T., 2011. Common ground for protein translocation: access control for mitochondria and chloroplasts. *Nature reviews. Molecular cell biology*, 12(1), pp.48–59.
- Schwake, M., Schröder, B. & Saftig, P., 2013. Lysosomal Membrane Proteins and Their Central Role in Physiology. *Traffic*, 14(7), pp.739–748.
- Selak, M.A. et al., 2000. Mitochondrial activity in Pompe's disease. *Pediatric Neurology*, 23(1), pp.54–57.

- Settembre, C. et al., 2012. A lysosome-to-nucleus signalling mechanism senses and regulates the lysosome via mTOR and TFEB. *The EMBO Journal*, 31(5), pp.1095–108.
- Settembre, C. et al., 2013. Signals from the lysosome: a control centre for cellular clearance and energy metabolism. *Nature reviews. Molecular cell biology*, 14(5), pp.283–96.
- Settembre, C. et al., 2011. TFEB Links Autophagy to Lysosomal Biogenesis. *Science*, 332(6036), pp.1429–1433.
- Shen, H.M. & Mizushima, N., 2014. At the end of the autophagic road: An emerging understanding of lysosomal functions in autophagy. *Trends in Biochemical Sciences*, 39(2), pp.61–71.
- Shibutani, S.T. & Yoshimori, T., 2014. A current perspective of autophagosome biogenesis. *Cell Research*, 24(1), pp.58–68.
- Shoubridge, E.A., 2001. Cytochrome c Oxidase Deficiency. *American Journal of Medical Genetics*, 106, pp.46–52.
- Sinha, R.A. et al., 2015. Thyroid hormone induction of mitochondrial activity is coupled to mitophagy via ROS-AMPK-ULK1 signaling. *Autophagy*, 11(8), pp.1341–1357.
- Smirnova, E. et al., 1998. A human dynamin-related protein controls the distribution of mitochondria. *Journal of Cell Biology*, 143(2), pp.351–358.
- Stagi, M. et al., 2014. Lysosome size, motility and stress response regulated by fronto-temporal dementia modifier TMEM106B. *Molecular and Cellular Neuroscience*, 61, pp.226–240.
- Steingrimsson, E. et al., 2002. Mitf and Tfe3, two members of the Mitf-Tfe family of bHLH-Zip transcription factors, have important but functionally redundant roles in osteoclast development. *Proceedings of the National Academy of Sciences of the United States of America*, 99(7), pp.4477–4482.
- Tanida, I. et al., 2005. Lysosomal turnover, but not a cellular level, of endogenous LC3 is a marker for autophagy. *Autophagy*, 1(2), pp.84–91.
- Terada, H., 1990. Uncouplers of oxidative phosphorylation. *Environmental Health Perspectives*, 87, pp.213–218.
- Tsai, M.H. et al., 2009. Mitochondrial genomic instability in colorectal cancer: no correlation to nuclear microsatellite instability and allelic deletion of hMSH2, hMLH1, and p53 genes, but

- prediction of better survival for Dukes' stage C disease. *Annals Surgical Oncology*, 16(10), pp.2918–2925.
- Tsuboi, S. & Ohsumi, Y., 1992. Autophagy in Yeast Demonstrated with Proteinase-deficient Mutants and Conditions for its Induction. *The Journal of Cell Biology*, 119(2), pp.301–311.
- Tsukada, M., 1993. Isolation and characterization of autophagy-defective mutants of *Saccharomyces cerevisiae*. *FEBS Letters*, 333(1), pp.169–174.
- Tsukihara, T. et al., 1996. The Whole Structure of the 13-Subunit Oxidized Cytochrome c Oxidase at 2.8 Å. *Science*, 272(31), pp.1136–1144.
- Vingtdeux, V. et al., 2010. AMP-activated protein kinase signaling activation by resveratrol modulates amyloid- β peptide metabolism. *Journal of Biological Chemistry*, 285(12), pp.9100–9113.
- Vygodina, T., Kirichenko, A. & Konstantinov, A.A., 2013. Direct Regulation of Cytochrome c Oxidase by Calcium Ions. *PLoS ONE*, 8(9).
- Wai, T. & Langer, T., 2016. Mitochondrial Dynamics and Metabolic Regulation. *Trends in Endocrinology & Metabolism*, 27(2), pp.105–117.
- West, A.P. et al., 2015. Mitochondrial DNA stress primes the antiviral innate immune response. *Nature*, 520(7548), pp.553–557.
- Wittig, I. et al., 2006. Supercomplexes and subcomplexes of mitochondrial oxidative phosphorylation. *Biochimica et Biophysica Acta*, 1757(9–10), pp.1066–1072.
- Xia, D. et al., 1997. Crystal Structure of the Cytochrome bc₁ Complex from Bovine Heart Mitochondria. *Science*, 277(5322), pp.60–66..
- Yan, W. et al., 2013. Impaired mitochondrial biogenesis due to dysfunctional adiponectin-AMPK-PGC-1 α signaling contributing to increased vulnerability in diabetic heart. *Basic Research in Cardiology*, 108(3).
- Yapici, N.B. et al., 2015. Highly stable and sensitive fluorescent probes (LysoProbes) for lysosomal labeling and tracking. *Scientific Reports*, 5, pp.1–8.
- Yoon, Y. et al., 2003. The Mitochondrial Protein hFis1 Regulates Mitochondrial Fission in Mammalian Cells through an Interaction with the Dynamin-Like Protein DLP1. *Molecular and Cellular Biology*, 23(15), pp.5409–5420.

- Youle, R.J. et al., 2012. Mitochondrial Fission, Fusion, and Stress. *Science*, 337, pp.1062–1065.
- Young, N.P. et al., 2016. AMPK governs lineage specification through Tfeb-dependent regulation of lysosomes. *Genes and Development*, 30(5), pp.535–552.
- Zaffagnini, G. & Martens, S., 2016. Mechanisms of Selective Autophagy. *Journal of Molecular Biology*, 428(9), pp.1714–1724.
- Zalman, L.S., Nikaido, H. & Kagawal, Y., 1980. Mitochondrial Outer Membrane Contains a Protein Producing Nonspecific Diffusion Channels. *The Journal of Biological Chemistry*, 255(5), pp.1771–1774.
- Zdolsek, J.M., Olsson, G.M. & Brunk, U.T., 1990. Photooxidative damage to lysosomes of cultured macrophages by acridine orange. *Photochemistry and Photobiology*, 51(1), pp.67–76.
- Zhang, C.S. et al., 2014. The lysosomal v-ATPase-regulator complex is a common activator for AMPK and mTORC1, acting as a switch between catabolism and anabolism. *Cell Metabolism*, 20(3), pp.526–540.
- Zhang, X. et al., 2016a. MCOLN1 is a ROS sensor in lysosomes that regulates autophagy. *Nature communications*, 7(May), p.12109.
- Zhang, X. et al., 2016b. MCOLN1 is a ROS sensor in lysosomes that regulates autophagy. *Nature Communications*, 7(12109).
- Zhou, G. et al., 2001. Role of AMP-Activated Protein Kinase in Mechanism of Metformin Action Role of AMP-activated protein kinase in mechanism of metformin action. *The Journal of Clinical Investigation*, 108(8), pp.1167–1174.
- Zhou, J. et al., 2013. Activation of lysosomal function in the course of autophagy via mTORC1 suppression and autophagosome-lysosome fusion. *Cell Research*, 23(4), pp.508–523.
- Zolov, S.N. et al., 2012. In vivo, Pikfyve generates PI(3,5)P₂, which serves as both a signaling lipid and the major precursor for PI5P. *Proceedings of the National Academy of Sciences of the United States of America*, 109(43), pp.17472–17477.
- Zong, H. et al., 2002. AMP kinase is required for mitochondrial biogenesis in skeletal muscle in response to chronic energy deprivation. *Proceedings of the National Academy of Sciences of the United States of America*, 99(25), pp.15983–15987.

Zorov, D.B., Juhaszova, M. & Sollott, S.J., 2014. Mitochondrial Reactive Oxygen Species (ROS) and ROS-Induced ROS Release. *Physiological Reviews*, 94(3), pp.909–950.

Zou, J. et al., 2015. Reactivation of Lysosomal Ca²⁺ Efflux Rescues Abnormal Lysosomal Storage in FIG4-Deficient Cells. *Journal of Neuroscience*, 35(17), pp.6801–6812.

Curriculum vitae

Personal information

Surname: Fernández Mosquera

Name: Lorena

Date of birth: 03/05/1982

Place of birth: Vigo (Spain)

Education

PhD in Molecular Medicine Georg-August-University Göttingen, Germany	Currently
Masters in Advanced Biotechnology (University of Vigo and University of A Coruña, Spain)	2012
Degree in Biology (Fundamental and Sanitary branch) (University of Vigo, Spain)	2009

Conferences

Ubiquitin and Autophagy (Frankfurt, Germany)	2016
Mitochondrial Medicine: Developng New Treatments for Mitochondrial Disease (Cambridge, UK)	2016
EMBO Conference “Autophagy signaling and progression in health and disease” (Sardinia, Italy)	2015
Euromit 2014: International Meeting on Mitochondrial Pathology (Tampere, Finland)	2014

Publications

Fernández-Mosquera L, Diogo CV, Yambire K.F., Stagi M., Milosevic I., Raimundo N.
Chronic mitochondrial respiratory chain deficiency down-regulates PI(3,5)P2
production and inhibits lysosomal calcium signaling. In preparation for submission
(EMBO Reports)

Fernández-Mosquera L., Diogo C.V., Yambire K. F., SantosG. L., Luna Sánchez M., Bénit P., Rustin P., Lopez L.C., Milosevic I., Raimundo N. Acute and chronic mitochondrial respiratory chain deficiency differentially regulate lysosomal biogenesis. *Science reports (reviewed, in revision)*

Raimundo, N., **Fernández-Mosquera, L.**, et al., 2016. Mechanisms of communication between mitochondria and lysosomes. *The International Journal of Biochemistry & Cell Biology*, 79, pp.345–349.

Raimundo, N., **Fernández-Mosquera, L.** & Yambire, K.F., 2016. Mitochondrial Signaling. In D. M. Hockenbery, ed. *Mitochondria and Cell Death*. Seattle, WA , USA: Springer Science+Business Media New York, pp. 169–186.
